Six-Motor Unmanned Aerial Vehicle Design Performance

Samaneh Abbaszadeh

A Thesis

In

The Department

Of

Mechanical, Industrial & Aerospace Engineering

Presented in Partial Fulfillment of the Requirements

For the Degree of Master of Applied Science at

Concordia University

Montreal, Quebec, Canada

April 2019

ABSTRACT

Six-Motor Unmanned Aerial Vehicle Design Performance

Samaneh Abbaszadeh

The topic of this thesis is on the unmanned aerial vehicle (UAV). Due to the growth of interests about this kind of equipment in different fields, the various features are under investigation. The specific type of UAV considered in this study is the multi-rotor drone. Basically, the kinematics and dynamics of the system are both reviewed in details within the fundamental concepts of this vehicle.

The main focus of the thesis is enhancing the performance of the quadrotor, mainly the forward speed. This vehicle is able to hover at any step of the flight and fast flight in forward direction. The Newton-Euler equations are used to model the quadrotor. Different strategies for adding rotor in the x direction are studied to make changes in the quadrotor to be able to fly fast in forward direction. The six-motor design is considered to cover all the requirements. This design is mathematically studied by using the Newton-Euler formulations. The dynamic model of six-motor design is developed based on existent models for UAVs.

Also, wind tunnel tests were carried out with the objective of extracting the aerodynamic forces. The quadrotor and one motor with its propeller are examined at different angles of installation. The results from the wind tunnel experiments are used in the simulation models.

The quadrotor and the six-motor UAV are both modeled and solved with MATLAB-Simulink. PID control is used for modeling the vehicles. The results of the simulations are compared. The performance of the quadrotor and six-motor UAV design are similar to the four rotor drone under the hovering conditions.

ACKNOWLEDGEMENTS

TABLE OF CONTENTS

List of Figures

List of Tables

Chapter 1

Introduction

1-1 Unmanned Aerial Vehicle

The autonomous flying object that its operator is located on the ground is called drone. Drone is controlled by an operator from the ground surface by means of wireless transmitters. Therefore, it is generally called unmanned aerial vehicle (UAV), however, there are different categories of such vehicle which may be named differently and which are briefly discussed below. This equipment is not in the category of the cruise missiles, ballistic and semi-ballistic vehicle, satellites and torpedoes, since this vehicle performs its mission and comes back and lands in the starting point of flight (take-off point) or anywhere where is programmed. There are different types of applications in both military and civil classes for this type vehicle which are discussed in further paragraphs. The UAV has ignited many studies over the current decade. In fact, by the advancement in fabrication of powered storage systems, remote control capabilities and navigation algorithms, the development of this vehicle has been possible in various fields for application for more precision while humans cannot carry the prospected mission in case of difficulties and dangerous circumstances such as environment contaminations (radiological, biological and chemical hazards), the risk of pilot life loss, longtime missions which lead the pilot to be fatigued and stressed.

1-2 Brief History of the UAV

In 1907, the first helicopter was invented by a French man Paul Cornu. The vehicle was a counter-rotating helicopter, with 20 foot rotors and 24 hp engine to provide support for lift and motion of the equipment. It could reach one-foot height and without tethering it was able to stay stable at that height. Though, the project was stopped due to some instability issues. Figure (1-1) shows Paul Cornu's helicopter [1]. In 1916 an UAV was proposed by Lawrence and Sperry [2] which was named "aviation torpedo" and flew about 30 miles (Figure 1-2). This achievement was the starting point of the aircraft automatic attitude control. At the end of 1950s, the UAVs development began and continued into the 1970s. The manufactured UAVs were tested in the Vietnam war and the cold war. After Vietnam war, the smaller and less expensive UAVs were developed by the U.S and Israel. These small aircrafts were powered by small engines, same as motorcycles or snow mobiles, carried the video cameras and transmitters images to the operator's location. They were called such as "Fire bee", "Bug" and etc. From 1960 to the mid-1970s, over 700 UAVs were built and used. In 1991, the Gulf war, The U.S used UAVs against Iraq and after these military applications, the UAVs progressed quickly [3, 4].

Figure 1-1: Paul Cornu's helicopter (1907)

The domestic utilization of UAVs was requested from FAA in 2005 for the surveillances in disasters and search and rescue processes, but the approval of these types of drones was released in May 2006. The U.S was not the only country that started the non-military utilization of UAVs. The European countries and Canada began to build applications in all fields from 2006 [5, 6, 7, 8].
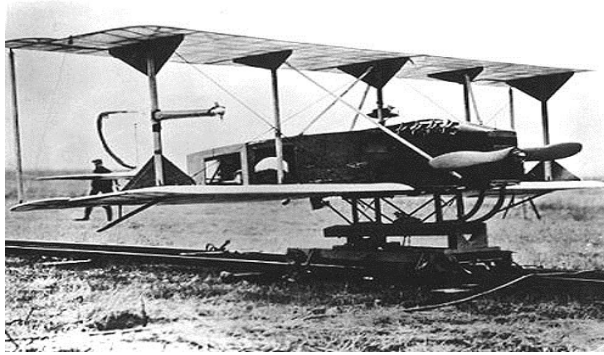
Figure 1-2: Lawrence's [1] UAV (1916)

With the time, the range of applications of UAVs has increased and significant research effort has been carried out in this area. In September 2013, searching for the words "unmanned aerial vehicle" Google would show more than six million entries which shows the influence of UAVs in these years [9].

During the past 15 years, there have been a lot of improvements in different sciences which lead to more enhancement and applications of drones. Miniaturization and cost reduction of controls, computing elements, power storage batteries, sensors, wireless communication units, microprocessors and development of fabrication lead to making tiny UAVs for specific applications and reducing the cost has been a significant selling target [10, 11, 12, 6] .

1-3 The UAV Applications

Unmanned aerial vehicle (UAV) application is growing in different industries. The applications consist of surveying, delivery, precision agriculture, firefighting, pollution monitoring, civil engineering, search and rescue, biotechnology, recreational hobbies, scientific research, inspection and monitoring and many other utilizations are accessible by making some minor changes in the configuration of the vehicle or adding some appropriate equipment on it. The following paragraphs have described some applications of UAVs in different fields briefly [8].

Whenever there would be a disaster, an emergency respond and proper information about the field condition is needed such that a suitable decision is taken. In these cases, UAVs can get real

time images by getting access to the out of reach areas. Therefore, by this remote observer more suitable support could be provided in disaster situations as the search and rescue which is called surveillance (figure 1-3). Moreover, monitoring crowded areas same as festivals, preventing theft, monitoring security threats or border surveillance are some sorts of order forces utilizations of the drones [13, 14].

The precision agriculture is the other application that by monitoring crops, plants, watering status and soil quality via progressed cameras, has led to improved cultivation (figure 1-4) [15, 16, 17, 18, 19].

Figure 1-3: The rescue mission and emergency action

Figure 1-4: The presicion agriculture application
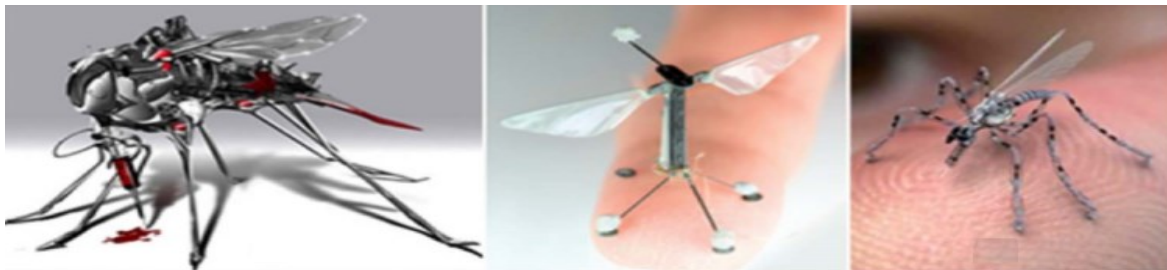
Figure 1-5: The biotechnological drones

The application of drones in biotechnology has been growing in the recent years, for transporting medicine and vaccine, cells, or some tiny surgery tools which can help maintaining human life (figure 1-5) [20, 21, 22, 23, 24].

For the precise 3D mapping that would be used in topology, assurance in different steps of building structure, road mapping and other affairs of civil engineering, UAVs play a crucial role that cannot be neglected. In addition, in many scientific investigations that include three D's "Dull, Dirty and Dangerous work", this vehicle can rectify the obstacles by having high resolution imagery and sensors, be able to use in remote and inaccessible areas [25, 26].

By passing the time and different applications of this vehicle, the funniest utilization can be called the recreational application as the toys for people who are interested in the flight and taking pictures by having a panoramic view.

There are many other applications that could be practical and bring more improvement in the different sciences. For instance, the increasing durations of commuting due to high traffic peaks in crowded cities may be alleviated by using this vehicle in a larger scale as the personal carriers which might significantly reduce the traffic by moving it from the ground in the air.

Another potential application is installing a public Wi-Fi on a multi-rotors drone to accelerate the public communication in a city whenever there is a disaster like earthquake, flood, volcanic and etc. This provided Wi-Fi at different points of the city can help surviving by the stronger network communication via cellphones. It has been known that the psychological aspect in such circumstances bring people together and their action should have more impact. It also can support transferring urgent alerts and notifications in addition to the latest news.

1-4 The Category of the UAVs by Considering MTOW

When classifying of drones, different parameters can be considered same as, weight, flight range and flight altitude. In this study, the MTOW (Maximum take-off weight) of vehicle is assumed as the classification item which has effect on the kinetic energy of the vehicle and is the first factor that makes influence on the flight safety (figure 1-6 shows a big sized drone and small

sized ones). The table (1-1) displays all the classified sorts of the unmanned aerial vehicle by considering the MTOW [27, 11, 7].

Figure (1-6): The DH.82B Queen Bee drone (Photo Credit: Adrian Pingstone) (on the left), small sized drones (on the right) [11]

Table 1-1:Unmanned Aerial Vehicle (UAV)categories by considering the weight [11]Category

No.	MTOW	Name	Notes
0	$< 1kg$	Micro	If damaged it does minimum damage and limited threaten to human life, this category is not considered in most countries
1	$\leq 1kg$	Mini	
2	$\leq 13.5\ kg$	Small	
3	$\leq 242\ kg$	Light/Ultralight	This category can be assumed as ultralight (FAR Part 103), LSA (Order 8130), or even normal aircraft (FAR Part 23) for airworthiness certification
4	$\leq 4,332\ kg$	Normal	This category is corresponded as the normal aircraft (FAR Part 23)
5	$> 4,332\ kg$	Large	This category is corresponded as the transport category (FAR part 25)

1-5 The Fixed Wing vs. The Rotary Wing UAVs

In addition to different categories of UAVs, there are two major structures for this vehicle. They are same as other aircrafts that are called, fixed-wings and multi-rotors which are similar to traditional airplanes and helicopters respectively but in the small scales. For both structures, there are some advantages and some disadvantages. The fixed-wing aircraft has rigid wings which are airfoils that produce lift by forward airspeed and lead the vehicle to continue the flight.

The multi-rotors UAVs contains the rotors and every rotor has 2 or 3 rotor blades which rotate around actuated by servomotors. They have different types of setup consisting of 4 rotors (quadcopter), 6 rotors (hexacopter), 8 rotors (octacopter) and also more number of rotors as 12 and 16 rotors (figure 1-7). The multi-rotors do not need a constant forward movement to maintain the airflow over the blades. The required airflow over the airfoil (produces lift) is generated by the constant movement of the blades. The variation in thrust and torque of rotors controls the multi-rotors UAV and all the attitude changes of a quadcopter is described in chapter 2 [28].

Figure 1-7: Different number of rotors configurations in multi-rotor drones [28]

1-5-1 Advantages and Demerits

Some merits and demerits of multi-rotor UAV are namely expressed as the two following paragraph respectively:

They are able to take-off and land vertically, so less substantial take-off and landing area is needed which is an important merit in the forest, mountains and urban environment. They have

the ability to hover and maneuver quickly which lead to their utilization in the inspections where precision maneuvering and focusing on a single target for a long time is required. There is no problem for their autonomous flight because of their mature controller that makes it easy to fly, take-off and landing.

The endurance and the operation speed is limited since the lift is produced during the complete flight by the rotors. Generally, the flight time is between 12 to 30 minutes, so short distance areas can be covered.

Some advantages and disadvantages of the fixed-wing UAV are stated as follows respectively:

The fixed-wings fly with high speed and have longer flight duration before changing the rechargeable batteries or re-fulling (more than 2 hours is feasible), so in less time, larger areas are covered. Their structure is simpler whenever are compared with the multi-rotors, so their maintenance is less complicated. They are able to glide without power. They are able to carry greater payloads in longer distances.

They have problems in some areas because they need to have an appropriate air flow. There would be damage during landing since they land at high speed. So, it might damage to the payload and if the payload is valuable it is unacceptable. In take-off status, a suitable airflow is needed or the drone must be thrown and it must stay in the constant forward motion [29, 30].

1-6 The Common Relevant Components of the UAVs

Many components are in common to build various UAVs. For instance, they need electrical

motors or fuel-driven engines to produce power and lift during the flight and the number of these power generators depend on the configuration of the UAV. The main body or the structure which all the other components are installed on it. The body shape is in direct relation with the drone configuration and application.

Moreover, there is the main tiny computer on board which can control all the input and output signals of the vehicle to perform a planned mission. There are different sensors (IMU, SONAR,

IR, GPS, …) that can be used for monitoring the various parameters such as temperature, flight altitude, gyroscopic, GPS, rpm of motors, voltage, airspeed and some other sensors which may be different by considering the application of the drone. In case of multi-rotor, propellers and gear sections are applied. Additionally, battery or fuel supply tank, receivers and transmitters, a remote control as a joy stick are the other parts of this vehicle. Also the drone utilization same as other vehicles has a great influence on the detailed component list and the parts type [31].

1-7 The Contribution of This Study

In this study, the proposed vehicle is a multi-rotors drone to perform a fast forward flight to take pictures and videos of plants, soil and the ground surface. This vehicle facilitates a trajectory which is explained as follows:

1- Vertical take-off from point (A). 2- Making orientation and setting the appropriate attitude of the flight. 3- Fast forward flight to reach point (B). 4- Finding the required orientation for landing. 5- Landing at the point (B).

As it is explained, this drone is able to hover at any point of the mission and moreover, to fly in the forward direction fast to perform the mission in less time. While, the drone can hover to make more focus on the required specific point of the mission. The defined trajectory would be utilized in the agricultural field, mining field, catastrophic events and many other applications.

Therefore, to understand the physics of the design and its reactions, firstly, the kinematics and dynamic equations of a quadrotor are studied. Secondly, the designed vehicle kinematics and dynamics equations are acquired. Hence, for a better stabilization it is crucial to determine the algorithm structure of the control and establish the model.

Both vehicles models are simulated by MATLAB-Simulink software which its results can help for performance debugging of the system. Moreover, a simple comparison between the standard quadrotor and the prospected design shows their merits and drawbacks.

Although, the design is not prototyped, a quadrotor which is named SYMA X5C has been selected as a basic model. All components and their dimensions and weights of the design are assumed as the granted vehicle. Some experiments have been performed to achieve the drag and lift forces of the mentioned vehicle in the wind tunnel. The vehicle and one motor with its assembled propeller have been tested individually in two steps in the wind tunnel. Their results are used in the simulation of various segments of a mission.

1-8 The Thesis Outline

This thesis contains five chapters which are as follows. The first chapter is the introduction that describes the purpose of the study. It includes a brief summary of the design objectives, steps to approach the planned objectives. This chapter also includes the targeted contribution of the thesis.

The mathematical model of a quadrotor and the actuators is presented in the second chapter. Basic concepts of the quadrotor and its flight status, the coordinate system, basic configuration and movements are explained in this chapter. The kinematics and the dynamics equations in conjunction with the actuators (motors, gearbox, propellers) equations are provided. The center of gravity position location and finding are presented.

In the third chapter development of different designs features to achieve the vehicle with the proposed characteristics are carried out. All the kinematics and dynamic equations of the designed drone is represented in this chapter. Many equations are common to various configurations while small changes are necessary only. Further the actuators equations are considered in coupled with the dynamics equations. The influence of the position of the center of gravity of the design is studied in this chapter.

In the fourth chapter, the wind tunnel experiments are explained and their results are illustrated in details. In addition, the standard quadrotor and the proposed design are simulated in the MATLAB-Simulink software and the results are presented. All the simulation outcomes are

investigated in this chapter and the results of the standard quadrotor and the proposed design are compared.

The fifth chapter presents the future work of this study and evaluates the conclusion of the thesis. In this chapter the goals of the study are summarized and some solutions are demonstrated to enhance the platform of this design.

CHAPTER 2

The Fundamental Principle of the Classical Quadrotor Model

In this chapter, the constitutive dynamics parameters and basic analysis of forces that are generated in a quadrotor are discussed. Also the quadrotor kinematics is investigated after the translation and rotation accelerations are determined from the dynamic model through the analysis of the variable lift forces acting within the range of directions and amplitudes. Unmanned Aircraft Vehicle (UAV) motions could be divided into the three important categories, according to the class of motion of the aerial vehicle. The three types of motion are lifting, hovering and following a direction in an orientation path (orientation about axes). All three motions are described by the same set of equations but each condition employs different relationship among the forces. Each type of motion may employ a large range of conditions such that a specific travel path. Thus, the displacement from a point to another could be achieved with many sets of forces along various paths. It is important to relate the motion of the UAV to these specific forces.

2-1 Basic Concepts

At first, there are some basic concepts that need to be discussed. As mentioned in chapter 1, any multi-rotor is made of four, six, eight or more (even number) propellers which are mounted on suitable actuators located at the end of two arms that are positioned at 90°, 60°,45° or other angles. The quadrotor must be built for one or multiple tasks. It requires a control board, the sensing for surrounding data processing, feedback control system and the other necessary

equipment to perform its function. Fixed-pitch blades are used in UAVs to produce downward airflow which results in upward lift of the quadrotor. The axes of rotation of the propellers are parallel and fixed.

It is assumed that the whole body of the quadrotor is rigid and the mass is invariant. All the motions need to be attained by varying the lift forces of the quadrotor in a suitable way. Thus, the control of the motion is accomplished through the individual control of the RPM at the four propellers. The equilibrium of moments is achieved through the suitable rotation of the propellers: the ones positioned at the two ends of a beam rotate in one direction while the ones from the other beam rotate in the opposite direction such that all yield the lift of the quadrotor without creating a rotation momentum. This setting is implemented to achieve the same role as a tail rotor in a helicopter to produce anti-torque for balancing the vehicle.

In figure 2-1, a schematic of a quadrotor is presented. The curved types of arrows show the circular velocity Ω_i(rad/s), (i = 1, 2, 3, 4) or the speed of the propellers, which are controlled while the vertical upward arrows illustrate the thrust force exerted at each propeller. The thrust is related to the circular velocity through the performance of the propellers.
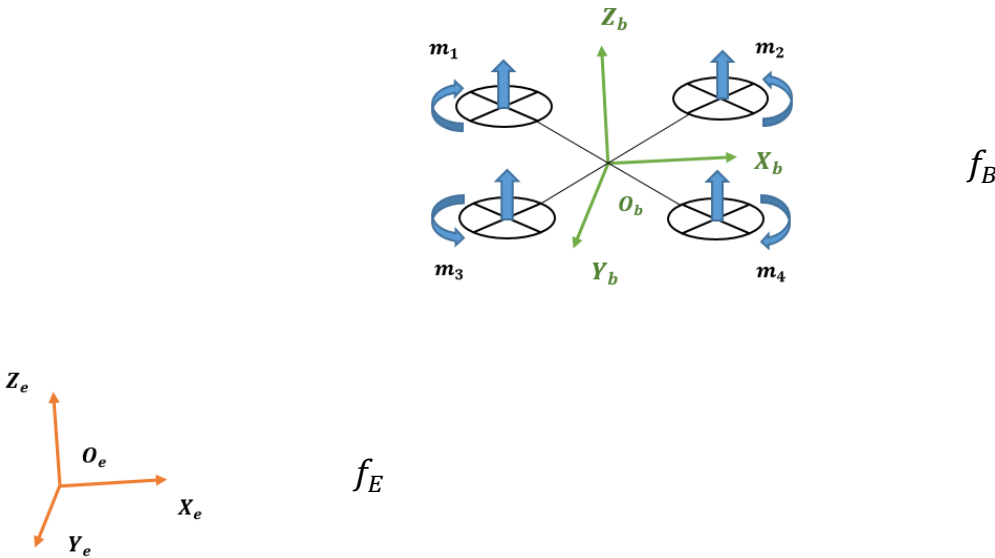
Fig 2-1: Schematics of a quadrotor with the associated frames (B-frame and E-frame)

By considering the movement of the quadrotor in relation with the earth, two frames are defined. The fixed frame is attached to the reference on the earth, Earth Frame (f_E), while the mobile one is attached to the quadrotor, namely is the Body Frame (f_B). The two frames with their axes are illustrated in Figure 2-1.

The motions of the quadrotor could be assessed based on the revolution speed of the four motors spinning the propellers. Assuming that all motors spin at the same rate, the drone moves vertically, it occupies a steady position or it moves downwards. The velocity of the motors for the steady position case should be such that the lift will balance the constant weight of the drone. If the total velocity of the motors is below this value, the drone will move downwards. If the speed of two adjacent motors is different from the other two, the plane of the drone will incline with respect to the horizontal position such that the lift force as well as the weight will exhibit a horizontal component that will cause the quadrotor to move in that direction. Finally, if two opposite motors spin at a different rate than the other two, the quadrotor will spin about its vertical axis in the direction of rotation of the higher speed propellers. This maneuver enables the quadrotor to control the directional position.
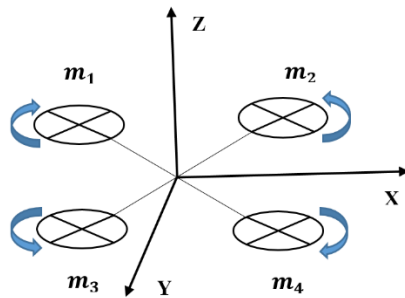
Fig 2-2: Schematics of the motors spin directions in a quadrotor motors

The quadrotor is equipped with four motors but it exhibits six degrees of freedom. The complex motion is enabled by the balance of the rotation rate of the four motors, figure 2-2, and table 2-1. There are three directions X, Y and Z. The direction of X is located where the attachment of the video camera is installed, this is, in the forward direction. The Y direction is defined as perpendicular to the X orientation in the horizontal plane. The third direction is Z, which is located in the vertical plane but perpendicular to the both X and Y directions. The differences

and changes in motions (translations) and rotations about all three directions are given in table 2-1 which are defined by comparing the RPM of all motors. Therefore, for obtaining a desired height and attitude, a controller should be designed by considering four accurate controllable variables which are named Roll, Pitch, Yaw and Altitude. Also propellers speed variation in definite patterns is the key factor in controlling the basic movements of a quadrotor.

Table 2-1: Six degrees of freedom of a quadrotor in relationship with motors RPM

NO	Types of Degree of Freedom	RPM Relations
1	Translation along Z (Vertical motion)	$RPM_1 = RPM_2 = RPM_3 = RPM_4 > RPM_h$
2	Translation along X in the positive direction	$RPM_1 = RPM_3 < RPM_2 = RPM_4$
3	Translation along Y in the positive direction	$RPM_1 = RPM_2 > RPM_3 = RPM_4$
4	Rotation about Z (Clockwise)	$RPM_1 = RPM_4 > RPM_2 = RPM_3$
5	Rotation about X (Clockwise)	$RPM_1 = RPM_2 < RPM_3 = RPM_4$
6	Rotation about Y (Clockwise)	$RPM_2 = RPM_4 < RPM_1 = RPM_3$

In the following, few of the possible maneuvers of the quadrotor are discussed. Let us assume that Δ_A and Δ_B are small positive variables used to produce changes in rotational speed of propellers which result in translation motion and rotation about the three axes.

2-1-1 Altitude Control (U₁)

The change in the quadrotor altitude can be reached by applying the same speed at all propellers in their respective rotational direction. By increasing or decreasing the angular speed of the propellers at the same time, climbing, hovering or descending are

achieved.

$$\Omega_i = \Omega_h + \Delta A \quad \text{for i} = 1, 2, 3, 4$$

In this equation, ΔA represents some increment which will yield a higher angular speed than the hover angular speed and which will lead to the upwards motion of the drone as illustrated in figure 2-3.

$$\Omega_i = \Omega_h - \Delta B \quad \text{for i} = 1, 2, 3, 4$$

In the above equation, ΔB represents some reduction amount in the angular speed at the propellers which causes the drone to descend. The reasonable assumption made here is that the quadrotor will keep the same mass during the entire mission.
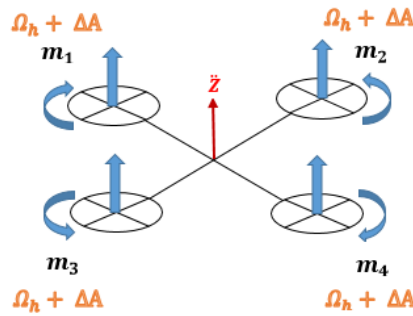
Fig 2-3: Propellers speed in moving up

By increasing the angular speed of two adjacent motors aligned one side and the other of the forward axis OX, the forward speed will increase but there are some caveats to this condition. The attitude of the quadrotor will change as discussed above. Moreover, the aerodynamic forces become important at the high RPMs of the rotors and are affected by the velocity changes of the rotors.

Generally speaking, there are various kinds of drag force for each type of flying objects. For example, helicopters and airplanes may encounter different kinds of drag forces. The reasons of the differences are their structures, configurations, speed, power resources and others. Fundamentally, there are many similarities between the helicopters and quadcopters. When considering drag forces, the most remarkable difference between these two types of vehicle is their sizes. The drag force contributions of a quadrotor are as follows [32]:

a) The propeller rotation in the air generates the thrust. Thus, there is an opposite reaction of the propellers on the air by considering the Newton's third law. In the area that high pressure air of

the upper section of propeller and the low pressure air in the lower section of the propeller are joint, there would be a vortex and spiral at the trailing edge and tip of the rotor. This vortex leads to a force which is called induced drag.

Therefore, the direction of the induced drag force is the rearward direction of the propeller's rotation. Hence, in the neighborhood of the propeller, this force deflects the airflow downward and causes in downwash. By increasing the thrust, the induced drag force increases and it is directly proportional to the rotation peed of the propeller.

b) The profile drag is due to the spin of the airfoil blades induced by horizontal velocity of the quadrotor. This drag is zero in hover. Profile drag is affected by the airspeed which includes the wind.

c) The resulted drag force by the non-lifting components of the vehicle, such as airframe, motors, camera, etc. is called the parasite drag. It is quite considerable at high speeds for large sized rotorcrafts. For the quadrotor with the moderate speed of up to 5 m/s, this drag can be neglected.
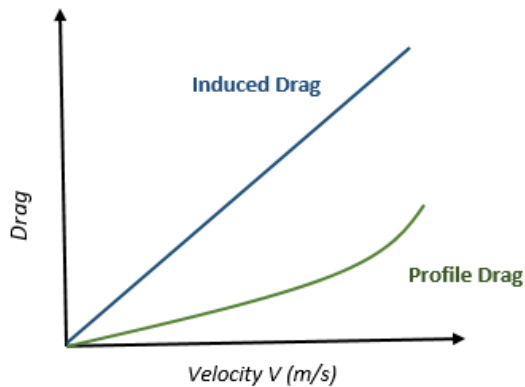
Fig 2-4: Drag-velocity qualitative relationship [32]
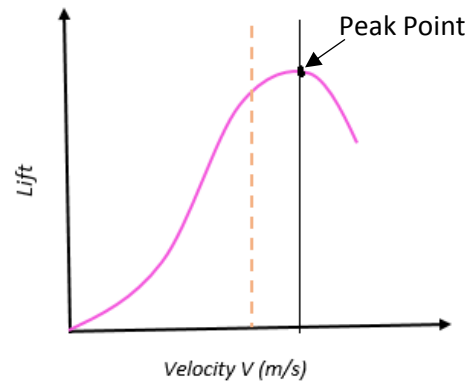
Fig 2-5: Lift-velocity qualitative relationship [33, 34]

Among the above drag force, only the profile and induced drag must be considered for a small rotorcraft as the quadrotor. Hence, the total drag force for the quadrotor is directly affected by the velocity. The figure 2-4 shows the qualitative relation of the profile drag, induced drag and the velocity. It is obvious that by increasing the velocity, the induced drag force will dramatically rise up. The profile drag force will slightly increase.

This graph shows that by raising the airspeed there is an increment in the total drag given the profile of both drag forces lines. Therefore, there must be a limitation in increasing the airspeed when it leads to reverse effect on the efficiency. In other words, by increasing the airspeed, the required power for compensating the total drag will increase while the drag may lead to stall and the vehicle cannot continue its mission as being out of control. The equation (2-1), shows the drag equation which can be produced by an airfoil. Here, ρ $[kg\ m^{-3}]$ is the airflow density, $V[m\ s^{-2}]$ is the airfoil velocity, A $[m^2]$ is the airfoil area and c_d is the drag coefficient and dimensionless which is different by changing the velocity.

$$D = \frac{1}{2}\ \rho\ V^2\ A\ c_d \tag{2-1}$$

$$L = \frac{1}{2}\ \rho\ V^2\ A\ c_l \tag{2-2}$$

The other aerodynamic force which needs to be considerable in the flight is the lift force. The equation (2-2) is expressed as the lift force. Where, ρ $[kg\ m^{-3}]$ is the airflow density, $V[m\ s^{-2}]$ is the airflow or airfoil velocity, A $[m^2]$ is the airfoil area and c_l is the lift coefficient which is dependent on velocity and dimensionless. The lift force of an airfoil is resulted from the pressure differences between the upper and lower surfaces of the airfoil. When the pressure under the airfoil is higher than the pressure above the airfoil, an upward force will generate as the lift force. Bernoulli equation, states that by increasing the velocity of the flow, its pressure will decrease. Hence, when the velocity of the air above the airfoil increases (because of the higher length of airfoil at top surface), its pressure will decrease. Hence, the pressure difference between the upper and lower surfaces of the airfoil will increase. Thus, more lift force will be generated by increasing the airfoil velocity. But the lift force increment would not continuously increase with the velocity. Above specific value of the velocity, the lift force increment converts to the decrement and stall will occur [33, 34].

By raising the kinetic energy of the boundary layer on the upper surface of the airfoil, the Reynolds number will increase. So the turbulent flow will be initiated. This turbulent flow may yield the separation of the airflow from the airfoil. This may cause the airfoil stall and no more lift could be produced. After the airfoil induces stall, any increase in the airflow speed will induce a decrease in the lift force.

Therefore, the air speed cannot be raised without limitation. This limitation is different for various airfoils and it depends on its surface and shape, the Mach number, the airfoil angle of attack and shape and flow factors. For keeping a flight in a safe condition, a margin of safety must be considered before reaching the stall point (peak point of the figure 2-5). This safety margin is illustrated by the dashed line in the figure 2-5.

2-1-2 The Roll (U2)

Roll motion is defined as the rotation about the X axis. For changing the orientation of the UAV about the X axis, the angular speed of motor 1 and 2 are the same and less than the angular speed of motor 3 and 4 which are the same, figure 2-6. This rotation is accompanied by some lateral displacement in the lateral direction.

$$\Omega_1 = \Omega_2$$

$$\Omega_3 = \Omega_4$$

(Clockwise Roll)
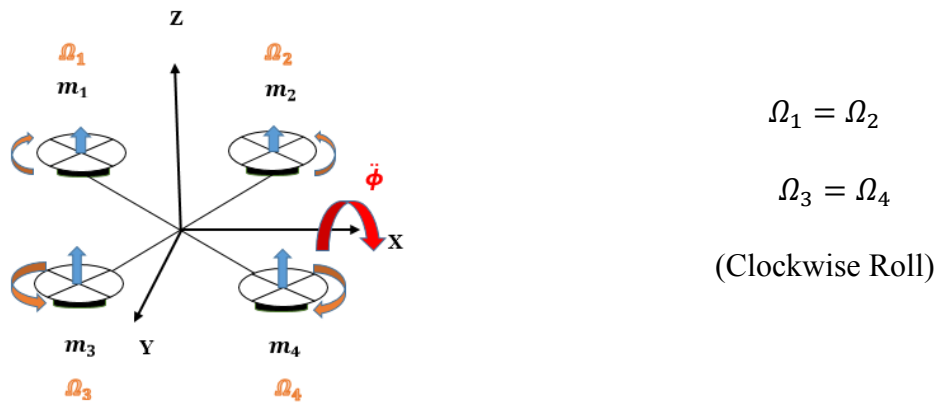
Fig 2-6: Propellers speed distribution in roll movement

2-1-3 The Pitch (U₃)

The pitch fundamental concept is the same as rolling but the movement is about the Y axis and makes the vehicle tilt forward and backward. In this motion the right and left angular speeds are the same as the hover angular speed but the fore one has increment (or decrement) and the aft one has decrement (or increment), figure 2-7. Along with the forward pitch the quadrotor will also move forward as a consequence of the balance of forces.
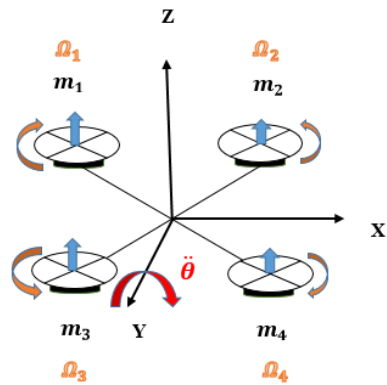
$$\Omega_2 = \Omega_4$$
$$\Omega_1 = \Omega_3$$
(Clockwise Pitch)

Fig 2-7: Propellers speed in pitch rotation

2-1-4 The Yaw (U$_4$)

Yaw is defined as the rotation about the Z axis. By comparing the two former discussed rotational movement and the yaw movement, there is a difference. The direction of yaw is given by the higher RPM of the two opposite rotors spinning in the desired direction of yaw. When Ω_1 and Ω_4 increase (or decrease) simultaneously, Ω_2 and Ω_3 are reduced (or increased). This contrast creates a moment which produces the vehicle rotation about the Z axis, figure 2-8.
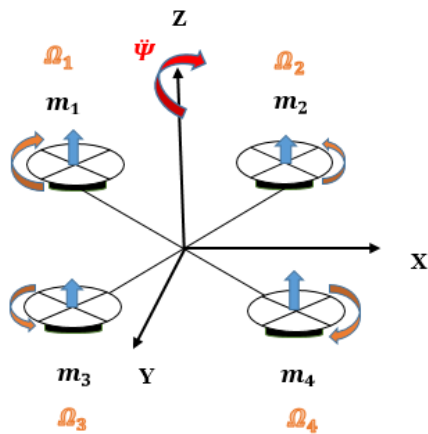
$$\Omega_1 = \Omega_4$$
$$\Omega_2 = \Omega_3$$
(Clockwise Yaw)

Fig 2-8: Propellers speed distribution in yaw rotation

20

2-2 Newton Euler Model

In this section, by using the defined frames in the section 2-1 (figure 2-1) (f_E) and (f_B), the quadrotor equations for generic motions are expressed and the mathematical model is derived from the Newton-Euler formulation.

At first, a generic 6-DOF rigid body is identified. As the kinematics laws require to know the accelerations of the body along the six directions (three translations and three rotations), the evaluation of the accelerations is carried out from the dynamic equilibrium equations. The accelerations are expressed when the dynamics equilibrium is reached. Hence, the two formulations are necessary to solve the kinematics of the drone. In the following equations, all bolded symbols are vectors.

2-2-1 The Kinematic Model

In kinematics [35, 36, 37, 38], the interest is the three laws of motion: acceleration, velocity and displacement. Once the accelerations in the three directions are found, the entire motion becomes fully determined. The quadrotor may move along 6 DOF while there are only four actuators that control the motion. Thus, six coupled equations will describe the entire motion of the system. The position vector in the E-Frame (f_E) is illustrated as $\boldsymbol{\xi}$. The challenge of this problem consists of converting the linear and angular velocities in the Frame B need to be moved to the fixed reference Frame E.

The linear position vector $\boldsymbol{\tau}^E [m]$ is specified by coordination of the origin of the B-Frame and the origin of the E-Frame (translational).

$$\boldsymbol{\tau}^E_{(3,1)} = \begin{bmatrix} x \\ y \\ z \end{bmatrix} \quad , \quad \boldsymbol{\theta}^E_{(3,1)} = \begin{bmatrix} \varphi \\ \theta \\ \psi \end{bmatrix}$$

The angular position vector $\boldsymbol{\theta}^E [rad]$ is specified by the position of the B-Frame with respect to the E-Frame and considering the main three rotations about the main axes, Euler angles (φ,

θ , ψ) (rotational). These rotational motions about the three axes by considering both frames are illustrated in figure 2-9 (a, b, c).

$$\xi = [\tau^E \ \theta^E]^T = [\ x \ y \ z \ \varphi \ \theta \ \psi \ ]^T$$

By using right handed orientation in the quadrotor motion vectors system, all the three above rotations are individually expressed in the Appendix A:

- Rotation about the X-axis of φ angle (Roll) through R (x, φ) figure 2-9(a).

- Rotation about the Y-axis of θ angle (Pitch) through R (y, θ) figure 2-9(b).

- Rotation about the Z-axis of ψ angle (Yaw) through R (z, ψ) figure 2-9(c).
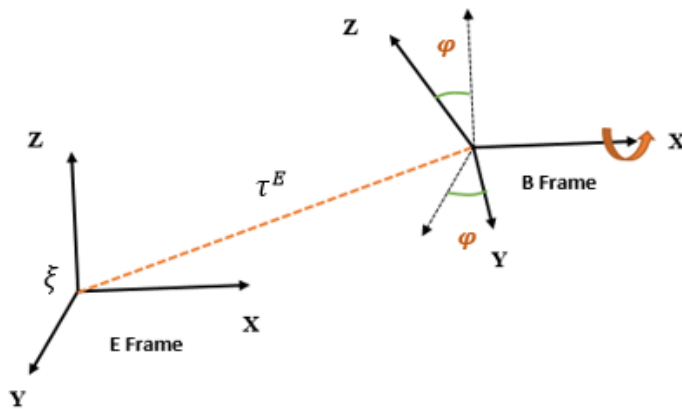
Fig 2-9(a): Rotation about X-axis by considering E-Frame as a fix frame
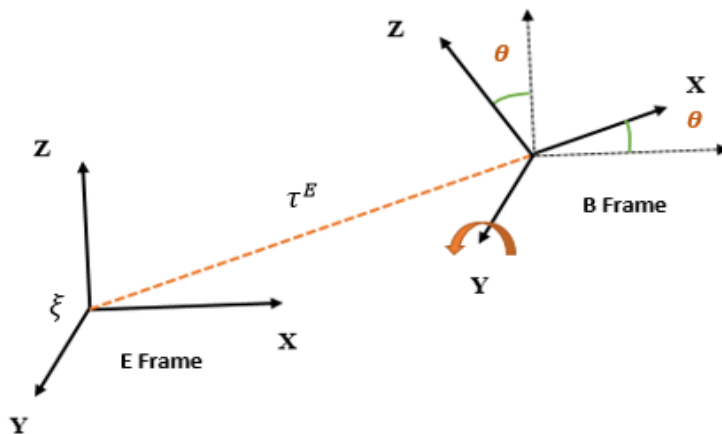
Fig 2-9(b): Rotation about Y-axis by considering E-Frame as a fix frame
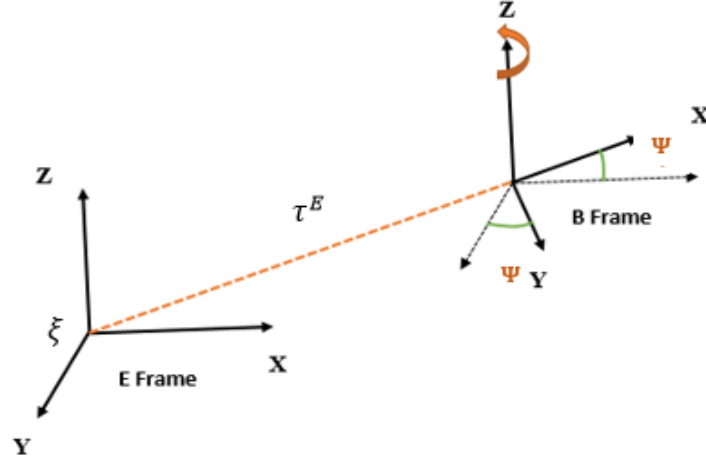
Fig 2-9(c): Rotation about Z-axis by considering E-Frame as a fix frame

There are two fundamental transformation matrices which are used in the rotational and translational derivations [39]. The processes of concluding the rotational matrix R_θ (2-3) and the translational matrix Γ_θ (2-8) are detailed in the Appendix B. Where, in the matrix R_θ, "s" represents sine and "c" represents cosine.

$$R_\theta = \begin{bmatrix} c\psi\ c\theta & -s\psi\ c\varphi + c\psi\ s\theta\ s\varphi & s\psi\ s\varphi + c\psi\ s\theta\ c\varphi \\ s\psi\ c\theta & c\psi\ c\varphi + s\psi\ s\theta\ s\varphi & -c\psi\ s\varphi + s\psi\ s\theta\ c\varphi \\ -s\theta & c\theta\ s\varphi & c\theta\ c\varphi \end{bmatrix} \tag{2-3}$$

The linear velocity in E-Frame is concluded according to the rotation of the linear velocity vector in B-Frame by the rotation matrix R_θ.

$$\boldsymbol{V^E} = \dot{\boldsymbol{\tau}}^E = R_\theta.\boldsymbol{V^B} \tag{2-4}$$

Where linear velocity is defined as:

$$\boldsymbol{V^B} = \begin{bmatrix} u & v & \omega \end{bmatrix}^T \tag{2-5}$$

The angular velocity in E-Frame is concluded according to the rotation of the angular velocity matrix in B-Frame by matrix Γ_θ (Transfer Matrix).

23

$$\omega^E = \dot{\theta}^E = \Gamma_\theta \cdot \omega^B \qquad (2\text{-}6)$$

Where angular velocity is defined as:

$$\omega^B = [p \quad q \quad r]^T \qquad (2\text{-}7)$$

Here, Γ_θ is given by:

$$\Gamma_\theta = \begin{bmatrix} 1 & 0 & -s\varphi \\ 0 & c\varphi & c\theta\, s\varphi \\ 0 & -s\varphi & c\theta\, c\varphi \end{bmatrix}^{-1} \qquad (2\text{-}8)$$

Particularly, the generalized velocity vector $\dot{\xi}$ in E-Frame is composed of conversion of generalized velocity vector $\boldsymbol{v}$ in B-Frame by means of generalized Matrix J_θ that is shown as equation (2-10). Accordingly, the equation (2-11) represents the expansion of (2-9).

$$\dot{\xi} = J_\theta\, \boldsymbol{v} \qquad (2\text{-}9)$$

$$J_\theta = \begin{bmatrix} R_{\theta\,3\times3} & 0_{3\times3} \\ 0_{3\times3} & \Gamma_{\theta\,3\times3} \end{bmatrix} \qquad (2\text{-}10)$$

$$\begin{bmatrix} \dot{\tau}^E \\ \dot{\theta}^E \end{bmatrix} = \begin{bmatrix} R_\theta & 0_{3\times3} \\ 0_{3\times3} & \Gamma_\theta \end{bmatrix} \begin{bmatrix} V^B \\ \omega^B \end{bmatrix} \qquad (2\text{-}11)$$

Therefore, the generalized velocity vector ($\boldsymbol{v}$) in the B-Frame includes quadrotor linear V^B [$m\ s^{-1}$] and angular ω^B[$rad\ s^{-1}$] velocity vectors which are written as the equation (2-12):

$$\boldsymbol{v} = [V^B \omega^B]^T = [\, u\ v\ w\ p\ q\ r\,]^T \qquad (2\text{-}12)$$

For evaluating the dynamic behavior of an object, its mass and moments of inertia in the conventional rotation axes should be determined. Hence the accumulated inertia, which is

described in the Appendix C, is used in the following formulation while there are some following assumptions which might simplify the inertia matrix.

1. The propellers are assumed rigid.
2. The structure is considered symmetric and fully rigid.
3. The B-frame base (O_B) is coincidentally assumed to be at the body center of mass.
4. The thrust and drag have remarkable variations in relation with the velocity changes which are illustrated in figures 2-4 and 2-5. Hence, in this study the drag and lift are experimentally measured and the details are given in chapter 4.
5. The vehicle mass is considered constant.

As initially all equations are described in the B-frame (f_B), in order to reduce the complexity in the acceleration terms, two assumptions provided below are considered:

a- The origin of the B-frame (f_B) O_B is coincident with the center of mass of the body. If the two points are not coincident, the body equations will become considerably complex.
b- The B-frame axes are assumed such that they coincide with the body principal axes of inertia where, the inertia matrix I is hence diagonal. The two assumptions will yield significantly less complicated formulations.

2-2-2 The Dynamic Model

Although the objective of the computation is to establish the kinematic laws of motion of the quadrotor, it is necessary to work through the dynamics equations. The dynamics in translation and rotation will reveal the laws of the acceleration along and about the three axes. The laws of the acceleration will be used to express velocity and displacement. In addition, the motion of the quadrotor will be related to the propulsion forces and drag forces which could be evaluated by observing the RPM of the individual motors. The second Newton-Euler's law is used in equations (2-13) and (2-18) to find the force vector $\boldsymbol{F}^E$ (N) and the torque vector $\boldsymbol{T}^E$ (Nm) [40, 36, 37].

$$m\ddot{\boldsymbol{r}}^{\,E} = \boldsymbol{F}^E \tag{2-13}$$

Where, $\ddot{\tau}^E (ms^{-2})$ is the linear acceleration of the quadrotor with respect to the E- frame and $m\ (kg)$ is the mass of the quadrotor.

This formulation (2-13) can be derived in the B-frame (f_B) as the equation (2-14) which is presented in detail in the Appendix D.

$$m \widehat{\dot{R_\theta\ V^B}} = R_\theta\ F^B \qquad \text{or} \qquad m\left(\dot{R_\theta}\ V^B + R_\theta \dot{V^B}\right) = R_\theta\ F^B \tag{2-14}$$

For expressing the equation (2-14) in more detail, the derivative of the rotation matrix $\dot{R_\theta}$ can be substituted by the equation (2-15) which is defined in the following paragraph.

Shiy U Zhao [41] presented the relationship of the derivative of the rotation matrix and the rotation matrix which the result is the equation (2-15) that can be substituted in the previous formula (2-14). The skew symmetric matrix $S(\omega)$ is defined when the given vector is in the general form of $k = [k_1 \quad k_2 \quad k_3]^T$ as shown in matrix (2-16) and in detail in the Appendix E. $[S(\omega)V = \omega \times V$ for any vector $V \in \mathbb{R}^3$, where $\times$ denote the vector cross-product]

$$\dot{R_\theta} = R_\theta\ S(\omega) \tag{2-15}$$

$$S(k) = \begin{bmatrix} 0 & -k_3 & k_2 \\ k_3 & 0 & -k_1 \\ -k_2 & k_1 & 0 \end{bmatrix} \tag{2-16}$$

After substitution, equation (2-14) is simplified and rewritten as equation (2-17):

$$mR_\theta\left(S(\omega)V^B + \dot{V^B}\right) = R_\theta\ F^B \qquad \text{or} \qquad m\omega^B V^B + m\dot{V^B} = F^B \tag{2-17}$$

In addition, the moment of forces by considering the Euler's second law is defined by the equation (2-18).

$$I\ddot{\theta}^E = T^E \tag{2-18}$$

In the equation (2-18), $I(Nms^2)$ is the body inertia matrix, $\ddot{\theta}^E$ $(rad\ s^{-2})$ is the angular acceleration vector by considering the E-frame.

The formula (2-18) can be derived in the B-frame (f_B) as the equation (2-19).

$$I \overline{\dot{R_\theta \omega}^B} = R_\theta \, \boldsymbol{T}^B \quad \text{or} \quad I(\dot{R}_\theta \omega^B + \dot{\omega}^B R_\theta) = R_\theta \, \boldsymbol{T}^B \tag{2-19}$$

The equation (2-19) can be simplified as the equation (2-20) by using the skew symmetric matrix (details in the Appendix E):

$$(\Gamma_\theta \, s(\omega)\omega^B + \dot{\omega}^B \Gamma_\theta) = \Gamma_\theta \, \boldsymbol{T}^B \quad \text{or} \quad I\omega^B \omega^B + I\dot{\omega}^B = \boldsymbol{T}^B \tag{2-20}$$

By combining the equations (2-17) and (2-20), the translational and rotational equations of motions of a 6 DOF rigid body are defined as follows (2-21):

$$\begin{bmatrix} mI_{3\times3} & 0_{3\times3} \\ 0_{3\times3} & I_{3\times3} \end{bmatrix} \begin{bmatrix} \dot{V}^B \\ \dot{\omega}^B \end{bmatrix} + \begin{bmatrix} \omega^B \times (mV^B) \\ \omega^B \times (I\omega^B) \end{bmatrix} = \begin{bmatrix} \boldsymbol{F}^B \\ \boldsymbol{T}^B \end{bmatrix} \tag{2-21}$$

In the above equation (2-21), the matrix $\begin{bmatrix} \dot{V}^B \\ \dot{\omega}^B \end{bmatrix}$ is the generalized acceleration vector ($\boldsymbol{v}$) which includes the linear acceleration vector ($\dot{V}^B$) and the angular acceleration vector ($\dot{\omega}^B$). Moreover, the matrix $\begin{bmatrix} \boldsymbol{F}^B \\ \boldsymbol{T}^B \end{bmatrix}$, is the generalized force vector ($\boldsymbol{Q}$) which contains the force vector ($\boldsymbol{F}^B$) and the torque vector ($\boldsymbol{T}^B$) and is expanded as the equation (2-22) and will describe further in this chapter.

$$\boldsymbol{Q} = [\boldsymbol{F}^B \quad \boldsymbol{T}^B]^T = [F_X \quad F_Y \quad F_Z \quad T_X \quad T_Y \quad T_Z]^T \tag{2-22}$$

By considering the two assumptions (a and b) in the paragraph (2-2-1), the equation (2-21) can be investigated in more details below while is rewritten as the equation (2-23).

$$M_B \dot{\boldsymbol{v}} + C_B(\boldsymbol{v})\boldsymbol{v} = \boldsymbol{Q} \qquad (2\text{-}23)$$

In the above equation, M_B represents the inertia matrix. This is constant and expressed as diagonal matrix. The expression of M_B is given in (2-24). The generalized acceleration vector ($\dot{\boldsymbol{v}}$) in the equation (2-23) is equal to $\begin{bmatrix} \dot{V}^B \\ \dot{\omega}^B \end{bmatrix}$ by considering the B-frame.

The Coriolis-centripetal matrix is shown as C_B in the equation (2-23) and is expanded as the equation (2-25) [42]. The Coriolis force is created by the effect of the Earth's rotation on the moving objects. It does not have notable influence on moving objects which moves slowly and travel short distances by comparing the size and rotation speed of the Earth. Therefore, there is no effect by this force on a small and low speed vehicle such as a drone. But this force is considered for fast-moving objects such as airplanes and rockets. Meanwhile, pilots must take the Earth's rotation into account when charting flights over long distances. So, the Coriolis force is not discussed in this study.

The next force which is represented in the matrix (2-25) is the centripetal or centrifugal force. This force effects on the objects with the rotating movements. For example, when the trajectory of the drone is defined as an acrobatic maneuvering like as a member of a group of drones (same as a flock of birds), the centripetal force would be considered. However, the trajectory of this quadrotor is not a rotating movement and it flies in the forward direction directly as it was explained in the first chapter. Therefore, the centripetal force is ignored in this study. Therefore, the equation (2-23) is rewritten as the equation (2-26).

$$M_B = \begin{bmatrix} m_{3\times3} & 0_{3\times3} \\ 0_{3\times3} & I_{3\times3} \end{bmatrix} = \begin{bmatrix} m & 0 & 0 & 0 & 0 & 0 \\ 0 & m & 0 & 0 & 0 & 0 \\ 0 & 0 & m & 0 & 0 & 0 \\ 0 & 0 & 0 & I_{XX} & 0 & 0 \\ 0 & 0 & 0 & 0 & I_{YY} & 0 \\ 0 & 0 & 0 & 0 & 0 & I_{ZZ} \end{bmatrix} \qquad (2\text{-}24)$$

$$C_B(v) = \begin{bmatrix} 0_{3\times3} & -m\,S(V^B) \\ 0_{3\times3} & -S(I\omega^B) \end{bmatrix} = \begin{bmatrix} 0 & 0 & 0 & 0 & m\omega & -mv \\ 0 & 0 & 0 & -m\omega & 0 & mu \\ 0 & 0 & 0 & mv & -mu & 0 \\ 0 & 0 & 0 & 0 & I_{ZZ}r & -I_{YY}q \\ 0 & 0 & 0 & -I_{ZZ}r & 0 & I_{XX}p \\ 0 & 0 & 0 & I_{YY}q & -I_{XX}p & 0 \end{bmatrix} \qquad (2\text{-}25)$$

$$M_B\dot{v} = Q \qquad (2\text{-}26)$$

The generalized force (Q) which is expressed in the equation (2-23), must be clarified in this step. It includes three components as follows:

1. The gravity force of the quadrotor $G_\theta\,(\xi)$, which is expanded in this chapter further.
2. The gyroscopic effect produced by the rotation of propellers $O_B(v)\Omega$, is explained as the equation (2-29).
3. The lift and drag forces and also torques which are directly produced by rotors motion, $U_B(\Omega)$ which is described in detail in the equation (2-35).

By contribution of the above three components of generalized force vector (Q), the equation (2-26) is rewritten as equation (2-27) :

$$M_B\dot{v} = G_\theta\,(\xi) + O_B(v)\Omega + U_B(\Omega) \qquad (2\text{-}27)$$

Due to the gravitational acceleration $g(ms^{-2})$, the first component on the right side of the equation (2-27) is the gravitational force which is defined as in (2-28). This force has components about Z axis on the fixed coordinate system and is considered only in the linear equations and not angular ones. With respect to the dynamic model which is expressed in the f_B (body frame), it is required to transfer the gravitational vector from f_E to f_B by multiplying the F_G^E by the inverse of the rotational matrix (R). In the equation (2-28), F_G^B is the gravitational force vector with respect to the body frame (f_B) and $0_{(3,1)}$ is a vertical vector with three zeros.

$$G_\theta(\xi) = \begin{bmatrix} F_G^B \\ 0_{(3,1)} \end{bmatrix} = \begin{bmatrix} R_\theta^{-1} F_G^E \\ 0_{(3,1)} \end{bmatrix} = \begin{bmatrix} R_\theta^T \begin{bmatrix} 0 \\ 0 \\ -mg \end{bmatrix} \\ 0_{(3,1)} \end{bmatrix} = \begin{bmatrix} mg\, s\theta \\ -mg\, c\theta\, s\varphi \\ -mg\, c\theta\, s\varphi \\ 0 \\ 0 \\ 0 \end{bmatrix} \qquad (2\text{-}28)$$

The rotations of two propellers spinning same direction induce gyroscopic moments that are compensated by counter-rotation of the other two. The algebraic summation of all propellers speeds should be zero to avoid the quadrotor overall misbalance. The axes of all four propellers (spin axes) are parallel to the Z axis. Additionally, when the pitch and roll rates are different from zero, the platform is subjected to the gyroscopic moment (the second component in the right hand side of equation (2-27)) according to the equation (2-29).

$$O_B(\boldsymbol{v})\boldsymbol{\Omega} = \begin{bmatrix} 0_{(3\times1)} \\ -\sum_{k=1}^{4} J_{TP}\left(\boldsymbol{\omega}^B \times \begin{bmatrix} 0 \\ 0 \\ 1 \end{bmatrix}\right)(-1)^k \, \boldsymbol{\Omega}_k \end{bmatrix} = \qquad (2\text{-}29)$$

$$\begin{bmatrix} \mathbf{0}_{(3\times1)} \\ J_{TP}\begin{bmatrix} -q \\ p \\ 0 \end{bmatrix} \boldsymbol{\Omega} \end{bmatrix} = J_{TP} \begin{bmatrix} 0 & 0 & 0 & 0 \\ 0 & 0 & 0 & 0 \\ 0 & 0 & 0 & 0 \\ q & -q & q & -q \\ -p & p & -p & p \\ 0 & 0 & 0 & 0 \end{bmatrix} \boldsymbol{\Omega} =$$

$$J_{TP} \begin{bmatrix} 0 & 0 & 0 & 0 \\ 0 & 0 & 0 & 0 \\ 0 & 0 & 0 & 0 \\ q & -q & q & -q \\ -p & p & -p & p \\ 0 & 0 & 0 & 0 \end{bmatrix} \begin{bmatrix} \Omega_1 \\ \Omega_2 \\ \Omega_3 \\ \Omega_4 \end{bmatrix} = J_{TP} \begin{bmatrix} 0 \\ 0 \\ 0 \\ -q\Omega \\ p\Omega \\ 0 \end{bmatrix}$$

The moment matrix of the propellers is given as $O_B(\boldsymbol{v})$. The total rotational moment of inertia about the propeller axis $J_{TP}(Nms^2)$ is further discussed. The following equation (2-30), expresses the total speed of the propellers $\boldsymbol{\Omega}\,(rad/s)$ which has been used in the previous equation (2-29). Where $\Omega_1(rad/s)$ is the front rotational propeller speed, $\Omega_2(rad/s)$ is the right rotational propeller speed, $\Omega_3(rad/s)$ is the rear rotational propeller speed and $\Omega_4[rad\,s^{-1}]$ is the left rotational propeller speed.

$$\boldsymbol{\Omega} = \begin{bmatrix} \Omega_1 \\ \Omega_2 \\ \Omega_3 \\ \Omega_4 \end{bmatrix} \tag{2-30}$$
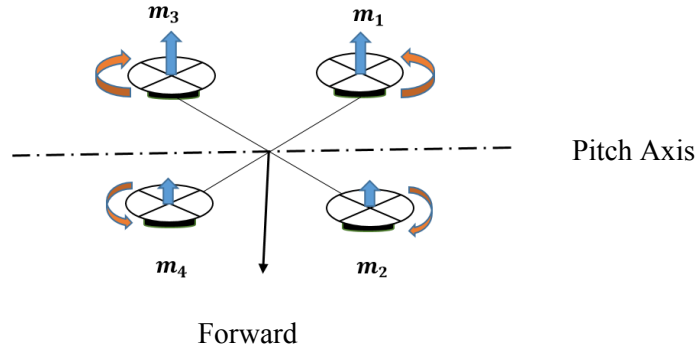
Fig 2-10: Symmetric structure of the quadrotor when is tilting about Y axis

The gyroscopic moment is proportional to the RPM. If the quadrotor performs a tilting, the orientation should be with regards to an axis that divides the quadrotor in two symmetric structure. Thus, the orientation of the vehicle towards the front direction should be along this axis as illustrated in the figure 2-10.

The last component of the generalized force vector (Q) which includes the forces and the torques are directly produced by the rotor spins. These forces and torques are explained in the following paragraphs. They concluded of a unique matrix as the motion matrix (E_B) which is multiplied by the square of the propeller rotational speed. So, the result is the motion vector $\boldsymbol{U_B}(\boldsymbol{\Omega})$ that is expanded in the equation (2-34).

Given that there are of no propeller in the direction X and Y, there is no propeller created force in those directions. It is illustrated in the motion vector $\boldsymbol{U_B}(\Omega)$ that all four elements of the first and second raw in the matrix are zero. Hence, in the Z direction there are four rotors and for all three Euler-angles, there are momentum to induce motion in φ, θ, ψ angles.

Each motor has a net torque that applies to the rotor shaft. This torque results in the thrust force T_i which is derived in the equation (2-31).

$$T_i = \frac{1}{2} \, b \, \rho A \, \Omega_i^2 \tag{2-31}$$

Generally, there are two types of drag force for a quadcopter in different flight statuses. When the vehicle is flying in the forward direction there would be a drag force in the opposite direction of its travel which is generated by the movement of the whole body through the air. This drag force is proportional to the drone forward speed as it is described in section 2-2-1. The second drag force is generated by the propellers rotation in the air. This force is proportional to the rotational speed of the propellers.

Therefore, the both thrust and drag forces are proportional to the square of the propellers rotational speed which are shown in the equations (2-32) and (2-33) in a simplified manner for each propeller.

$$T_i = b\Omega_i^2 \tag{2-32}$$

$$D_i = d\Omega_i^2 \tag{2-33}$$

Where in the equation (2-32), T $[N]$ represents thrust force, i the number of motor, b the thrust coefficient which is dimensionless and Ω $[rad \, s^{-1}]$ the rotational speed.

In the equation (2-33), D_P $[N]$ represents propeller drag force, i the number of motor, d the drag coefficient which is dimensionless and $\mathbf{\Omega}$ $[rad \, s^{-1}]$ the rotational speed.

All drag, lift and thrust coefficient are dimensionless. However, they are important for calculation of force on the quadrotor and directly depends on the velocity. All the aerodynamics contributions are explained and derived in detail in the Appendix F.

Then, by multiplication of the square of the rotation speed $\mathbf{\Omega^2}$ $[rad^2 \, s^{-2}]$ to the motion matrix (E_B), the motion vector $\mathbf{U_B(\Omega)}$ is resulted, equation (2-34).

$$U_B(\Omega) = E_B\Omega^2 = \begin{bmatrix} U_1 \\ U_2 \\ U_3 \\ U_4 \\ U_5 \\ U_6 \end{bmatrix} = \begin{bmatrix} 0 & 0 & 0 & 0 \\ 0 & 0 & 0 & 0 \\ b & b & b & b \\ 0 & -bl & 0 & bl \\ -bl & 0 & bl & 0 \\ -d & d & -d & d \end{bmatrix} \begin{bmatrix} \Omega_1^2 \\ \Omega_2^2 \\ \Omega_3^2 \\ \Omega_4^2 \end{bmatrix} =$$ (2-34)

$$\begin{bmatrix} 0 \\ 0 \\ b(\Omega_1^2 + \Omega_2^2 + \Omega_3^2 + \Omega_4^2) \\ bl(\Omega_4^2 - \Omega_2^2) \\ bl(\Omega_3^2 - \Omega_1^2) \\ d(\Omega_2^2 + \Omega_4^2 - \Omega_1^2 - \Omega_3^2) \end{bmatrix}$$

In the equation (2-34), $l(m)$ is the distance from the center of the propeller to the center of the vehicle, b is the thrust coefficient and d is the drag coefficient. $U_1, ..., U_4$, are the motion vector components which are related to each propeller. $\Omega_1, ..., \Omega_4$ are the propellers' speed.

In accordance with the effectiveness of each motor in each direction, the resultant thrust or drag forces of each direction are different. These forces are concluded of the rotation of propellers by servomotors. So, the propellers drag and thrust are both given by the RPM of the rotors. The motors RPM are controlled through their applied DC voltage. Moreover, the motion matrix (E_B) as a constant matrix is expanded in the equation (2-35) which is used in the equation (2-34).

$$E_{B\,(6\times4)} = \begin{bmatrix} 0 & 0 & 0 & 0 \\ 0 & 0 & 0 & 0 \\ b & b & b & b \\ 0 & -bl & 0 & bl \\ -bl & 0 & bl & 0 \\ -d & d & -d & d \end{bmatrix}$$ (2-35)

In this step, all the forces use in the formulation of the generalized force equation (2-27) are defined. By rewriting this equation to the equation (2-36), the generalized acceleration vector ($\dot{v}$) in relation to the B-frame (f_B) is extracted.

$$\dot{\boldsymbol{v}} = \frac{\boldsymbol{G}_\theta\left(\boldsymbol{\xi}\right) + O_B(\boldsymbol{v})\boldsymbol{\Omega} + E_B\boldsymbol{\Omega}^2}{M_B} \tag{2-36}$$

To show all the components of the generalized acceleration vector ($\dot{\boldsymbol{v}}$) can be written as six equations for the six degrees of freedom of the vehicle. Therefore, by using all previous equations, the equation (2-36) is rewritten as the equation (2-37) in six sub equations for each element of the generalized acceleration vector (derivative of the generalized velocity vector, equation (2-12)) with respect to the B-frame.

$$\dot{\boldsymbol{v}} = \begin{cases} \dot{u} = g\ s\theta \\ \dot{v} = -g\ c\theta s\varphi \\ \dot{w} = -g\ c\theta s\varphi + \dfrac{U_3}{m} \\ \dot{p} = \dfrac{J_{TP}}{I_{XX}}q\Omega + \dfrac{U_4}{I_{XX}} \\ \dot{q} = \dfrac{J_{TP}}{I_{YY}}p\Omega + \dfrac{U_5}{I_{YY}} \\ \dot{r} = \dfrac{U_6}{I_{ZZ}} \end{cases} \tag{2-37}$$

All four defined forces are used in the above equation. For example for the first sub equation that are expressed the first element of the acceleration vector ($\dot{u}$), the following related forces are considered.

The first force of interest is the gravitational force which is expressed in the equation (2-28) for all six equations of motion. As it was explained, there is no gravitational force for the angular equations (last three ones). However, the first equation is expressed as ($mg\ s\theta$) and is divided by the mass (m). Hence, it is written as ($g\ s\theta$) where, s and c expressed sin and cosine, respectively. The next phenomenon of interest is the gyroscopic couple. This force is shown in the equation (2-29). It was detailed that this force is not applicable to the linear equations of motion (the first three ones). Hence, there is no gyroscopic force to appear in the first equation ($\dot{u}$). However, for the angular equations, by considering the equation (2-29), this force appears in the last three sub equations of the equation (2-37). The last effects are given by the drag and thrust forces (motion force vector) which are provided by each motor, while there is no

motion force in the first linear equation. These forces are specified as the equation (2-34) and are written as the last element of each sub equations (2-37).

All parameters of the equations (2-37) are written in the B-frame. However, the dynamic equations in E-frame makes the control purposes more practical. So, it is better to write the dynamic equations in the E-frame. For this transformation, the linear and angular accelerations are considered separately. It is clear that due to no movement assumption in hover condition, the transfer matrix Γ_θ is assumed as the identity matrix $I_{3\times3}$. Therefore, the equation (2-6) is rewritten as the equation (2-38) which the angular velocity in the E-frame is equal to the angular velocity in the B-frame. So, there is no difference between the angular acceleration in the B-frame and the E-frame. Then by assuming $\Gamma_\theta = I_{3\times3}$, the equation (2-10) is rewritten as the given equation (2-39).

$$\omega^E = \omega^B = \dot{\theta}^{\ E} \tag{2-38}$$

$$\begin{bmatrix} \dot{\tau}^E \\ \dot{\theta}^E \end{bmatrix} = \begin{bmatrix} R_{\theta\ 3\times3} & 0_{3\times3} \\ 0_{3\times3} & I_{3\times3} \end{bmatrix} \begin{bmatrix} V^B \\ \omega^B \end{bmatrix} \tag{2-39}$$

By considering the above equation (2-39), all the angular equations of the equation (2-37) include no changes when are transferring to the E-frame. While, the linear equations are multiplied by rotational matrix ($R_{\theta\ 3\times3}$) to result in the equations of the E-frame. Therefore, the generalized velocity vector ($\dot{\xi}$) is expressed as the equation (2-40) and the equation (2-36) is changed to the equation (2-41) by considering the frames transformation from f_B to f_E.

$$\dot{\xi} = \begin{bmatrix} \dot{\tau}^E \\ \omega^B \end{bmatrix} = \begin{bmatrix} \dot{X} \\ \dot{Y} \\ \dot{Z} \\ p \\ q \\ r \end{bmatrix} \tag{2-40}$$

$$\dot{v} = \frac{G(\xi) + O(\xi)\Omega + U(\Omega)}{M} \tag{2-41}$$

The inertia matrix in the E-frame is same as the B-frame, equation (2-42).

$$M = M_B = \begin{bmatrix} mI_{3\times3} & 0_{3\times3} \\ 0_{3\times3} & I_{3\times3} \end{bmatrix} = \begin{bmatrix} m & 0 & 0 & 0 & 0 & 0 \\ 0 & m & 0 & 0 & 0 & 0 \\ 0 & 0 & m & 0 & 0 & 0 \\ 0 & 0 & 0 & I_{XX} & 0 & 0 \\ 0 & 0 & 0 & 0 & I_{YY} & 0 \\ 0 & 0 & 0 & 0 & 0 & I_{ZZ} \end{bmatrix} \tag{2-42}$$

The gravitational force vector is rearranged to the equation (2-43) which is expressed as the gravitational force in the E-frame as there are only linear terms in this force.

$$G(\xi) = \begin{bmatrix} F_G^E \\ 0_{3,1} \end{bmatrix} = \begin{bmatrix} 0 \\ 0 \\ -mg \\ 0 \\ 0 \\ 0 \end{bmatrix} \tag{2-43}$$

The final gyroscopic force (2-44) is the same as the gyroscopic force in the B-frame (2-29).

$$O(\xi)\Omega = O_B(v)\Omega = \begin{bmatrix} 0_{(3\times1)} \\ -\sum_{k=1}^{4} J_{TP}\left(\omega^B \times \begin{bmatrix} 0 \\ 0 \\ 1 \end{bmatrix} \right)(-1)^k \, \Omega_k \end{bmatrix} \tag{2-44}$$

$$= \begin{bmatrix} 0_{(3\times1)} \\ J_{TP} \begin{bmatrix} -q \\ p \\ 0 \end{bmatrix} \Omega \end{bmatrix} = J_{TP} \begin{bmatrix} 0 \\ 0 \\ 0 \\ -q\Omega \\ p\Omega \\ 0 \end{bmatrix}$$

The last force, motion force vector $U(\Omega)$ includes both linear and angular terms. So, in case of linear terms the (U_1, U_2, U_3 in the equation (2-34)) are multiplied by the rotation matrix ($R_{\theta\,3\times3}$) to be transferred to the E-frame by considering the equation (2-39). In addition, the angular terms (U_4, U_5, U_6 in the equation (2-34)) do not make any changes. Therefore, the extracted motion force vector by considering both linear and angular elements is written in the equation (2-45).

$$U(\Omega) = \begin{bmatrix} R_{\theta\,3\times3} & 0_{3\times3} \\ 0_{3\times3} & I_{3\times3} \end{bmatrix} U_B(\Omega) = \begin{bmatrix} R_{\theta\,3\times3} & 0_{3\times3} \\ 0_{3\times3} & I_{3\times3} \end{bmatrix} E_B \Omega^2$$

(2-45)

$$= \begin{bmatrix} (c\varphi s\theta c\psi + s\varphi s\varphi)U_3 \\ (c\varphi s\theta s\psi - s\varphi c\psi)U_3 \\ (c\varphi c\theta)U_3 \\ U_4 \\ U_5 \\ U_6 \end{bmatrix}$$

Hence by using all the explained forces (equations (2-43), (2-44) and (2-45)) in the E-fame, the equation (2-37) can be rewritten as the equation (2-46).

(2-46)

$$\dot{\xi} = \begin{cases} \ddot{x} = (C\varphi\,S\theta\,C\psi + S\varphi\,S\psi)\dfrac{U_3}{m} \\[2mm] \ddot{y} = (C\varphi\,S\theta\,S\psi - S\varphi\,C\psi)\dfrac{U_3}{m} \\[2mm] \ddot{z} = -g + (C\varphi\,C\theta)\dfrac{U_3}{m} \\[2mm] \ddot{\varphi} = \dfrac{J_{TP}}{I_{XX}}(\Omega_T)\dot{\theta} + \dfrac{U_4}{I_{XX}} \\[2mm] \ddot{\theta} = \dfrac{J_{TP}}{I_{YY}}(\Omega_T)\dot{\varphi} + \dfrac{U_5}{I_{YY}} \\[2mm] \ddot{\psi} = \dfrac{U_6}{I_{ZZ}} \end{cases}$$

2-3 The Actuation (The DC Motor)

Once the equations of motion have been expressed, the interest of the investigation goes towards the actuation of the rotors. The scheme of actuation will produce any desired motion. However, the motions will be affected by constraints which are related to the performances of the actuators. This sub-chapter deals with these aspects.

The Kirchhoff's second law indicates that all the lost energy through the resistances is equal to the electrical energy charge in a closed loop circuit. This statement is another way that is expressed the conservation of the energy. The DC motor circuit in the figure (2-11) contains the resistor R (Ω), the electric inductance L (H), the voltage source v (V), and the potential generator $e(V)$. It demonstrates the Kirchhoff's second law by considering the equation (2-47).
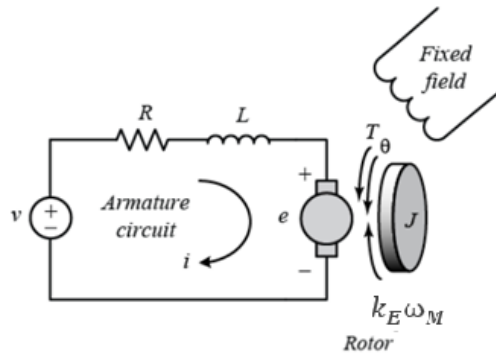
Fig 2-11: DC motor circuit

$$v = v_R + v_L + e \tag{2-47}$$

where $v_R(V)$ is the difference of potential on the resistor (R) and $v_L(V)$ is the potential difference on the inductance L. This equation (2-47) can be rewritten as the equation (2-48).

$$v = R\,i + L\,\frac{d_i}{d_t} + K_E\,\omega_M \qquad\qquad (2\text{-}48)$$

Where, i (A) is the current in the motor, K_E $(V\,s\,rad^{-1})$ is the motor torque constant and $\omega_M (rad\,s^{-1})$ is the motor angular speed. In the above equation, Ri is substituted by v_R and the inductance differential equation $v_L = L\,\frac{\partial_i}{\partial_t}$ is used for the second term in the equation (2-47).

The inductor effects can be neglected in the equation (2-48) and be rewritten as the equation (2-49) in order to the following three reasons:

- In robotics, most of the servo-motors (mostly miniature servomotors) show small inductance because of the construction optimization.
- Solving the first order differential equation is easier than solving a second order differential equation.
- The inductor is formed by two parts: the electrical part and the mechanical part. The response of the electrical part is much faster than the response of the mechanical part. For the overall system the slowest speed contribution is assumed only.

$$v = R\,i + K_E\,\omega_M \qquad\qquad (2\text{-}49)$$

Moreover, by considering $J_{TM}(N\,m\,s^2)$ as the total motor mass moment of inertia, $\dot{\omega}_M\,(rad\,s^{-2})$ the motor angular acceleration, $T_M(N\,m)$ the motor torque, $T_L(N\,m)$ the load torque (figure 2-12) and the use of the Newton second law, the equation (2-50) can be used to describe the dynamics of the motor. The equation shows that when the motor torque and the load torque are not equal, there is an acceleration or deceleration of the motor angular speed ω_M . The changes in the speed is related to the total motor moment of inertia J_{TM}. It means, when the J_{TM} value is smaller, the acceleration will be higher [36].

$$J_{TM}\dot{\omega}_M = T_M - T_L \qquad\qquad (2\text{-}50)$$
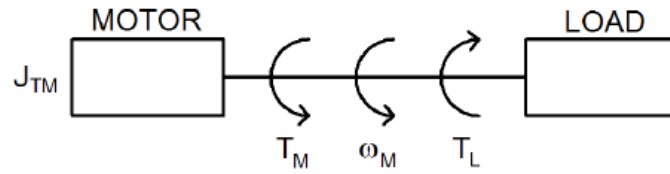
Fig 2-12: The motor and load system in a general configuration

In addition, there is a linear relation between the motor torque T_M and the electrical current i which is related to $K_M (N\ m\ A^{-1})$: $T_M = K_M\ i$. Therefore, equation (2-51) is written instead of equation (2-50).

$$J_{TM}\ \dot\omega_M = K_M\ i - T_L \tag{2-51}$$

From the equation (2-49) the current i can be expressed as the equation (2-52). Then by substituting the equation (2-52) in the equation (2-51), the equation (2-53) is:

$$i = \frac{v - K_E\ \omega_M}{R} \tag{2-52}$$

$$J_{TM}\dot\omega_M = \frac{K_M}{R} v - \frac{K_M K_E}{R}\omega_M - T_L \tag{2-53}$$

In motors with high RPM, a gear set for the RPM reduction of each motor must be considered as high RPM would lead to the reduction in lift performance of the propellers. The gear set reduces the speed of the propellers versus the motors speed, $\frac{\omega_M}{\omega_P}$. Some energy is lost by friction in the gear set. For example, there is another factor in relation with the gear set which is gear

conversion efficiency η and which connects the mechanical power of the motor axis P_M to the power at the propeller axis, P_P $(N\ m\ s^{-1})$.

The efficiency is included in the equation (2-54). The mechanical power in the motor axis P_M is equal to the multiplication of the motor angular speed ω_M $(rad\ s^{-1})$ by the propeller torque $T_{P_M}(N\ m)$ in the same direction (the motor axis). In addition, the mechanical power in the propeller axis P_P is the multiplication of the propeller angular speed ω_P $(rad\ s^{-1})$ by the motor torque $T_{M_P}(N\ m)$ in the same direction (the propeller axis).

$$P_M\ \eta = \ P_P \qquad\qquad \text{or} \qquad\qquad \omega_M T_{P_M}\ \eta = \ \omega_P T_{M_P} \qquad\qquad (2\text{-}54)$$

The equation (2-51) is expanded to the equations (2-55) and (2-56) for the motor and propeller respectively. Here, $J_M(N\ m\ s^2)$ is the rotor moment of inertia about the motor axis, $J_P(N\ m\ s^2)$ the rotor moment of inertia about the propeller axis, $\dot{\omega}_P(rad\ s^{-2})$ the propeller angular acceleration, $T_P(N\ m)$ the propeller torque.

Hence, the dynamics of the gear system can be expressed as it follows:

$$J_M \dot{\omega}_M = T_M\ - T_{PM} \qquad\qquad (2\text{-}55)$$

$$J_P \dot{\omega}_P = T_{MP}\ - T_P \qquad\qquad (2\text{-}56)$$

Therefore, equation (2-54) can be rewritten in (2-57) by substituting the equations (2-55) and (2-56) as follows:

$$\omega_M(T_M - J_M \dot{\omega}_M)\ \eta = \ \omega_P(T_P + J_P \dot{\omega}_P) \qquad\qquad (2\text{-}57)$$

$$(J_M + \frac{J_P}{\eta\ N^2})\ \omega_M = T_M - \frac{T_P}{\eta\ N} \qquad\qquad (2\text{-}58)$$

The above formulation (2-58) is resulted by substituting ω_P with $\frac{\omega_P}{\omega_M}\dot{\omega}_M$ and N with $\frac{\omega_M}{\omega_P}$ in the equation (2-57).

The structure of the equation (2-58) and (2-50) are the same. Hence, by comparing these two equations, the values of T_L and J_{TM} are expressed as below:

$$T_L = \frac{T_P}{\eta\,N} \tag{2-59}$$

$$J_{TM} = J_M + \frac{J_P}{\eta\,N^2} \tag{2-60}$$

Moreover by using aerodynamic calculation and considering $d\ [N\ m\ s^2]$ as the aerodynamic drag factor, the propeller torque is defined as equation (2-61).

$$T_P = d\,\omega_P^2 = \frac{d\,\omega_M^2}{N^2} \tag{2-61}$$

Then equation (2-59) is rewritten as the equation (2-62) by substitution of the equation (2-61) to express the final load torque T_L.

$$T_L = \frac{d\,\omega_M^2}{\eta\,N^3} \tag{2-62}$$

In accordance with the equations (2-60) and (2-62), the equation (2-53) can be rewritten as equation (2-63) which is related to the motor system. Therefore, by using $N = \frac{\omega_M}{\omega_P}$ reformulating this equation (2-63), the equation of the propeller system can be written as equation (2-64).

$$\left(J_M + \frac{J_P}{\eta\,N^2}\right)\dot{\omega}_M = -\frac{K_M K_E}{R}\omega_M + \frac{K_M}{R}v - \frac{d\omega_M^2}{\eta\,N^3} \tag{2-63}$$

$$\left(J_P + \eta\,N^2 J_M\right)\dot{\omega}_P = -\frac{K_M K_E}{R}\eta\,N^2\omega_P + \frac{K_M}{R}\eta\,N\,v - d\omega_P^2 \tag{2-64}$$

By considering the Newton second law, the total rotational moment of inertia around the propeller axis $J_{TP}[N\,m\,s^2]$ is extracted from the equation (2-64) as the equation (2-65).

$$J_{TP} = J_P + \eta\,N^2 J_M \tag{2-65}$$

By substituting the $\frac{K_M K_E}{R\,J_{TP}}\,\eta\,N^2$ with $\frac{1}{r}$, the equation (2-65) is rewritten as the equation (2-66).

$$\dot{\omega}_P = -\frac{1}{r}\omega_P + \frac{1}{N\,r\,K_E}v - \frac{d\omega_P^2}{J_{TP}} \tag{2-66}$$

The following equation (2-67) represents the above non-linear equation (2-66) in a simple form by using the first order Taylor series method.

$$\dot{\omega}_P = A_P\omega_P + B_P\,v + C_P \tag{2-67}$$

Where, $A_P\,[rad\,s^{-1}]$ is the linearized propeller's speed coefficient, $B_P\,[rad^2s^{-2}V^{-1}]$ is the linearized input voltage coefficient and $C_P\,[rad^2s^{-2}]$ is the linearized constant coefficient. The value of these coefficients are obtained by using the equations (2-68), (2-69) and (2-70).

$$A_P = \left.\frac{\partial \dot{\omega}_P}{\partial \omega_P}\right|_{\omega_P = \omega_H} = -\frac{K_E K_M \eta N^2}{J_{TP} R} - \frac{2\,d}{J_{TP}} \omega_H \tag{2-68}$$

$$B_P = \left.\frac{\partial \dot{\omega}_P}{\partial v}\right|_{\omega_P = \omega_H} = \frac{K_M \eta N}{J_{TP} R} \tag{2-69}$$

$$C_P = \left. \left(\dot{\omega}_P - (A_P \omega_P + B_P v) \right) \right|_{\omega_P = \omega_H} = \frac{d}{J_{TP}} \omega_H^2 \tag{2-70}$$

Therefore, by using the three above equations, the dynamics of all four motors can be described.

2-4 The Center of Gravity (CG)

Basically, there are few aspects to be considered in relation with the airborne system design. Three important physical aspects are considered in this work, namely, weight, center of gravity position and moment of inertia. It is obvious that weight is a simple problem however it is crucial for calculating the thrust and evaluating the payload in conjunction with the performance of the vehicle. There are different methodologies to evaluate the mass of a drone [43]. The other major issue in designing an aircraft is the positioning of the center of gravity. An accurate evaluation of the center of gravity will require balance of the equation under static condition. Without static balance, the control of vehicle would not be achievable or may result in lots of energy being consumed. For instance, during the flight of a statically imbalanced vehicle, the propulsion will tend to compensate that unevenness by pulling the tendency of the vehicle to reduce the move in the opposite direction (compensation). This reaction will lead to higher energy consumption and time delays. Moreover, the higher required RPM on the servomotor that is assigned to compensate the imbalance will be below the threshold of the thrust which pushes down all the performance of all other servos. Although it takes time to design a vehicle statically balanced, it is the starting step of a suitable design. Therefore, the evaluation of the center of gravity (CG) position represents one of the basic requirement for designing a drone in this thesis. The CG position should coincide with the center of symmetry.

There are various methods to evaluate the position of the center of gravity [43]. The moment which is created by all masses about the three coordinate axes is zero in a specific point in space. This specific point is called the center of gravity. Though, the determination of the CG of a physically un-built system is rather a complex task. Actually, the components in the drone are positioned such that the CG coincides with the intersection of the two axes connecting the axes of the opposite motors (rotors). It is essential to have the CG located as much as possible into the center of symmetry. Also there is no mass variation in a quadrotor which needs to be compensated by the DC motors. This feature is not applicable to other UAVs that use fuel instead of electric batteries as the source of energy.

When a strongly irregular object is the subject of the evaluation, the weights can comprise of small homogenous entities. Analytics is then used to incorporate the result of these weights and

the differential partitions. The 3D configuration associated with the lack of homogeneity rise the complexity of the performance.

The center of gravity position for regularly shaped objects, such as circles, squares, spheres, and cubes, are at their geometric centers. In case of other configurations, either experimental method or analytical method are used. The experimental determination of center of gravity position is more effortless than the calculation. For suspended objects which can move freely, the position of the center of gravity is always directly beneath the suspension point.

In experimental work, the center of gravity is attained by hanging the object from several points and finding the line of intersection of the extended lines. A feasible line is used to record the vertical direction. The point at which two or more vertical lines are intersected from the feasible line is the CG of the object. For more clarification, a non-symmetric object is selected in figure 2-13 to show the center of gravity position by hanging on the object [44].

Step 1   Step 2
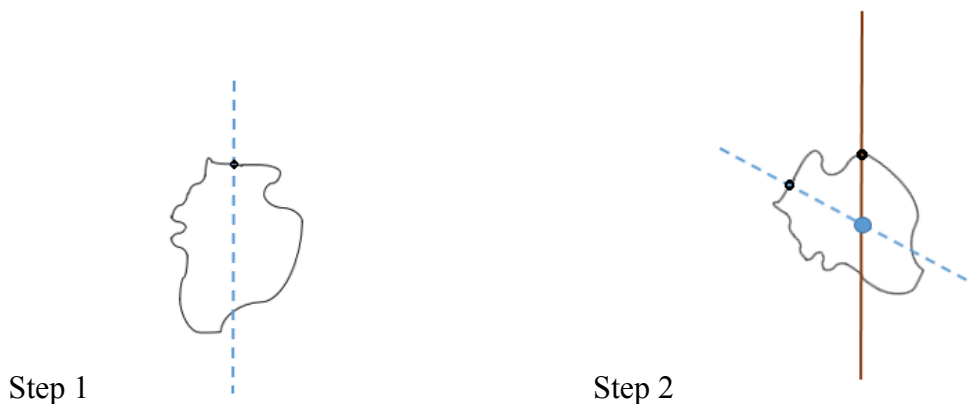
Fig 2-13: A non-symmetric object center of gravity position is specified in two steps by hanging on the object from different suspension points.

For all airborne vehicles, the center of gravity is measured in two planes, the vertical and the lateral planes. This experiment has been done for a quadrotor in both planes and its pictures are figures 2-14 and 2-15.

In the first step, the vehicle is attached to a string in the vertical plane and by using a vertical extension line to the sting. The first vertical line is recorded, figure 2-13(a).

The next step consists of attaching the quad by another arm and perform same operation process through extending the wire line and obtaining another vertical line as illustrated in, figure 2-13(b).

Finally, by intersecting these two figures 2-13(a) and 2-13(b) within the vertical plane, the intersection point of these two line represents the center of gravity of this vehicle in figure 2-13(c). The position of the CG is located in the center point (symmetric point) of the vertical plane of the vehicle in our case.

For the lateral CG, the vehicle must be attached on same plane where the vertical CG is located. Hence, the way to find the lateral CG is the same as the vertical CG, except the location of the plane of suspension. The three following pictures show the steps of the finding the lateral CG for the quadrotor illustrated in figure 2-14.

a. Recording first vertical line   b. Recording second vertical line   c. Correspondence of two lines

Fig 2-14: Method of finding the position of vertical CG in three steps by hanging on the quadcopter and recording the feasible lines

a. Recording 1st vertical line   b. Recording 2nd vertical line   c. Correspondence of two lines

Fig 2-15: Illustration of finding the position of lateral CG in three steps by hanging on the quadcopter and recording the feasible lines

By comparing figures 2-14(a) and 2-14(b) for the lateral plane, the intersection of both lines, the CG would be located in the center point of the lateral plane which shows the real position of the center of mass of the vehicle (figure 2-14(c)).

Quadcopter is built as a symmetric vehicle. Thus, the center of gravity position must be in the center point of the vehicle in each plane. If the quadrotor center of gravity position would not be at the point of the quadrotor center of symmetry, controlling the vehicle would be hard. Moreover, whenever the vehicle is not level in flight, it cannot properly fly to perform its mission.

Therefore, the center of gravity position for this quadrotor is located in the symmetric point of the body in the both planes (vertical and lateral). If the center of gravity position moves by making change in the configuration or location of different parts, an imbalance might happen and it needs to compensated by applying more loads on some motors. This more loads will lead to momentum imbalance and the vehicle would be out of control. Therefore, the correspondence of CG position and symmetric point of the drone is crucial to be able to fly. If the drone changes to the six-motor type with two extra rotors in lateral plane, another consideration must be taken to reach the drone center of gravity position. This is another step which is described in the following chapter.

CHAPTER 3

A Solution to Enhance the Forward Displacement Performance of a Quadrotor

UAVs have been used for many applications that includes inspection, condition assessment, transportation and delivery. Their mission may consist of periods of forward displacement as well as accurate and steady positioning in the space. The way the drone is conceived enables all the above. However, if one of the performances needs to be improved, some constructive modification to the present configuration of a quadrotor might be considered. In this chapter, a potential solution to enhance the front displacement performance of a quadrotor is discussed.

3-1 Basic Concepts

Basically, for getting higher speed in direct flight and shortening the flight time in different missions, a fifth propeller is suggested. Generally, it must be installed below the vehicle for more stability and less drag force generation. Therefore, there are two possibilities for installing the fifth motor, in the front or rear of the drone. By installing the fifth motor in forward direction of the vehicle as like as figure 3-1, it would obstruct the vision of the front camera. Moreover, the vehicle would yield nose-down due to additional weight in front of the vehicle. Then, the nose down yield will lead to the directional instability. However, the front installation of the fifth motor will cause the balanced thrust. Therefore, it would result in the stability in the motions of the vehicle in comparison with the rear installation of the fifth motor. In the rear installation of the fifth motor, the thrust would be produced in the forward direction to push forward the drone

as well. Therefore, there would be instability in the motions of the drone. Hence, it is better to choose the front installation of the additional motor and using a longer pod for the camera mounting. Then, there would not be any obstruction of the camera vision.

Totally, there is more energy consumption by adding one motor to the standard quadrotor. Meanwhile, fast movement in the forward flight can compensate this consumption. Moreover, this solution might provide more stability to the vehicle. Although, there are some mechanical complexities and weight problems the possibility of producing more thrust in the forward direction might compensate these drawbacks.

In the mathematical formulation of such a configuration, some of the quadrotor equations will be affected by adding the fifth rotor. Totally, all the former four rotors are in the same location and status in comparison with the quadrotor. By adding the fifth rotor in the X direction of the vehicle, some unbalance may appear which translate into the difficulties in attitude stability. Two major forces that create unbalance are the gyroscopic force and the momentum of the fifth rotor. In fact, the gyroscopic momentum, which is produced by the fifth rotor, may lead to the roll the drone. This phenomenon creates disturbance in the vehicle attitude and balance. It is clear that the drone cannot carry out any stable flight under such conditions. Moreover, in the five-rotor drone, there is an odd number of rotors and the fifth one creates a momentum that cannot be compensated by the other rotors momentum. There is an extra RPM, however in lateral plane but it is the only rotor in that plane and its action might not be easy to compensate from the other four rotors in the horizontal plane. The imbalanced issue can be corrected by using more energy and RPM from other four motors to recover the intended attitude and motion. Then those four motors tolerate some more loads in the whole process of the flight and significant loss of efficiency might be encountered. Meanwhile, the planned mission might not be completed. This momentum can be neutralized by introducing another rotor, which spins in the opposite direction. There are some options to neutralize the fifth rotor momentum. Two of them are discussed in the following.

Firstly, using counter-rotating propellers instead of the fifth rotor is quite useful. These propellers must be concentric and counter-rotating which are actuated by one motor, the fifth motor of the drone. This is explained further in paragraph 3-1-1. Secondly, installing two propellers at two opposite locations, the fore and the aft of the vehicle can counter the imbalance.

Two motors spin these propellers individually, in inverse direction. The fore propeller spins in the clockwise and the aft one in the counterclockwise direction, which is shown in figure 3-4 and is described in detail in paragraph 3-1-2. However, the two propellers should provide, under the above conditions, thrust in only one direction.

3-1-1 The Concentric Shafts for the Fifth Motor

The counter-rotating propellers are named the fifth rotor since they both rotate from
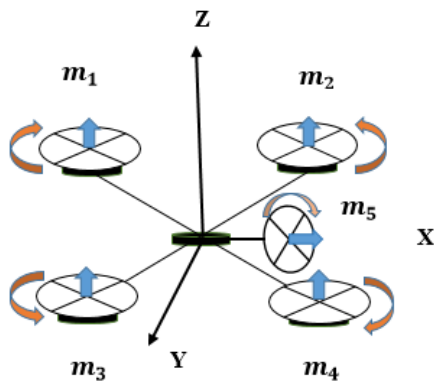
Fig 3-1: Five-rotor, five-motor UAV   Fig 3-2: Six-rotor, five-motor UAV
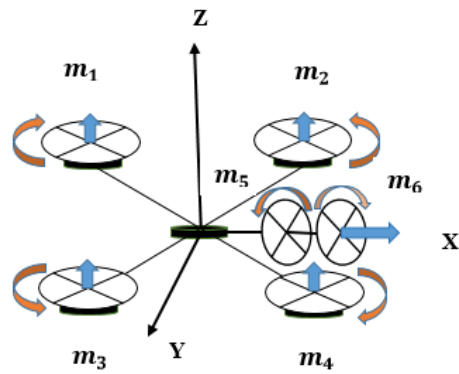
the same motor. The location of this propeller is shown in figure 3-2 where the counter-rotating rotors are located in the forward position, exactly in the X direction.

The counter-rotating propellers are clearly illustrated in figure 3-3 in a detail representation. The rotations of the propellers are adverse which is shown by the arrows. The counter rotation of propellers leads to nullifying their produced momenta in the X direction. It is noticeable that these two counter-rotating propellers are twisted in opposed way. The front rotor is an inboard one which produce thrust in the forward direction, pulling force, and it rotates clockwise. Although the aft one is an outboard rotor that produce thrust in the forward direction as well, it produces pushing force that results in pushing the vehicle in the forward direction while the direction of rotation of the aft propeller is counterclockwise. In conclusion, the outcome thrusts

of both rotors of the fifth motor have the same direction which lead to increasing the speed of the drone in the forward flight (cruise flight).

The other issue which must be considered about counter-rotating propellers is their drive shafts. There are two shafts which are concentric. One of them is a hollow shaft and the other one is solid. Since both shafts must be spun by the same motor, the set of gears must be matched as is shown in figure 3-3. This small transmission with a suitable design can transfer the power of the fifth motor to each lateral axis propeller. As it is illustrated, there is some complexity and extra cost to prepare a small vehicle with these tiny gears. The other noticeable issue is that the void space between these two shafts leads to play in their positions, so bearings must be placed between these two shafts to reduce the play. The size that these sleeve bearings should be selected upon is the difference of the outer shaft and the inner shaft sizes as the play should be minimized to reduce the imbalance of the counter-rotating propellers [45].

The above scenario on the transmission is perfect at a theoretical sight but practically there are some drawbacks that are listed in the following paragraph which lead to choosing another solution for neutralizing the momentum of the fifth rotor.
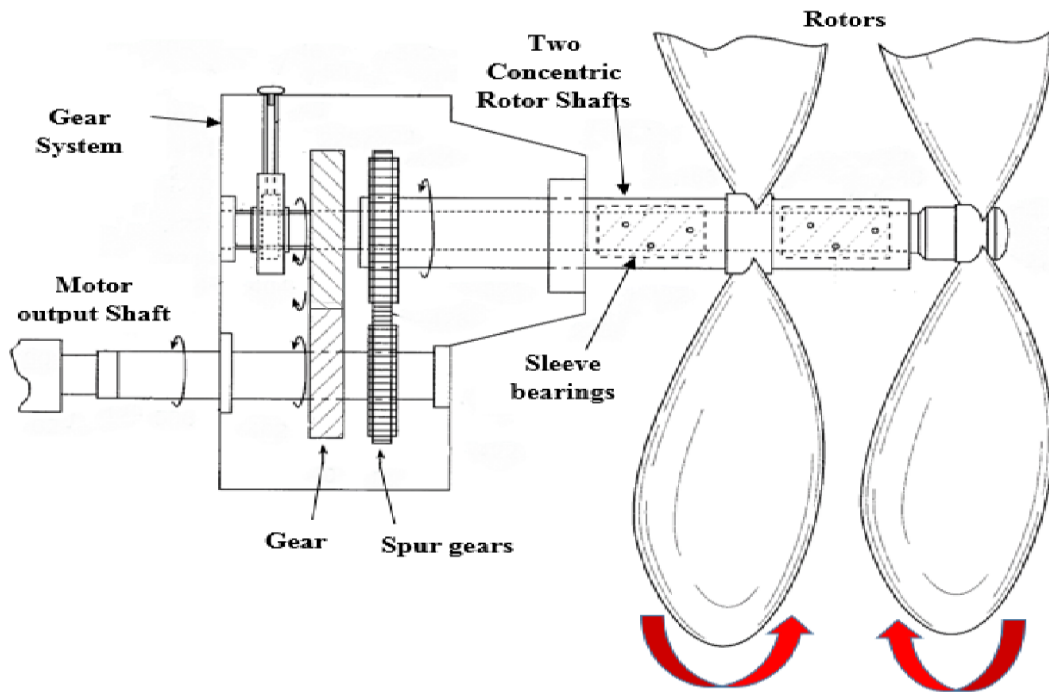
Fig 3-3: The gear system of counter-rotating rotors with two concentric shafts in detail [45]

One of the most significant difficulties which is included in two concentric shafts is the imbalance status of the vehicle. Since there is not the same weight in the aft position of the vehicle and the camera is installed in the forward position as well. This imbalance happens and causes the movement of the center of gravity from the center point of vehicle to the front. It is important to point out that the best design would position the CG of the vehicle at its center of symmetry. This phenomenon causes problems in order to achieve a moderate flight and includes wasting a significant amount of energy for correcting the imbalance. The second important aspect is the weight of the whole transmission part. The gear set makes the vehicle heavier and produce more drag while the fifth motor spins two propellers. Therefore, the vehicle consumes more energy to fly. The next effective consequence of assembling the gear system is the elaboration and the cost of preparing all these miniature parts for a small sized drone.

3-1-2 Two Solid Shafts and Motors in Opposite Direction in Lateral Plane

The split-away locations of both lateral axis propellers can solve some of the complications in many aspects. Both lateral rotors are considered as one because they rotate to produce the same direction of thrust as is shown in figure 3-4. Obviously, both rotors produce the same thrust value and direction according to their configurations. Their opposed twist airfoils lead the fact that the forward one which rotates clockwise and has the pushing twist shape produce the same thrust force and in the same direction as the aft one. The aft one rotates counterclockwise at the same speed and has the pulling twist shape of the airfoil. In addition, different directions of rotation of both lateral axis rotors neutralize the gyroscopic forces and momentums which are their outcomes. The spinning directions of all rotors are illustrated in figure 3-4. The X direction is considered the forward direction of the drone which is parallel with the axis of rotation of both rotors.
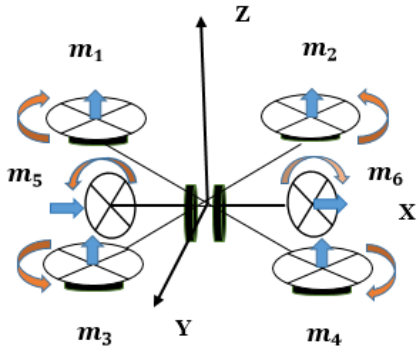
Fig 3-4: Six-motor UAV

In this design, the fifth and sixth motors are located under the main body and two shafts transmit their power to rotors. This configuration causes more stability and balance attitude due to the position of center of gravity which will be described in the paragraph 3-3. Therefore, by eliminating the gear system and adding one motor in comparison with the former design one gains more performance. More thrust is produced by the two motors in contrast with one motor. However, there is some additional weight by considering the 6th motor, but the gear system and its complexity are rectified by this design. The weight of all additional parts for both five-motor and six-motor designs are figured in the table 3-1. This table shows an approximate weight comparison between these two designs. As shown, the total additional weight of six-motor is about 11.62 grams by considering two rotors and motors. On the other hand, the total weight of five-motor is about 43.62 grams by considering two rotors, two motors and gear system. While, there is more created power in six-motor design. Hence, the next paragraphs are exploring the physical and mathematical model of the recommended design (six-motor).

Table 3-1: An approximate comparison of the weight of the added parts for 5-motor (5th rotor is counter-rotating) vs 6-motor (with 6 rotors)

Part name	Weight for 5-motor (g)	Part name	Weight for 6-motor (g)
Rotors	2 x 1.91	Rotors	2 x 1.91
Motors	3.9	Motors	2 x 3.9
Gear system	32	-	-
Total	43.62	Total	11.62

Obviously, all the above explanation for designing a drone with the fast forward flight capability is completed by considering the inclined degree of the vehicle. In case of rotor wing drones and helicopters purely straight or nose up flights are not possible. There must be a nose down degree inclination. In the following, the produced thrust of a standard quadcopter and the 6-motor design are compared by considering two different inclination degrees, at 15° and 30°.

Totally when the vehicle is inclined, some of the vertical force reduces and the motors need to speed up faster to make sure that the vehicle is able to hover. The forward motors spin speed is slower to stable the inclination. This reaction of the motors at 30° makes the thrust component to be reduced and the height of the vehicle will reduce. It is possible that the vehicle slips and gets in instability condition at 30° inclination.

Figure (3-5) shows the thrust components of the motor.
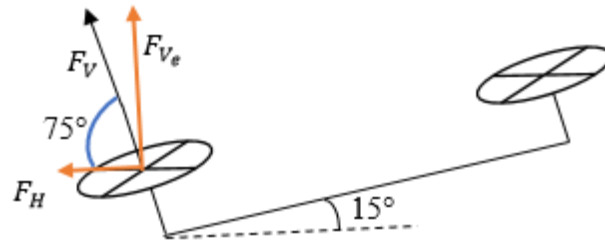
Fig 3-5: The motor inclination

The total thrust is given by all four motors in quadcopter and six motors in 6-motor design. The advancement thrust by considering the inclined degree as 15° is calculated in the equation (3-1).

$$4F_H = 4F_V \cos 75 = F_V \qquad (3\text{-}1)$$

$$2F_H = 2F_V \cos 15 = 1.92F_V$$

$$F_T = F_V + 1.92\,F_V = 2.92\,F_V$$

Where, $4F_H$ is the produced thrust by a quadcopter, $2F_H$ is the produced thrust by two horizontal motors and F_T is the total generated thrust of the 6-motor design. It is clear that the produced thrust of the 6-motor design is about three times of the quadcopter.

It is interesting that at 30° the produced thrust of four vertical motors is relatively half of the two horizontal motors. Although at 15° inclination the drag is higher (experimental results), for fast forward advancement, this is a more suitable position.

3-2 Newton Euler Model

The dynamics motion of the six-rotor vehicle is obtained by the Newton-Euler model as well. Two frames are defined same as for the standard quadrotor, Earth frame (f_E) and Body frame (f_B). These two frames are illustrated in figure 3-6. Hence, the whole system movements can be clarified by the dynamics and the kinematics equations. However, there is no difference in the kinematic modeling of this design and quadrotor since the fifth and sixth motors are installed in the horizontal direction. In the following paragraph there is a short briefing for the kinematic model of the specified drone.
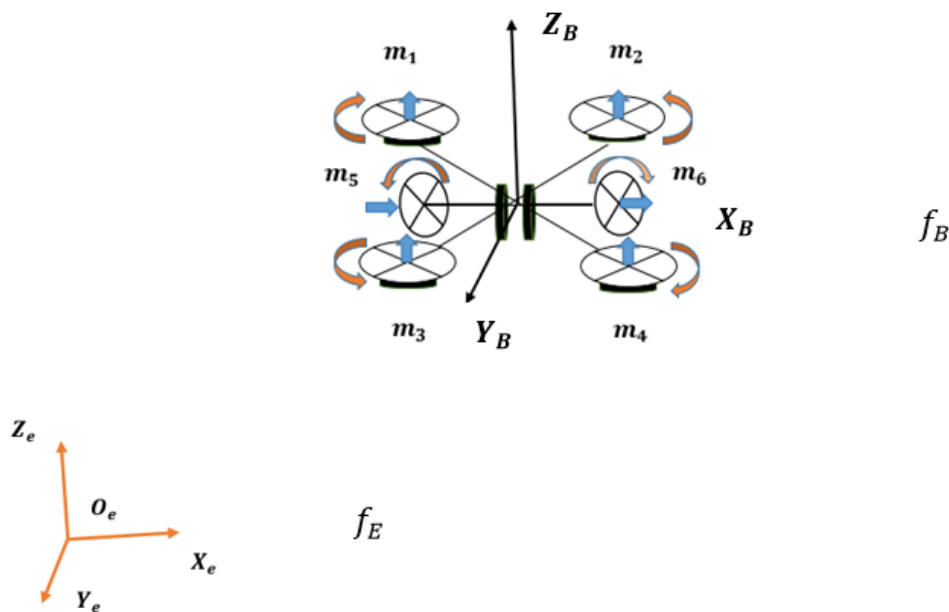
Fig 3-6: The schematics of the 6-motor drone with its frames (B-frame and E-frame)

3-2-1 The Kinematic Model

In this model, the three laws of motions: acceleration, velocity and displacement need to be considered [35, 40, 36]. The position in the E-frame will be defined by ξ. The linear position $\tau^E[m]$ can be specified by the position of E-frame with respect to the B-frame. The angular velocity $\theta^E[rad]$ is specified by the position of the B-frame with respect to the E-frame and considering the main three rotations around the main axes, Euler angles (φ θ ψ).

$$\xi = \begin{bmatrix} \tau^E \\ \theta^E \end{bmatrix}$$

While,
$$\tau^E = \begin{bmatrix} x \\ y \\ z \end{bmatrix} \quad \text{and} \quad \theta^E = \begin{bmatrix} \varphi \\ \theta \\ \psi \end{bmatrix}$$

Then,
$$\xi = \begin{bmatrix} \tau^E \\ \theta^E \end{bmatrix} = \begin{bmatrix} x \\ y \\ z \\ \varphi \\ \theta \\ \psi \end{bmatrix} = [\, x \; y \; z \; \varphi \; \theta \; \psi \,]^T$$

Three main rotations of the body around main axes known as Roll, Pitch, and Yaw, which all the three rotations are defined in the paragraph (2-2-1). By adding two motors to the quadrotor in the lateral plane, no changes will occur for the rotation matrix R_θ, equation (2-3) (details in the Appendix B). So for the 6-motor design, there is no change in the formulation of the linear and angular velocity vectors of the E-frame (V^E, ω^E) by considering the velocity vectors of the B-frame (V^B, ω^B) in comparison with the standard quadrotor.

In this chapter, transfer matrix Γ_θ, is the same matrix with the same terms as the one in the second chapter, this is equation (2-8). Therefore, J_θ (generalized matrix) and finally $\dot{\xi}$ (velocity

vector in E-frame) are same as they are presented in the second chapter, the equations (2-9), (2-10) and (2-11).

Moreover, all assumptions that are listed in the second chapter, at the end of the paragraph (2-2-1) are entirely applicable to the six-motor drone design.

3-2-2 The Dynamic Model

By considering the fact that all the equations used for formulating a quadrotor as basic dynamic model are presented in the chapter 2. In this chapter for the proposed vehicle, most of the equations [35, 37] would be the same and just the different equations will be pointed out. With respect to the E-frame and using the second Newton-Euler law, the force and torque vectors which are created by the vehicle are described by equations (2-13) and (2-18). Hence, by using the skew symmetric matrix for angular velocity(ω), equations (2-15) and (2-16), the equations (2-17), (2-19) and (2-20) are exactly the steps to achieve the generalized force vector (Q) in this design as $\begin{bmatrix} F^B \\ T^B \end{bmatrix}$. The formulation contains the force matrix (F^B) and the torque matrix (T^B) and is expanded as the equation (2-22).

Same as the quadrotor generalized force vector formula (2-21), M_B and C_B are the system inertia matrix and the Coriolis-centripetal matrix respectively. These two matrices are exactly as like as the equations (2-24) and (2-25) since there is no changes in the fundamental concepts of the vehicle. In this configuration, the summation of the system inertia matrix and the Coriolis-centripetal matrix is equal to the summation of the gravity force G_θ (ξ) of the vehicle, the gyroscopic force $O_B(v)\Omega$, the motion force $U_B\Omega$ and the frontal body aerodynamics forces W_B, as in equation (3-2) [46, 47, 36].

$$M_B\dot{v} + C_B(v)v = G_\theta(\xi) + O_B(v)\Omega + U_B(\Omega) + W_B \tag{3-2}$$

The Coriolis-centripetal matrix is ignored due to the low speed movement of the vehicle in comparison with the earth speed as it was described in Chapter 2. Moreover, there is no

rotational movement and the trajectory of drone is the forward flight consideration which is written in the first Chapter. Therefore, the equation (3-2) is rewritten as the equation (3-3).

$$M_B \dot{\boldsymbol{v}} = \boldsymbol{G}_\theta\left(\xi\right) + \boldsymbol{O}_B(\boldsymbol{v})\boldsymbol{\Omega} + \boldsymbol{U}_B(\boldsymbol{\Omega}) + \boldsymbol{W}_B \tag{3-3}$$

However, only the equation of the gravity and gyroscopic forces of this design are the same as the quadcopter (equations (2-28) and (2-29)) and the other forces (the motion force and the aerodynamics forces of the frontal body) are different in comparison with the standard quadrotor. Hence, these forces are presented in the following paragraphs.

The 5th and 6th propellers are rotating in an opposite direction and same speed ($\Omega_5 = \Omega_6$) which the algebraic summation of both propellers speed should be zero to prohibiting the vehicle overall momentum misbalance same as the standard quadcopter. Therefore, their gyroscopic momentum would be neutralized by each other and there would be no additional gyroscopic momentum in comparison to the standard quadrotor. Hence, in case of the 5th or 6th rotor failure, there would be an additional momentum. The equation (3-4) and (3-5) describe the additional gyroscopic momentum by considering the failure of 5th or 6th propellers.

The axes of the four propellers (spin axes) are parallel to the Z axis and there are two more propellers with the horizontal axis and parallel to the X axis. The gyroscopic precession will only affect an aircraft when the attitude is changing. Making distinction between the gyroscopic force and an asymmetrical thrust is not easy. As soon as the aircraft encounters a pitch or yaw rotation, asymmetric thrust will amplify pitching or yawing (3-4).

In the equation (3-4), for $k = 1\ to\ 4$ (rotor number 1 to 4), the angle between the plane of rotation of the propellers and the Z direction (θ_k) is 90° and for the two lateral propellers (when $k = 5, 6$) this angle(θ_k) is 0°. Therefore, by substitution of these observations, the equation (3-4) is resulted which expresses momentum, not only that the angle between R_5 and R_6 is zero as their rotational axes coincide.

$$O_B(v)\Omega = \begin{bmatrix} 0_{3\times 1} \\ -\sum_{k=1}^{6} J_{TP}\left(\omega^B \times \begin{bmatrix} C\theta_k \\ 0 \\ -S\theta_k \end{bmatrix}\right)(-1)^k\Omega_k \end{bmatrix} \tag{3-4}$$

$$O_B(v)\Omega = \begin{bmatrix} 0_{3\times 1} \\ -\sum_{k=1}^{4} J_{TP}\left(\omega^B \times \begin{bmatrix} 0 \\ 0 \\ 1 \end{bmatrix}\right)(-1)^k\Omega_k \end{bmatrix} + \begin{bmatrix} 0_{3\times 1} \\ -\sum_{k=5}^{6} J_{TP}\left(\omega^B \times \begin{bmatrix} 1 \\ 0 \\ 0 \end{bmatrix}\right)(-1)^k\Omega_k \end{bmatrix}$$

$$O_B(v)\Omega = \begin{bmatrix} 0_{3\times 1} \\ -\sum_{k=1}^{4} J_{TP}\begin{bmatrix} -q \\ p \\ 0 \end{bmatrix}\Omega_k \end{bmatrix} + \begin{bmatrix} 0_{3\times 1} \\ -\sum_{k=5}^{6} J_{TP}\begin{bmatrix} 0 \\ r \\ p \end{bmatrix}\Omega_k \end{bmatrix} \tag{3-5}$$

$$= J_{TP}\begin{bmatrix} 0 & 0 & 0 & 0 & 0 & 0 \\ 0 & 0 & 0 & 0 & 0 & 0 \\ 0 & 0 & 0 & 0 & 0 & 0 \\ q\Omega_1 & -q\Omega_2 & q\Omega_3 & -q\Omega_4 & 0 & 0 \\ -p\Omega_1 & p\Omega_2 & -p\Omega_3 & p\Omega_4 & -r\Omega_5 & r\Omega_6 \\ 0 & 0 & 0 & 0 & -p\Omega_5 & p\Omega_6 \end{bmatrix}$$

The gyroscopic momentum matrix of the propeller is shown by $O_B(v)$ and J_{TP} $[Kg\ m^2]$ is the total rotational moment of inertia about the propeller axis.

In the equation (3-5), there are components as propellers speed Ω_k $[rad\ s^{-1}]$ which are classified by the number of propellers. For example, the rotational speed of the first propeller has the subscript 1 and is shown as Ω_1 $[rad\ s^{-1}]$.

Kaan T. Oner [46] has defined the details of mathematically modeling of a drone with the vertical and horizontal rotor axes. The required steps to reach the final motion vector equation $U_B(\Omega)$ for the six-rotor UAV are represented in detail in the Appendix G. The forces and torques which are defined as the motion vector $U_B(\Omega)$ are explained in the following paragraphs [46, 47].

Given that there is no propeller in the direction Y, there is no propeller created force in that direction. It is illustrated in the motion vector $\boldsymbol{U_B}(\Omega)$ that all six elements of the second raw in the matrix are zero. In the other directions, X and Z, there are rotors and for all three Euler-angles, there are momentum to induce motion in φ, θ, ψ angles. Each motor has a net torque that applies to the rotor shaft. This torque results in the thrust force T_i which is derived in the equation (3-6).

$$T_i = \frac{1}{2} b \, \rho A \, \Omega_i^2 \qquad\qquad (3\text{-}6)$$

Generally, there are two types of drag force for a quadcopter in different flight statuses. When the vehicle is flying in the forward direction there would be a drag force in the opposite direction of its travel which is generated by the movement of the whole body through the air. This drag force is proportional to the drone forward speed as it is described in the section 2-2-1.

The second drag force is generated by the propellers rotation in the air. This force is proportional to the rotational speed of the propellers. These both thrust and drag forces are proportional to the square of the propellers speed which are shown in the equations (2-32) and (2-33) in a simplified manner for each propeller.

$$T_i = b\Omega_i^2 \qquad\qquad (3\text{-}7)$$

$$D_i = d\Omega_i^2 \qquad\qquad (3\text{-}8)$$

Where in the equation (3-7), T $[N]$ represent thrust force, i the number of motors, b the thrust coefficient which is dimensionless and Ω $[rad\ s^{-1}]$ the rotational speed.

In the equation (3-8), D $[N]$ represent drag force, i the number of motors, d the drag coefficient which is dimensionless and Ω $[rad\ s^{-1}]$ the rotational speed.

All drag, lift and thrust coefficients are dimensionless. However, they are important for calculations. All the aerodynamic contributions are explained and derived in detail in the

Appendix F. By considering the aerodynamics, it shows that forces and torques are proportional to the squared propellers speed.

Therefore, by multiplication of the square of the propeller rotational speed $\Omega^2 [rad^2\ s^{-2}]$ to the unique motion matrix (E_B) (3-10), the motion vector $U_B(\Omega)$ relation (3-9) is resulted. As it was explained in chapter one, the proposed trajectory of this design is to travel with the constant height and forward speed, on a given path from A to B to perform visualization inspections. Thus, there are three steps of the flight mission for which the motion forces are changing from a state to the other.

1) The vehicle lifts to a required height. In this design the four vertical propellers produce force to lift the vehicle and at the same time they produce drag since they are mover upwards and encounter the air. Hence, the horizontal propellers do not create any aerodynamics force while they do not drag the air.

2) The drone gains the desired attitude and orientation (they might be modified and corrections applied). All four vertical propellers are engaged to change the orientation of the vehicle and produce aerodynamics force in this step. The horizontal propellers do not have any involvement in creating the aerodynamics force.

3) The vehicle keeps horizontal and activates the horizontal propellers to reach the required speed along the selected direction. Therefore, the aerodynamics force is generated by the horizontal propellers which are encountered with the air. In this step all four vertical propellers are in hover status. Hence, there would be an ignorable drag force induced by these propellers and the body as well.

By considering the above steps of the drone mission, for the first and second steps, the motion vector $U_B(\Omega)$ is the same as the standard quadrotor (equation (2-34)) since there is no remarkable aerodynamics forces via the horizontal propellers. Hence, the third step describes that the motion vector $U_B(\Omega)$ is changed in comparison with the standard quadrotor while the

horizontal propellers are the only ones which are involved in generating the aerodynamics forces. Hence, the equation (3-8) describes the motion vector $\boldsymbol{U_B}(\Omega)$ in this step.

$$\boldsymbol{U_B}(\Omega) = E_B\Omega^2 = \begin{bmatrix} U_1 \\ U_2 \\ U_3 \\ U_4 \\ U_5 \\ U_6 \end{bmatrix} = \begin{bmatrix} 0 & 0 & 0 & 0 & b & b \\ 0 & 0 & 0 & 0 & 0 & 0 \\ b & b & b & b & 0 & 0 \\ 0 & 0 & 0 & 0 & d & -d \\ 0 & 0 & 0 & 0 & 0 & 0 \\ -d & d & -d & d & 0 & 0 \end{bmatrix} \begin{bmatrix} \Omega_1^2 \\ \Omega_2^2 \\ \Omega_3^2 \\ \Omega_4^2 \\ \Omega_5^2 \\ \Omega_6^2 \end{bmatrix} \tag{3-9}$$

$$= \begin{bmatrix} b\Omega_5^2 + b\Omega_6^2 \\ 0 \\ b(\Omega_1^2 + \Omega_2^2 + \Omega_3^2 + \Omega_4^2) \\ d(\Omega_5^2 - \Omega_6^2) \\ 0 \\ d(\Omega_2^2 + \Omega_4^2 - \Omega_1^2 - \Omega_3^2) \end{bmatrix}$$

$$E_B = \begin{bmatrix} 0 & 0 & 0 & 0 & b & b \\ 0 & 0 & 0 & 0 & 0 & 0 \\ b & b & b & b & 0 & 0 \\ 0 & 0 & 0 & 0 & d & -d \\ 0 & 0 & 0 & 0 & 0 & 0 \\ -d & d & -d & d & 0 & 0 \end{bmatrix} \tag{3-10}$$

In the equation (3-8), $l(m)$ is the distance from the center of the propeller to the center of the vehicle, b is the thrust coefficient and d is the drag coefficient. $U_1, ..., U_6$, are the motion vector components which are related to each propeller. $\Omega_1, .., \Omega_6$ are the propellers' speed.

As it was explained in the chapter 2, there are aerodynamics forces (lift and drag) in the horizontal flight which are proportional to the forward speed. These aerodynamics forces are generating by encountering of the air with the airfoil. The airfoil which produces these forces is the frontal area of the body. It is the first area that air encounters with it. Therefore, in the

horizontal flight of the proposed vehicle, the aerodynamic lift and drag forces of the front struts are considered in dynamic modeling of the vehicle. These forces are not taken into account for the dynamic modeling of the vertical flight and are assumed as external disturbance. These forces are written as (3-11) and (3-12). Moreover, the aerodynamics forces of an airfoil are explained in the Appendix F in details.

$$L = \frac{1}{2} \rho V^2 A c_l \qquad (3\text{-}11)$$

$$D = \frac{1}{2} \rho V^2 A c_d \qquad (3\text{-}12)$$

Where, ρ $[kg\ m^{-3}]$ is the airflow density, $V [m\ s^{-2}]$ is the airfoil velocity, $A\ [m^2]$ is the airfoil area which encounter with the air in forward movement and c_d is the drag coefficient that is various in different velocities. The experimental measurements of drag coefficient of the standard quadrotor in the wind tunnel is used for this design and are described in the chapter four in detail.

The frontal body aerodynamic forces are taken into account just for the translational movements in forward direction. Therefore, there is no frontal body aerodynamic force for the angular motions. Thus, the following matrix (3-13) shows the frontal body aerodynamic forces.

$$W = \begin{bmatrix} W_1 \\ W_2 \\ W_3 \\ W_4 \\ W_5 \\ W_6 \end{bmatrix} = \begin{bmatrix} -\frac{1}{2} \rho V^2 A c_d \\ 0 \\ \frac{1}{2} \rho V^2 A c_l \\ 0 \\ 0 \\ 0 \end{bmatrix} \qquad (3\text{-}13)$$

All four forces (the gravity force, the gyroscopic force, the motion force vector and the frontal body aerodynamics force vector) are contributed in the generalized force vector (Q). By considering the three steps of the flight trajectory, the equation (2-27) is not changed for the first and second steps of the drone mission as there are no changes in the gravity, gyroscopic and aerodynamics forces. Additionally, there is no aerodynamics force of the frontal body in these formulations, though in the third step of the drone mission, the aerodynamics force is changed and the equation (2-27) is changed to the equation (3-3).

The equation (3-3) is rearranged in the following formulation (3-14) to yield the generalized acceleration vector ($\dot{v}$) with respect to the B-frame.

$$\dot{v} = \frac{G_\theta\left(\xi\right) + O_B(v)\Omega + U_B\Omega + W_B}{M_B} \tag{3-14}$$

To show all the components of the generalized acceleration vector ($\dot{v}$), it can be written as six equations for the six directions of motion of the vehicle. Therefore, by using all previous equations, the equation (3-14) is rewritten as the equation (3-15) in six scalar equations for each element of the generalized acceleration vector (derivative of the generalized velocity vector (2-12)) with respect to the B-frame.

$$\dot{v} = \begin{cases} \dot{u} = g\ s\theta + \dfrac{U_1}{m} + \dfrac{W_1}{m} \\[2mm] \dot{v} = g\ c\theta\ s\varphi \\[2mm] \dot{\omega} = g\ c\theta\ s\varphi + \dfrac{U_3}{m} + \dfrac{W_3}{m} \\[2mm] \dot{p} = -\dfrac{J_{TP}}{I_{XX}}q(\Omega_2 - \Omega_1 + \Omega_4 - \Omega_3) + \dfrac{U_4}{I_{XX}} \\[2mm] \dot{q} = \dfrac{J_{TP}}{I_{YY}}p(\Omega_2 - \Omega_1 + \Omega_4 - \Omega_3) + \dfrac{J_{TP}}{I_{YY}}r(\Omega_5 - \Omega_6) \\[2mm] \dot{r} = \dfrac{J_{TP}}{I_{YY}}p(\Omega_5 - \Omega_6) + \dfrac{U_6}{I_{ZZ}} \end{cases} \tag{3-15}$$

Where the propellers speed inputs and frontal body aerodynamics forces are respectively given as (3-16) and (3-17):

$$
U = \begin{cases}
U_1 = b(\Omega_5^2 + \Omega_6^2) \\
U_2 = 0 \\
U_3 = b(\Omega_1^2 + \Omega_2^2 + \Omega_3^2 + \Omega_4^2) \\
U_4 = d(\Omega_5^2 - \Omega_6^2) \\
U_5 = 0 \\
U_6 = d(\Omega_2^2 + \Omega_4^2 - \Omega_1^2 - \Omega_3^2)
\end{cases}
\tag{3-16}
$$

$$
W = \begin{cases}
W_1 = -\dfrac{1}{2}\,\rho\,V^2\,A\,c_d \\
W_2 = 0 \\
W_3 = \dfrac{1}{2}\,\rho\,V^2\,A\,c_l \\
W_4 = 0 \\
W_5 = 0 \\
W_6 = 0
\end{cases}
\tag{3-17}
$$

All five defined forces and momentum in the equation (3-14) are used in the equation (3-15). For more clarification, the first line of the equation (3-15) is explained in the following paragraph and is used to express all five forces and momentums. It is shown by $(\dot{u})$ as the first element of the acceleration vector.

The first force is the gravitational force which is expressed in the equation (3-14) for all six equations of motion. Therefore, it is expressed as $(mg\ s\theta)$ and same as the first force it is divided by the mass (m). So it is written as $(g\ s\theta)$ where, s and c expressed sin and cosine respectively.

The second force of concern is the gyroscopic momentum. This momentum is shown in the equation (3-5). It was previously discussed in the chapter 2 where was concluded that this force is not applicable to the linear equations of motion (the first three ones). Therefore, there is no

gyroscopic momentum in the first equation. However, for the angular expressions of acceleration, by considering the equation (3-5), these forces (momentums) are yield by the last three equations of (3-15).

The next force of interest is the motion force vector $\boldsymbol{U_B \Omega}$ which is expressed in the equation (3-9) and its elements $(U_1, \dots, U_6)$ in the equation (3-16). As it is written, for the first scalar equation in (3-15), there is U_1 as the thrust force. The last force of concern is the frontal body aerodynamics forces which is written in the first equation of motion as W_1. This force does not apply on the angular motions. It is presented in detail in the equation (3-17).

All parameters of the equations (3-15) are written in the B-frame. However, the dynamic equations in E-frame describe the control purposes of a clear fashion. Hence, it is necessary to write the dynamic equations in the E-frame. For this transformation, the linear and angular accelerations are considered separately. It is obvious that due to no movement in the hover condition, the transfer matrix Γ_θ is assumed as identity matrix $I_{3\times3}$. Therefore, the equation (2-6) is rewritten as the equation (3-18) where the angular velocity in the E-frame is equal to the angular velocity in the B-frame. Hence, there is no difference between the angular acceleration in the B-frame and the E-frame. Then by assuming $\Gamma_\theta = I_{3\times3}$, the equation (2-10) is rewritten as the given equation (3-19).

$$\boldsymbol{\omega}^E = \dot{\boldsymbol{\theta}}^E \tag{3-18}$$

$$\begin{bmatrix} \dot{\boldsymbol{\tau}}^E \\ \dot{\boldsymbol{\theta}}^E \end{bmatrix} = \begin{bmatrix} R_{\theta\ 3\times3} & 0_{3\times3} \\ 0_{3\times3} & I_{3\times3} \end{bmatrix} \begin{bmatrix} \boldsymbol{V}^B \\ \boldsymbol{\omega}^B \end{bmatrix} \tag{3-19}$$

By considering the above equation (3-19), all the angular equations of the equation (3-16) include no changes when are transferring to the E-frame. Hence, the linear equations are multiplied by rotational matrix $(R_{\theta\ 3\times3})$ to result in the equations of the E-frame. Therefore, the generalized velocity vector $(\boldsymbol{\xi})$ is expressed as the equation (3-20) .

$$\xi = \begin{bmatrix} \dot{t}^E \\ \omega^B \end{bmatrix} = \begin{bmatrix} \dot{x} \\ \dot{y} \\ \dot{z} \\ p \\ q \\ r \end{bmatrix} \tag{3-20}$$

The inertia matrix in the E-frame is same as the B-frame, equation (3-21).

$$M_H = M_B = \begin{bmatrix} mI_{3\times3} & 0_{3\times3} \\ 0_{3\times3} & I_{3\times3} \end{bmatrix} = \begin{bmatrix} m & 0 & 0 & 0 & 0 & 0 \\ 0 & m & 0 & 0 & 0 & 0 \\ 0 & 0 & m & 0 & 0 & 0 \\ 0 & 0 & 0 & I_{XX} & 0 & 0 \\ 0 & 0 & 0 & 0 & I_{YY} & 0 \\ 0 & 0 & 0 & 0 & 0 & I_{ZZ} \end{bmatrix} \tag{3-21}$$

The gravitational force vector is rearranged to the equation (3-22) which is expressed as the gravitational force in the E-frame as there are only linear terms in this force.

$$G(\xi) = \begin{bmatrix} F_G^E \\ 0_{3,1} \end{bmatrix} = \begin{bmatrix} 0 \\ 0 \\ -mg \\ 0 \\ 0 \\ 0 \end{bmatrix} \tag{3-22}$$

There is no change in the gyroscopic effects, as there is no gyroscopic force in the linear equations. Hence, the final gyroscopic force (3-23) is the same as the gyroscopic force in the B-frame (3-5).

$$O(\xi)\Omega = O_B(v)\Omega = \begin{bmatrix} 0_{3\times1} \\ -\sum_{k=1}^{4} J_{TP} \begin{bmatrix} -q \\ p \\ 0 \end{bmatrix} \Omega_k \end{bmatrix} + \begin{bmatrix} 0_{3\times1} \\ -\sum_{j=5}^{6} J_{TP} \begin{bmatrix} 0 \\ r \\ p \end{bmatrix} \Omega_k \end{bmatrix} \tag{3-23}$$

$$= J_{TP} \begin{bmatrix} 0 & 0 & 0 & 0 & 0 & 0 \\ 0 & 0 & 0 & 0 & 0 & 0 \\ 0 & 0 & 0 & 0 & 0 & 0 \\ q\Omega_1 & -q\Omega_2 & q\Omega_3 & -q\Omega_4 & 0 & 0 \\ -p\Omega_1 & p\Omega_2 & -p\Omega_3 & p\Omega_4 & r\Omega_5 & -r\Omega_6 \\ 0 & 0 & 0 & 0 & p\Omega_5 & -p\Omega_6 \end{bmatrix}$$

The last, motion force vector $U(\Omega)$ includes both linear and angular terms. Hence, in case of linear terms the (U_1, U_2, U_3 in the equation (3-8)) are multiplied by the rotation matrix ($R_{\theta\,3\times3}$) to be transferred to the E-frame by considering the equation (2-39). In addition, the angular terms (U_4, U_5, U_6 in the equation (2-34)) do not require any changes. Therefore, the extracted motion force vector by considering both linear and angular elements is written in the equation (3-24).

$$E(\xi)\Omega^2 = \begin{bmatrix} R_{\theta\,3\times3} & 0_{3\times3} \\ 0_{3\times3} & I_{3\times3} \end{bmatrix} E_B \Omega^2 \tag{3-24}$$

$$= \begin{bmatrix} (c\psi c\theta)(U_1 + W_1) + (s\psi s\varphi + c\varphi^2 s\theta)(U_3 + W_3) \\ (s\psi c\theta)(U_1 + W_1) + (-c\psi s\varphi + s\psi s\theta c\varphi)(U_3 + W_3) \\ -s\theta(U_1 + W_1) + c\theta c\varphi(U_3 + W_3) \\ U_4 \\ 0 \\ U_6 \end{bmatrix}$$

Hence by using all the explained forces (equations (3-20), (3-21), (3-22) and (3-23)), the equation (3-14) can be rewritten as the equation (3-24).

$$
\dot{\xi} = \begin{cases}
\ddot{x} = (c\psi c\theta)\dfrac{U_1 + W_1}{m} + (s\psi s\varphi + c\varphi^2 s\theta)\dfrac{U_3 + W_3}{m} \\[2mm]
\ddot{y} = (s\psi c\theta)\dfrac{U_1 + W_1}{m} + (-c\psi s\varphi + s\psi s\theta c\varphi)\dfrac{U_3 + W_3}{m} \\[2mm]
\ddot{z} = -g - (s\theta)\dfrac{U_1 + W_1}{m} + c\theta c\varphi\dfrac{U_3 + W_3}{m} \\[2mm]
\ddot{\varphi} = \dfrac{J_{TP}}{I_{XX}}\dot{\theta}(\Omega_2^2 + \Omega_4^2 - \Omega_1^2 - \Omega_3^2) + \dfrac{U_4}{I_{XX}} \\[2mm]
\ddot{\theta} = \dfrac{J_{TP}}{I_{YY}}\dot{\varphi}(\Omega_2^2 + \Omega_4^2 - \Omega_1^2 - \Omega_3^2) + \dfrac{J_{TP}}{I_{YY}}\dot{\psi}(\Omega_5^2 - \Omega_6^2) \\[2mm]
\ddot{\psi} = \dfrac{J_{TP}}{I_{ZZ}}\dot{\varphi}(\Omega_5^2 - \Omega_6^2) + \dfrac{U_6}{I_{ZZ}}
\end{cases}
$$

3-3 The Five-Servo Motor Actuation

There is no doubt that by changing the number of motors, the equation of the angular acceleration for each motor and propeller do not change. Therefore, all the equations that have been used in the chapter 2 (quadcopter) are used for this study (six-motor) as well.

If the five-motor has been selected for this design, that will require some changes due to the gear set system. This would have effect on the gear conversion efficiency η. Therefore, there would be some more energy loss in five-motors (that are spinning six rotors). However, six-motor drone does not include a gear box system. All its motors and propellers components are same as the quadcopter. Hence, the produced energy for each motor may not be different by considering the standard quadcopter. The sole limitation will be related to the amount of energy that the battery would deliver to carry out the mission.

3-4 The Center of Gravity (CG)

The concept of the center of gravity is defined in the chapter 2. Therefore, by considering the configuration changes of the vehicle, there would be some differences in mass distribution within the drone. Both added motors and propellers are assumed to be install along the x direction of the vehicle. Therefore, the vehicle is a symmetric drone. In this case, in the vertical plane of the vehicle there would be some lowering in the center of gravity position. The center of gravity must be located exactly at the symmetry point of the vehicle. Hence, the symmetry is kept as well. Thus, the center of gravity position would be the symmetric point. However, this symmetry point will be located at a position that is lower than the original quadcopter symmetric point. Since in the lateral configuration, two more motors and propellers are added in the lower section of the vehicle body. Hence, the center of gravity position in the lateral plane would move a little lower than the quadcopter. Meanwhile, lower position of center of gravity in the vertical direction create more stability for the vehicle. Therefore, there is foresees no issue with mounting the horizontal motors below the drone.

CHAPTER 4

The Wind Tunnel Experiments and

Simulating the Design

Chapter 4 includes two parts. The first part presents experiments and the results of the measurements carried out in the wind tunnel test. These experiments are related to the selected quadcopter as a sample vehicle to find the drag and lift forces for different conditions. The results of this part are used in the second part which requires suitable estimates of drag and lift. The second part contains simulation and modeling a standard quadcopter and 6-motor drone by using the MATLAB-Simulink software.

In the second part of this chapter all the mathematical concepts of chapter 2 (standard quadcopter) and chapter 3 (6-motor drone) are simulated as the theoretical work. It contains four sections:

1) General concepts for simulating the drone
2) Control modelling of the standard quadcopter
3) Control modelling of the 6-motor drone
4) Comparing the result graphs of the standard quadcopter and 6-motor drone

Both parts of this chapter are explained in the following respectively.

Part 1

4-1 The Wind Tunnel Experiments of the Quadcopter and One Motor with Propeller

In this study, experiments in the wind tunnel has been carried out. The wind tunnel is a low speed tunnel which air is drawn in it by means of a fan spun by an electrical motor. The drawn air provides a specified flow speed and the experiment is visible through the transparent windows in the test area. The characteristics of the flow can be measured by special instruments. The main goal of the designed wind tunnel is to measure how the plunged object is affected by the surrounded airflow. The object can be a model, a vehicle or part of it and an engineering frame or structure that supports the test device. The size of the examined object has a direct influence on the size of the wind tunnel [48].

In this study, the wind tunnel experiments are described in detail with their results and provided in the following paragraphs. The test explained here were carried out in the subsonic wind tunnel. The wind tunnel is an open-loop type with a rectangular test section. The rectangular test section dimension is almost 90 cm long and 30 x 30 cm in cross section (figure 4-1). The suction air in the wind tunnel is supported by a 2 hp motor. The speed of the wind tunnel is changeable up to 50 m/s. While because of maximum speed of the tested vehicle, the maximum wind tunnel speed is considered 15 m/s. The temperature was 21°C and the pressure was 1 atmosphere. For more accuracy in this experiment, the flow speed has been measured by Pitot-static instrument.

Fig 4-1: The open-loop wind tunnel

As it is mentioned in chapter 2, no prototyped model was built in this study. Thus, a small quadcopter (figure 4-2) with the mentioned specifications in table (4-1) is selected to be used in the wind tunnel experiments. The scope of this test was to establish the procedure and analyze the matrice of experiments as suitable to such investigation.

Table 4-1: Selected quadcopter specification

Model: SYMA X5C			
Weight	98 gr	Flight Range	50 m
Dimension	31 x 31 x 8 cm	Battery	3.7V 500 mAh LiPo
Max speed	15 m/s	Battery charging time	40-45 min
Flight time	6-8 Min	Motor type, max power	Coreless, 7.4 W

Fig 4-2: The quadcopter SYMA X5C

In this investigation, the wind tunnel experiment has been performed in two phases. In phase one was performed the experiment for the quadrotor and phase two was performed the test for one motor with the installed propeller - in two steps.

4-1-1 The Wind Tunnel Experiments in Phase One

In phase one, by comparison of the wind tunnel size and the quadrotor dimensions, it was clear that the vehicle could not be run during the test. Since, the propeller did not have enough clearance for the rotation. Therefore, no power was applied on the vehicle during the test and it was a stationary (static) test.

During this test the wind tunnel speed has been changed between 5 to 15 m/s as normal velocity operation of a quadrotor, and at different angles of vehicle installation from 0° to 90° (0, 15, 30, 45, 60, 75, 90). The velocity corresponds to the intended forward speed of the quadrotor. Figure (4-3) illustrates the installed quadcopter in the wind tunnel with the angle of attack of 15° as an example. This angle corresponds to the attitude the quadrotor moves forward. The angle of installation is considered as the angle of attack of the vehicle in the wind tunnel.

Figure (4-4) shows the generated drag forces by the quadcopter body in stationary mode at the angle of attack 15° and wind tunnel speed from 5 to 15 m/s as a sample test [49, 50].

75

Fig 4-3: The quadcopter is installed in the wind tunnel

Fig 4-4: The produced drag forces by the quadcopter @ 15° angle of attack

4-1-2 The Wind Tunnel Experiments in Phase Two

In the second phase of the test [49, 50], one motor with its installed propeller was tested in two steps (stationary and dynamic) to get the actual results of the drag force during the flight. The first step of the second phase (figure 4-5) is very similar to the phase one, because there is no applied power on the motor. Thus, the output of the test is only the drag force in the stationary mode. Hence, there was not any lift to produce in this step as it is illustrated in the sample graph @ 15° (figures 4-6).
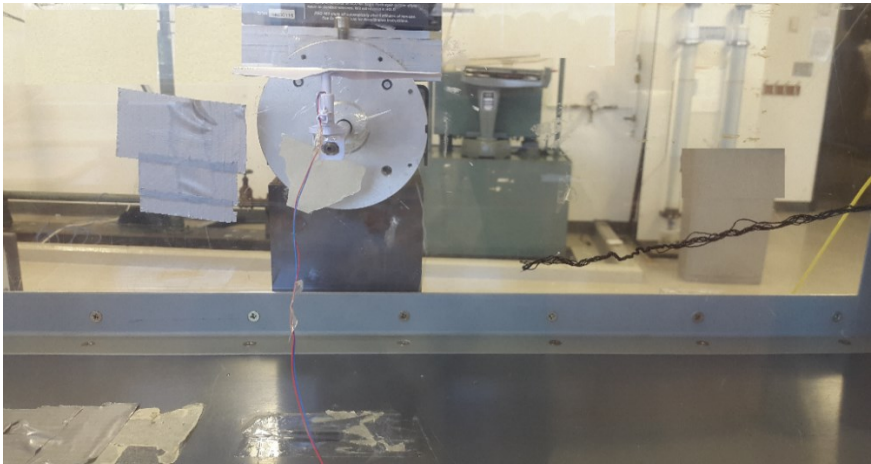
Fig 4-5: One motor with its propeller is installed in the wind tunnel @ 0°

Fig 4-6: The produced drag forces by one motor @ 15° angle of attack

In the second step of phase two, there is a remarkable change due to applying the power on the motor that rotates the propeller. So, the output graphs of this phase show the drag and lift forces. In order to ensure correctness of the resulted forces at different RPMs, this test was performed at four different RPMs. Therefore, due to rising the number of tests graphs to 28, just their outcomes are presented here along with some samples. There are three outcomes which are described below:

1- By comparing these graphs, it is concluded that there is a relation between the generated drag and the angle of attack ($d = \lambda \alpha$), where d is the drag force, α is the angle of attack and λ is the ratio. While all the relations were defined as the numerical values in these tests the relation between them needs to be found. Therefore, for each angle there is an equation which is extracted by comparing the drag values in different RPMs. Thus, all the equations are used in the second part of this chapter for simulating the vehicles. Figure (4-7) shows the drag graph and its equation at the angle of attack of 15 °.

The drag graph of one rotating motor at different RPMs @ angle = 15°

$y = 8E\text{-}06x^2 - 0.0002x + 0.0342$

Fig 4-7: The produced drag forces by one rotating propeller @ 15° angle of attack

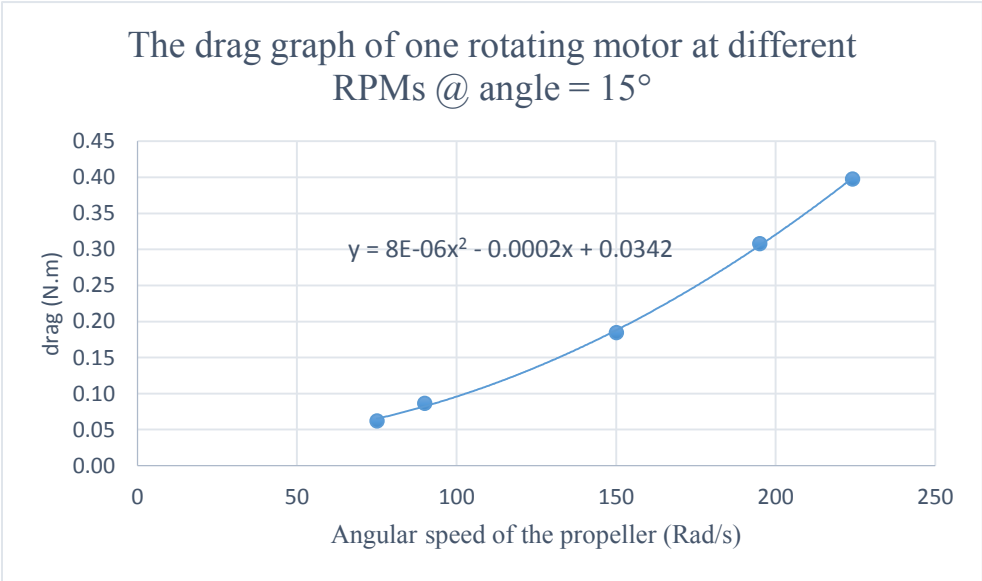Table (4-2): A small part of the table of the resulted of drag and lift forces @ different RPMs and angles

Degree: 0
One motor dynamic phase

rotor Speed	Voltage	Drag	Lift
75	2.36	0.05	0.06
90	2.36	0.08	0.08
150	2.6	0.17	0.09
195	2.68	0.29	0.1
224	2.74	0.37	0.11

Degree: 0
One motor dynamic phase

rotor Speed	Voltage	Drag	Lift
75	2.87	0.02	0.07
90	2.88	0.04	0.06
150	2.91	0.15	0.1
195	2.94	0.31	0.13
224	3.02	0.38	0.14

Degree: 15
One motor dynamic phase

rotor Speed	Voltage	Drag	Lift
75	3.32	0.06	0.28
90	3.34	0.09	0.28
150	3.49	0.18	0.23
195	3.55	0.32	0.21
224	3.61	0.4	0.2

Degree: 0

rotor Speed	Voltage	Drag	Lift
75	3.11	0.05	0.25
90	3.18	0.06	0.26
150	3.29	0.17	0.29
195	3.38	0.32	0.35
224	3.46	0.36	0.33

Degree: 0

rotor Speed	Voltage	Drag	Lift
75	3.27	0.08	0.3
90	3.3	0.12	0.32
150	3.42	0.21	0.34
195	3.5	0.35	0.35
224	3.57	0.37	0.36

Degree: 30

rotor Speed	Voltage	Drag	Lift
75	2.47	0.03	0.12
90	2.51	0.04	0.16
150	2.69	0.14	0.09
195	2.78	0.32	0.05
224	2.89	0.4	0.04

Degree: 0

rotor Speed	Voltage	Drag	Lift
75	3.35	0.08	0.3
90	3.38	0.12	0.33
150	3.52	0.21	0.35
195	3.6	0.34	0.36
224	3.63	0.4	0.38

Degree: 15

rotor Speed	Voltage	Drag	Lift
75	2.43	0.1	0.18
90	2.45	0.14	0.19
150	2.63	0.17	0.19
195	2.79	0.34	0.17
224	2.96	0.4	0.16

Degree: 30

rotor Speed	Voltage	Drag	Lift
75	3.18	0	0.16
90	3.19	0.03	0.16
150	3.32	0.14	0.12
195	3.39	0.31	0.06
224	3.47	0.38	0.04

All the drag and lift values for different RPMs and angles are written as a table which some parts of it is shown in table (4-2).

2- The figure (4-8) shows the drag and the lift forces when the angle of attack is 15° and the RPM is 40,500. It shows that at the point A, both produced drag and lift are equal and before the point A, the lift is higher than the drag. Hence, the vehicle is able to fly before this point. But, besides drag and lift, the weight of the vehicle is another factor that must be considered in the flight. Whenever the produced thrust and the vehicle weight are equal, the vehicle is able to hover.

Then, in addition to the drag, the weight of the vehicle is essential for flight performance. Therefore, the vehicle is flying before the point A, where it overcomes its weight and the lift force is more than drag force. The flight continues as long as these conditions are satisfied.
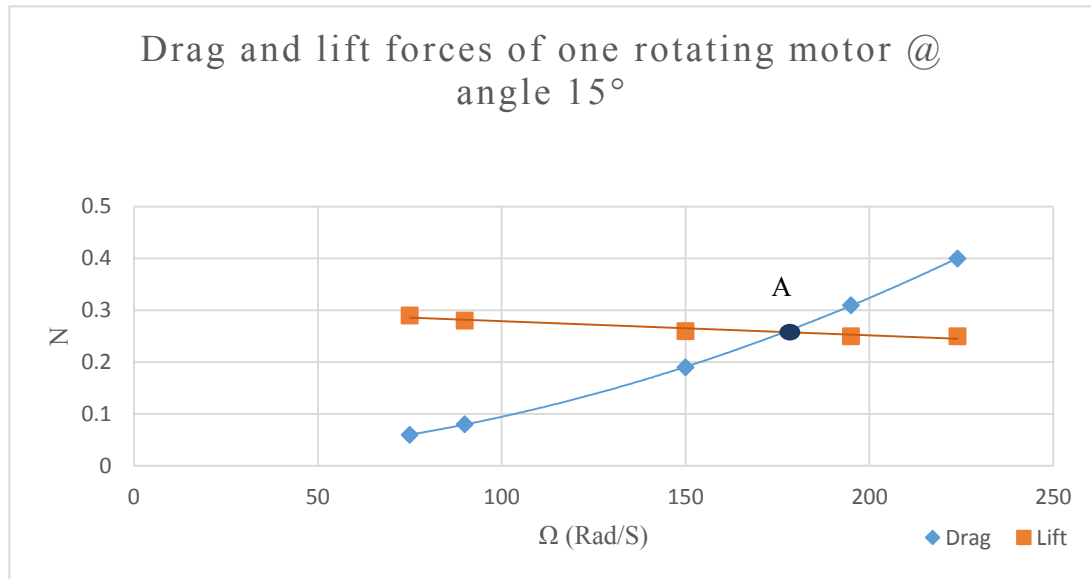

Fig 4-8: The relation between drag and lift forces of one rotating motor @ angle 15°

3- The other concept which is extracted from the graphs and comparison of the drag and lift factors in the figure (4-8) is the saturation point (point A). By comparing these two graphs, at point A, the drag and the lift forces are equal.

It is obvious that beyond point A, the drag force is increasing and lift force continues to decrease. Therefore, at the point A, the actuator starts to stall. The point A is the saturation point. By considering the margin which is needed before reaching the stall point, the flight speed must be controlled up to the margin of the point A. However, operating point should be selected to 80-90% of the margin.

All the results and consequents of the wind tunnel experiments are used in simulating the vehicles of chapter two and three in the following part of this chapter.

Part 2

4-2 Simulating and Modeling the Mathematical Concepts of Chapter Two and Three

In this study, MATLAB-Simulink software [51] is used for simulating the performance of the drone. This software is used to study, examine and design the systems and products in different fields by scientists and engineers. Some of its applications are named as mathematics, expanding the algorithms, do simulation and modeling, computer vison, computation, control design, robotics, image processing and many others. The base of this software is matrix computation which make the mathematics formulation very easy. There is a large library of toolboxes in it that take less time to write a system.

First section (4-2-2) includes the standard quadcopter simulation. All steps of simulating a quadcopter are explained same as the control system parameters, angular squared speed and dynamics.

Section two (4-2-3) presents the designed vehicle of this study. As it has been explained, the vehicle is a 6-motor drone acting in two planes. All the simulation steps like as the control system parameters, angular squared speed and dynamics are explained in details.

In the last section (4-2-4), both vehicles simulation results are compared and their graphs are shown and studied in details.

4-2-1 The General Concepts for Simulating the Drone

A general block diagram which is shown in figure (4-9) [35, 36, 52, 51], provides an overview of the quadcopter modelling. The objectives of each block are explained in the further paragraphs:(a) Trajectory block (b) Controller lock (c) Motor block (d) Dynamics block.
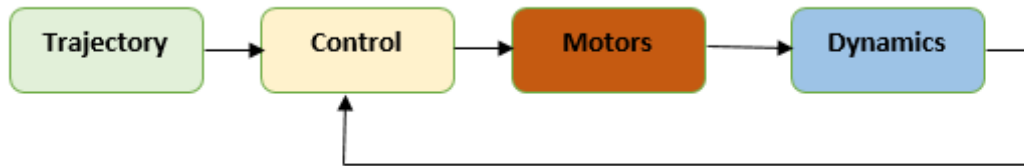

Figure 4-9: The block diagram of a quadcopter modeling

a) Trajectory block:

The propose of the vehicle is expressed by the trajectory block. There are two ways to implement this block. It may be put in the MCU's ROM as an autonomous feature or be transferred by the pilot via the wireless communication devices. In this case, the task can be changed by the user via utilizing the remote controller (RC) and RF transmitter which transmit the task details to the RF receiver that is located on the vehicle. While the vehicle is assumed as an autonomous one, no communication is needed. Since a prototyped drone is not made in this study, the autonomous consideration is implemented.

The flight trajectory must be considered as the first step of the plan in the simulating. Therefore, task block generates the desired trajectory for the flight. The vehicle follows the trajectory and the desired set of positions (X_d, Y_d, Z_d) and Euler angles $(\varphi_d, \theta_d, \psi_d)$ are established.

b) Controller block:

The feedback controller is used to control the quadcopter's position and attitude. This block represents an algorithm which grant the map, the plan of the trajectory and recognizing of the obstacles. The feedback helps the controller to evaluate the motion development of the vehicle. One of the practical techniques for controlling a system is PID techniques which are explained in following in details.

PID techniques as a controller:

One of the practical linear regulators in the industrial field is the PID type. There are three key reasons to implement it.

- Uncomplicated construction
- Suitable achievement in many operations
- Be adjustable in case of no special model for the controlled system.

Although, there are different algorithms which yield the better results than PID, due to the above reasons, PID is outmost selected. The basic control in the robotics are using the PID algorithms. The PID controller structure includes three tunable contributions (the proportional gain (K_P), the integral gain (K_I) and the derivative gain (K_D)) as shown in equation (4-1) and figure (4-10).

$$U(s) = K_P + \frac{K_I}{s} + K_D.s \qquad\qquad (4\text{-}1)$$
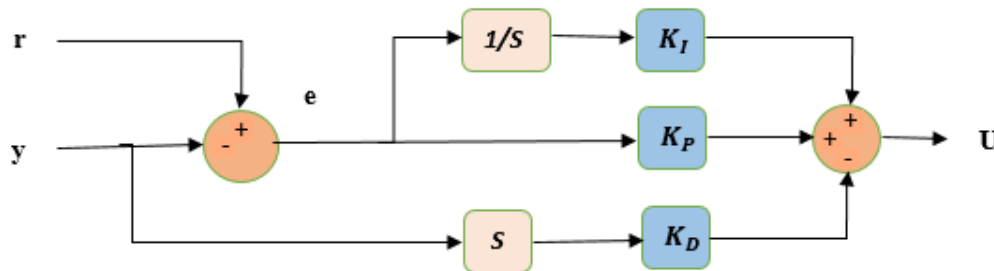

Figure 4-10: PID structure

In the above equation and figure, the derivation and integration operations are shown by s and $\frac{1}{s}$ respectively. Where U is the typical controlled variable.

1-Proportional gain (K_P):

The first element of the PID, (K_P) is proportional to the error and by increasing its value the required time to reach the desired output signal is reduced.

2-Integral gain (K_I):

By the integral of the error, the error is trended to zero. In order to rectify the steady-state error feedback system, this value (K_I) must be boosted. However, this increases the adjustment time.

3-Derivative gain (K_D):

This gain (K_D) is changed by the derivative of the error. By increasing this value, the overshoot time decreases. This gain does not have influence on the steady-state error instantly but it provides damping characteristic in the system.

Therefore, the model is allowed to use a larger K_P value by providing damping characteristic of the derivative gain (K_D).

c) The motor block:

The motor block calculates the angular speed of the propellers. The motor-propeller system is explained in chapter 2. This is obvious that by using mechanics and electronics components, the motor block connects the controller algorithms to the dynamics of the vehicle. The thrust and moment of the quadcopter is directly related to the square of the angular speed of the propeller.

d) Dynamics block:

This block contains the relations of the position and Euler angles. The angular speed of the propellers represents the inputs of this block to evaluate the body position and Euler angles. The output of this block which is the measured positions and Euler angles of the body are used as the feedback of the controller. These values are compared with the desired inputs of the controller. So the prospected trajectory is thus followed by minimization of the error.

4-2-2 The Modeling of the Control of the Standard Quadcopter

The most important part of the simulating is the modeling of the control unit [37, 35, 51]. The equations which are used in the control modelling of the standard quadcopter are presented below.

In the second chapter, the dynamics of the standard quadcopter presents in detail the equation of the motion of the quadrotor. Therefore, the fundamental aspect is repeated like as the equation (4-2) by considering the basic motion commands. These equations express the accelerations along the six degrees of freedom of the flying drone.

$$(4\text{-}2)$$

$$
\xi = \begin{cases}
\ddot{x} = (C\varphi\, S\theta\, C\psi + S\varphi\, S\psi)\dfrac{U_3}{m} \\[2mm]
\ddot{y} = (C\varphi\, S\theta\, S\psi - S\varphi\, C\psi)\dfrac{U_3}{m} \\[2mm]
\ddot{z} = -g + (C\varphi\, C\theta)\dfrac{U_3}{m} \\[2mm]
\ddot{\varphi} = \dfrac{J_{TP}}{I_{XX}}(\Omega_T)\dot{\theta} + \dfrac{U_4}{I_{XX}} \\[2mm]
\ddot{\theta} = \dfrac{J_{TP}}{I_{YY}}(\Omega_T)\dot{\varphi} + \dfrac{U_5}{I_{YY}} \\[2mm]
\ddot{\psi} = \dfrac{U_6}{I_{ZZ}}
\end{cases}
$$

The next equation (4-3) shows the relation of the propeller squared speed with the basic motions.

$$
\begin{cases}
U_3 = b(\Omega_1^2 + \Omega_2^2 + \Omega_3^2 + \Omega_4^2) \\
U_4 = bl(\Omega_4^2 - \Omega_2^2) \\
U_5 = bl(\Omega_3^2 - \Omega_1^2) \\
U_6 = d(\Omega_2^2 + \Omega_4^2 - \Omega_1^2 - \Omega_3^2)
\end{cases}
\qquad (4\text{-}3)
$$

The equation (4-4) displays the relation between the propellers' speed and motors' voltage by considering the dynamics of the motors.

$$(J_P + \eta \, N^2 J_M) \, \dot{\Omega} = -\frac{K_M K_E}{R} \eta \, N^2 \Omega + \frac{K_M}{R} \eta \, N \, v - d\Omega^2 \tag{4-4}$$

Theoretically, by double integrating the acceleration, the quadcopter position is achievable. Therefore, the internal state and the voltages of the motors must be taken into accounts for this operation which is necessary in formulating the direct kinematics and dynamics.

Given the need of stability of the quadcopter, the voltage fed to the motors must be found to position the quadcopter in the required point as the per the mission. This process is known as the inverse kinematics and dynamics. The inverse operation is an inverse problem with potential multiple solutions, unlike the direct operations. Hence, it would be more complicated to take in accounts the inverse operation. Therefore, all the dynamics concepts must be simplified to easily get an inverse model and be able to use it in the control algorithm. Due to the following assumptions, the equation (4-2) can be rearranged as the equation (4-5).

- The flight is taken into account at hovering condition, then no changes happen in the angular contributors (specifically for roll and pitch), and the gyroscopic effects are neglected.

- The transfer matrix Γ_θ which is used for transferring the angular velocity from the body frame to the earth frame is considered as the identity matrix, because of positioning in the hovering condition.

- In order to controlling the vehicle only with the four motors, more variables are not considered. Therefore, the control algorithm is assumed to stabilize the attitude and the height. Then from the six equations in the equation (4-2), the equation which are related to X and Y positions have been removed.

$$\begin{cases} \ddot{Z} = -g + (C \, \varphi \, C \, \theta) \dfrac{U_3}{m} \\ \ddot{\varphi} = \dfrac{U_4}{I_{XX}} \\ \ddot{\theta} = \dfrac{U_5}{I_{YY}} \\ \ddot{\psi} = \dfrac{U_6}{I_{ZZ}} \end{cases} \tag{4-5}$$

The control algorithm receives and processes data as the inputs, the data from the task and the feedbacks are received. This algorithm uses several constants and variables which are related to

the dynamics and the quadcopter states for the computation. The output of the algorithm is a signal for the four motors to make the required power to follow the trajectory.

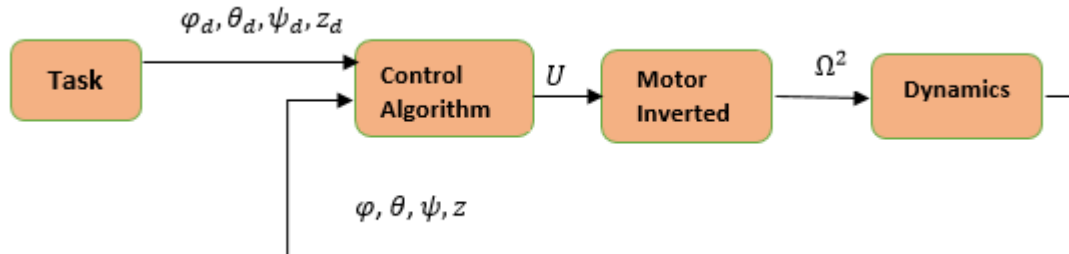The control consists of three components as illustrated in figure (4-11).

Figure 4-11: Control system diagram

In the control system, the first module is the control algorithm. The task and the feedback of the system are processed at this step. The output signal is the basic movements which the position error is stabilized through this block.

The block diagram of the four control systems for stabilizing the attitude and the height are shown and described in the following scheme
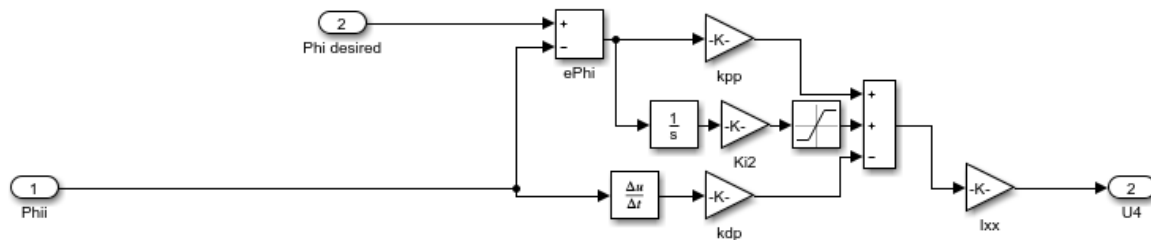
Roll Controller:

Figure 4-12: Roll control block diagram

where, φ_d (rad) is the desired roll angle, φ (rad) represents the measured roll angle, e_φ (rad) is the roll error and the required roll torque is represented as the U_4 (N.m). K_{P_p} (s^{-2}), K_{D_p} (s^{-1}) are control parameters and I_{XX} (N.m) is the moment of inertia of the body around the X-axis. This block diagram is made by considering the equation ($\ddot{\varphi} = \frac{U_4}{I_{XX}}$) which is results in the roll control U_4.
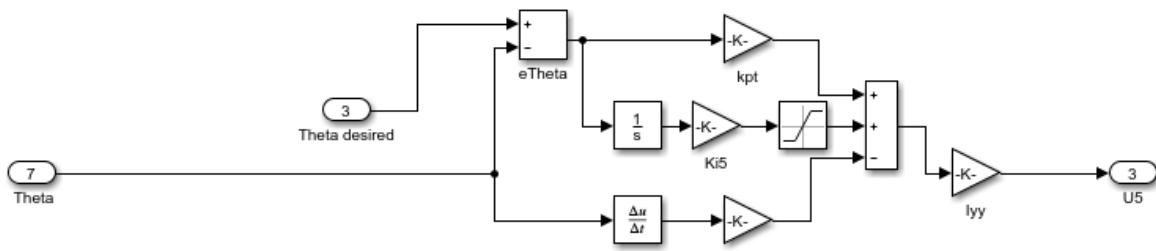
Pitch controller:

Figure 4-13: Pitch control block diagram

Where, θ_d (rad) is the desired pitch angle, θ (rad) represents the measured pitch angle, e_θ (rad) is the pitch error and the required pitch torque is represented as the U_5 (N.m). K_{P_t} (s^{-2}), K_{D_t} (s^{-1}) are control parameters for the pitch control and I_{YY} (N.m) is the moment of inertia of the body around the Y-axis. This block diagram is made by considering the equation ($\ddot{\theta} = \frac{U_5}{I_{YY}}$) which is resulted to the roll control U_5.

Yaw controller:

Figure 4-14: Yaw control block diagram

Here, ψ_d (rad) is the targeted yaw angle, ψ (rad) represents the measured yaw angle, e_ψ (rad) is the yaw error and the required yaw torque is represented as the U_6 (N.m). $K_{P_{ps}}$ (s^{-2}), $K_{D_{ps}}$ (s^{-1}) are control parameters for the yaw control and I_{ZZ} (N.m) is the moment of inertia of the body around the Z-axis. This block diagram is made by considering the equation ($\ddot{\psi} = \frac{U_6}{I_{ZZ}}$) which is resulted to the yaw control U_6.
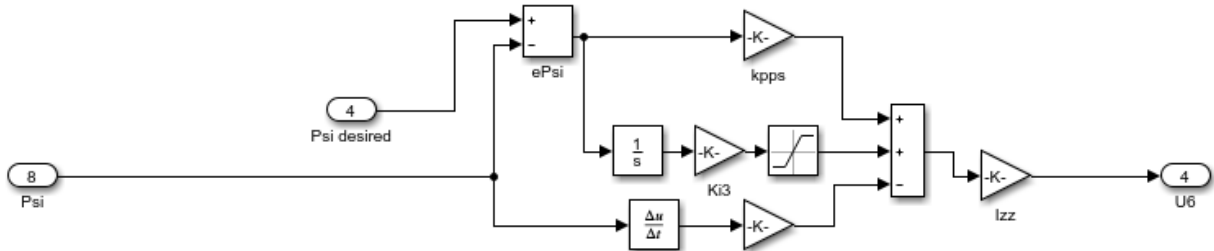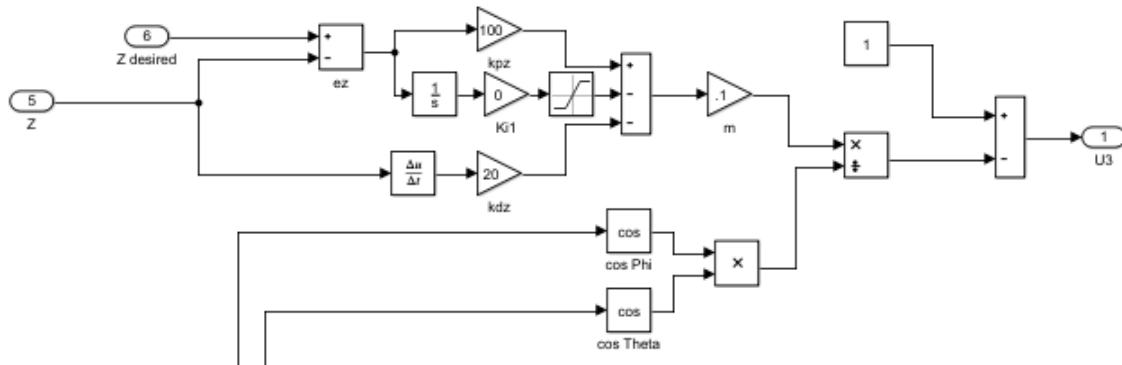
Height controller:

Figure 4-15: Height control block diagram

Where, Z_d (m) is the desired height, Z (m) represents the measured height, e_Z (m) is the height error and U_3 (N) is the required thrust. K_{P_Z} (s^{-2}), K_{D_Z} (s^{-1}) are control parameters for the height and I_{ZZ} (N.m) is the moment of inertia of the body around the Z-axis. g $(m \ s^{-2})$ is the gravity acceleration, m (Kg) is the mass of the quadcopter, $C\varphi$ is the roll angle cosine and $C\theta$ is the pitch angle cosine. This block diagram is built by considering the equation ($\ddot{Z} = -g + (C \varphi \ C \theta)\frac{U_3}{m}$) which is resulted to the height control U_3.

The second block of the control system (figure 4-11) is the inverted movements equations. By using the four basic motion signals from the first block, the squared speed of the propellers is computed. The movements matrix can be inverted to identify the relationship between the U and Ω in order to ensure nonzero determinant of this matrix. A snapshot of this block is shown as figure (4-16).
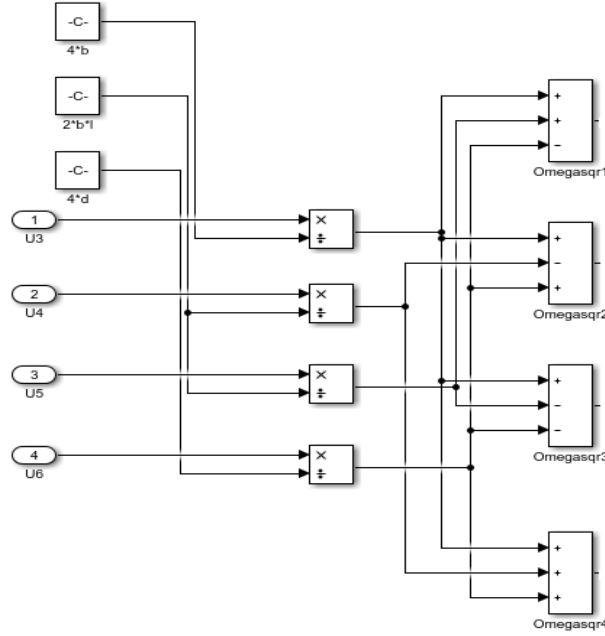
Figure 4-16: The relationship between U and Ω

The inverted equations are written as the equation (4-6).

$$\begin{cases} \Omega_1^2 = \dfrac{1}{4\,b}\,U_3 - \dfrac{1}{2\,b\,l}\,U_5 - \dfrac{1}{4\,d}\,U_6 \\[2mm] \Omega_2^2 = \dfrac{1}{4\,b}\,U_3 - \dfrac{1}{2\,b\,l}\,U_4 + \dfrac{1}{4\,d}\,U_6 \\[2mm] \Omega_3^2 = \dfrac{1}{4\,b}\,U_3 + \dfrac{1}{2\,b\,l}\,U_5 - \dfrac{1}{4\,d}\,U_6 \\[2mm] \Omega_4^2 = \dfrac{1}{4\,b}\,U_3 + \dfrac{1}{2\,b\,l}\,U_4 + \dfrac{1}{4\,d}\,U_6 \end{cases} \qquad (4\text{-}6)$$

In the above equation b and d are the coefficients of the lift and drag forces respectively. In this study, these dimensionless values are attained from the wind tunnel experiments which are described in the first part of this chapter.

The last block of the control system is the dynamics block. A snapshot of this block content is shown in figure (4-17). In MATLAB-Simulink software, using pre-built blocks instead of software codes helps to save the time of makes the computation user friendly. Therefore, this block contains a lot of hardware blocks to gain the positions (x, y, z) and Euler angles (φ, θ, ψ). By double integrating the linear acceleration vector (ddx, ddy, ddz) and the angular acceleration vector (dp, dq, dr), the position and the Euler angles of the vehicle are achieved respectively.
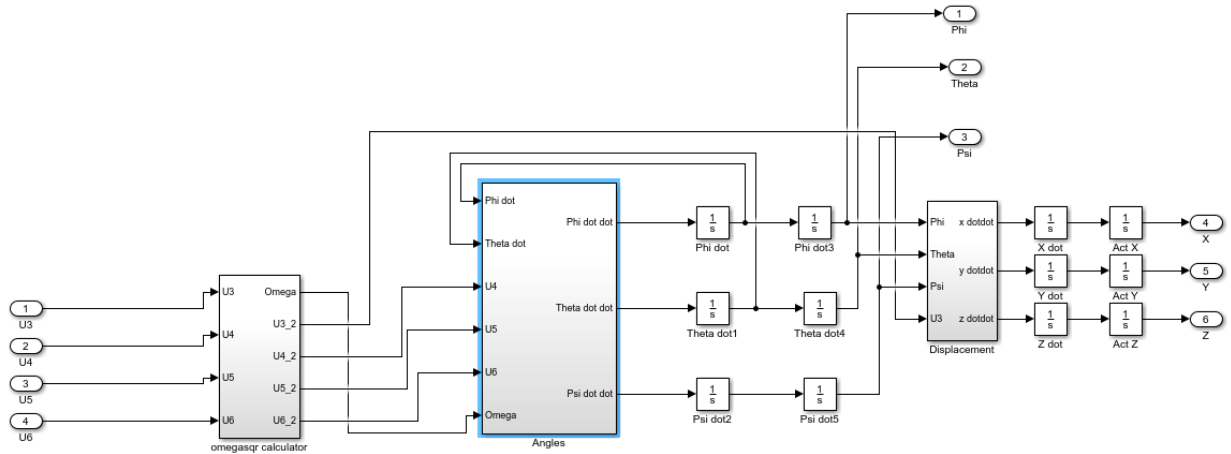
Figure 4-17: Dynamics implementation

4-2-3 The Control Modelling in Details for the Six-Motor Drone

The control system for quadcopter and the 6-motor drone is different in the forward flight only. However, in the take-off and landing conditions and changing the orientations for both models, the control system is same.

In the quadcopter, by using the Euler angles, the vehicle flight to the desired point while follows the laws of motion that have been discussed above. However, in the 6-motor drone, the vehicle reaches the desired point in the forward direction by using the 5th and 6th rotors which are installed for motion in the X direction.

Therefore, in the forward flight, the control system is different from the quadcopter. Four forces are generated in this condition which contributes in performing the flight. They are lift and drag forces which are produced by the four vertical propellers and the two horizontal ones.

Therefore, same as quadcopter, this vehicle is under-actuated due to four forces to control the vehicle and six degree of freedom. Hence, the first force is the generated lift in the x direction and the second one is the drag forces of the 5th and 6th propellers about the φ direction of Euler angle. There are lift and drag forces about z and ψ direction of Euler angle are generated by the four vertical propellers.

91

As it is explained in the first section of part two of this chapter, the desired trajectory of the flight plays an important role in the design of the control system of a drone which obviously, it requires a model of motion for the drone [53, 54, 55, 56, 57]. The equations which are used in this section are extracted from chapter 3. In chapter 3, the dynamics of the 6-motor drone is presented in detail.

Hence, by considering the above paragraphs, the important concepts are repeated as the equation (4-7). By considering the basic motion commands, this equation expresses the acceleration elements of the desired vehicle.

$$
\dot{\xi} = \begin{cases}
\ddot{x} = (c\psi c\theta)\left(\dfrac{U_1 + W_1}{m}\right) + (s\psi s\varphi + c\varphi^2 s\theta)\left(\dfrac{U_3 + W_3}{m}\right) \\[2mm]
\ddot{y} = (s\psi c\theta)\left(\dfrac{U_1 + W_1}{m}\right) + (-c\psi s\varphi + s\psi s\theta c\varphi)\left(\dfrac{U_3 + W_3}{m}\right) \\[2mm]
\ddot{z} = -g - (s\theta)\left(\dfrac{U_1 + W_1}{m}\right) + (c\theta c\varphi)\left(\dfrac{U_3 + W_3}{m}\right) \\[2mm]
\ddot{\varphi} = \dfrac{J_{TP}}{I_{XX}}(\Omega_2^2 + \Omega_4^2 - \Omega_1^2 - \Omega_3^2)\dot{\theta} + \dfrac{U_4}{I_{XX}} \\[2mm]
\ddot{\theta} = \dfrac{J_{TP}}{I_{YY}}(\Omega_2^2 + \Omega_4^2 - \Omega_1^2 - \Omega_3^2)\dot{\varphi} \\[2mm]
\ddot{\psi} = \dfrac{J_{TP}}{I_{ZZ}}(\Omega_5^2 - \Omega_6^2)\dot{\varphi} + \dfrac{U_6}{I_{ZZ}}
\end{cases}
\tag{4-7}
$$

The next equation (4-8) shows the relation of the propellers squared speed associated with the basic motions.

$$
U = \begin{cases}
U_1 = b\left(\Omega_5^2 + \Omega_6^2\right) \\
U_2 = 0 \\
U_3 = b(\Omega_1^2 + \Omega_2^2 + \Omega_3^2 + \Omega_4^2) \\
U_4 = d\left(\Omega_5^2 - \Omega_6^2\right) \\
U_5 = 0 \\
U_6 = d(\Omega_2^2 + \Omega_4^2 - \Omega_1^2 - \Omega_3^2)
\end{cases}
\tag{4-8}
$$

The equation (4-9) shows the lift and drag forces which are produced by the body of the vehicle (wing).

$$W = \begin{cases} w_1 = -\dfrac{1}{2}\,\rho\,V^2\,A\,c_d \\ w_2 = 0 \\ w_3 = \dfrac{1}{2}\,\rho\,V^2\,A\,c_l \\ w_4 = 0 \\ w_5 = 0 \\ w_6 = 0 \end{cases} \qquad (4\text{-}9)$$

The equation (4-10) displays the relation between the propellers speed and motors power voltage by considering the motors dynamics.

$$(J_P + \eta\,N^2 J_M)\,\dot{\boldsymbol{\Omega}} = -\frac{K_M K_E}{R}\,\eta\,N^2\boldsymbol{\Omega} + \frac{K_M}{R}\,\eta\,N\,v - d\boldsymbol{\Omega}^2 \qquad (4\text{-}10)$$

The control model of all the take-off, landing and orientations is the same as what is written in section two of this part (give the equations#). Though, in the forward flight, the control model is different from the one of the standard quadrotor. Therefore, in order for the following consideration, the equation (4-7) is rearranged as the equation (4-11).

$$\dot{\xi} = \begin{cases} \ddot{x} = (c\psi c\theta)\left(\dfrac{U_1 + W_1}{m}\right) + (s\psi s\varphi + c\varphi^2 s\theta)\left(\dfrac{U_3 + W_3}{m}\right) \\ \ddot{z} = -g - (s\theta)\left(\dfrac{U_1 + W_1}{m}\right) + (c\theta c\varphi)\left(\dfrac{U_3 + W_3}{m}\right) \\ \ddot{\varphi} = \dfrac{J_{TP}}{I_{XX}}(\Omega_2^2 + \Omega_4^2 - \Omega_1^2 - \Omega_3^2)\dot{\theta} + \dfrac{U_4}{I_{XX}} \\ \ddot{\psi} = \dfrac{J_{TP}}{I_{ZZ}}(\Omega_5^2 - \Omega_6^2)\dot{\varphi} + \dfrac{U_6}{I_{ZZ}} \end{cases} \qquad (4\text{-}11)$$

All four vertical propellers are rotating in the same speed to maintain the hover condition. Therefore, there is no trend to move the vehicle about any axis (x, y, z) and no movement happens with respect to Euler angles. The only motion is in the forward direction (X-direction) and all the gyroscopic effects are neglected. The only forces are the drag and lift forces which are

generated by all 6 rotors in different directions. By changing these forces, the vehicle can be controlled. Thus, there are four forces and six degree of freedom, the design is under-actuated. Then, from the 6 equations of (4-7), y position and θ Euler angle are not used in the control model given the fact that there is no force in these two directions and hence, no control is achieve them.

Hence, the control model for this design is the same as the quadcopter (figure 4-11). However, their blocks contents are different due to the differences of the constitutive equations.

The first block in the control model is the control algorithm which is shown in the figure below (4-18).
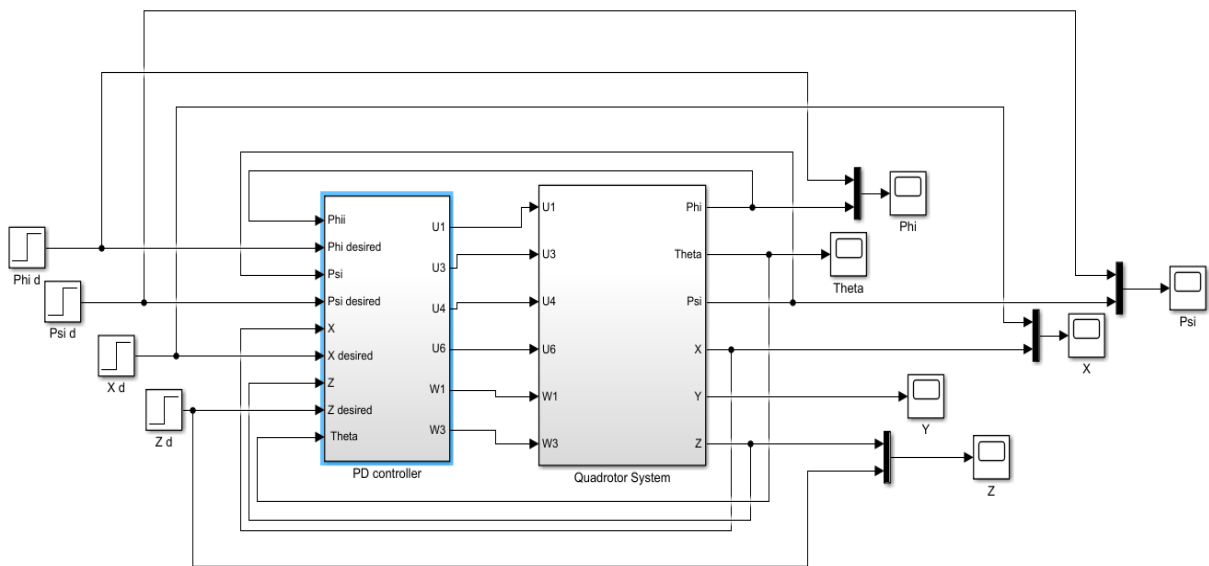

Figure 4-18: The PID controller block contains the control algorithm

All the control parameters are presented in the following paragraphs and their flowcharts in the Simulink software are illustrated for more clarification. Figure (4-19) shows some part of the X controller and Z controller as a screenshot.

The forward motion controller:

In the figure (4-19), X_d (m) is the desired forward distance , X (m) represents the measured forward distance, e_X (m) is the distance error and U_1 (N) is the required thrust. K_{P_X} (s^{-2}), K_{D_X} (s^{-1}) are control parameters for the distance and I_{XX} (N.m) is the moment of inertia of the body

around the X-axis. m (Kg) is the mass of the vehicle, $c\varphi$ is the roll angle cosine, $c\theta$ is the pitch angle cosine, $c\psi$ is the yaw angle cosine, $s\theta$ is the pitch angle sine, $s\psi$ is the yaw angle sine. This block diagram is built by considering the equation ($\ddot{x} = (c\psi c\theta)\left(\frac{U_1+W_1}{m}\right) +$ $(s\psi s\varphi + c\varphi^2 s\theta)\left(\frac{U_3+W_3}{m}\right)$) which is resulted to the X (forward distance) control U_1.
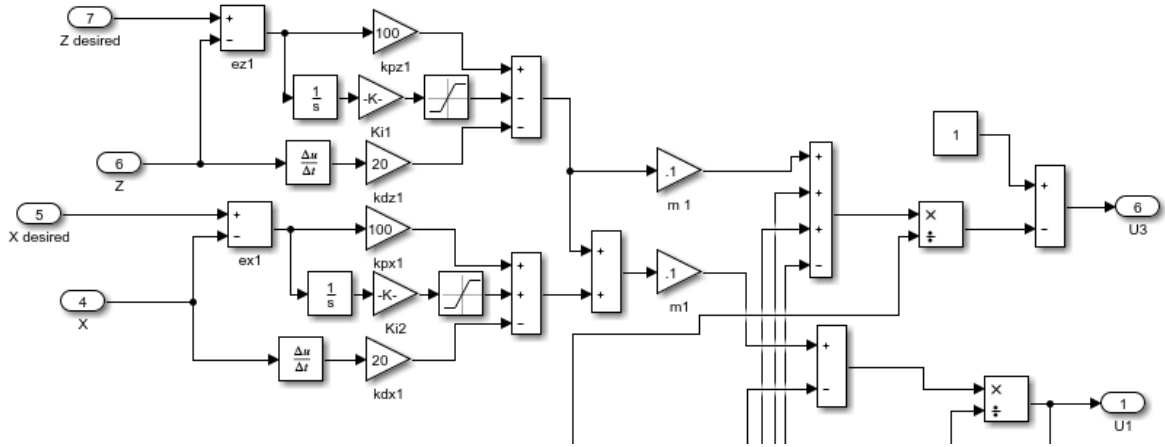

Figure 4-19: Some part of the X controller and Z controller

The height controller:

In the figure (4-19), Z_d (m) is the desired height, Z (m) represents the measured height, e_z (m) is the height error and U_3 (N) is the required thrust. K_{P_Z} (s^{-2}), K_{D_Z} (s^{-1}) are control parameters for the height and I_{ZZ} (N.m) is the moment of inertia of the body around the Z-axis. g ($m\ s^{-2}$) is the gravity acceleration, m (Kg) is the mass of the quadcopter, $C\varphi$ is the roll angle cosine, $C\theta$ is the pitch angle cosine $s\theta$ is the pitch angle sine. This block diagram is built by considering the equation ($\ddot{z} = -g - (s\theta)\left(\frac{U_1+W_1}{m}\right) + (c\theta c\varphi)\left(\frac{U_3+W_3}{m}\right)$) which is resulted to the height control U_3.
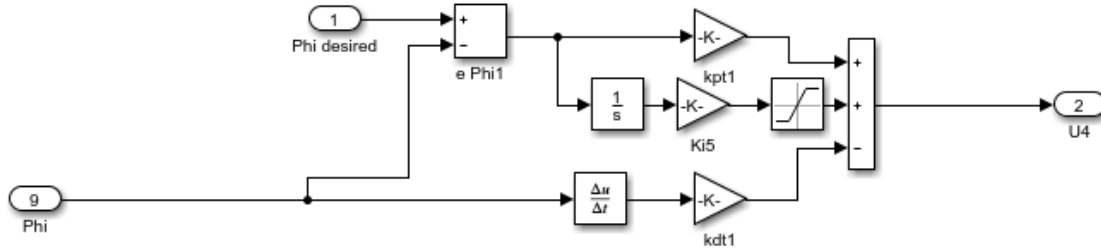
Roll Controller:

Figure 4-20: Roll control block diagram for 6-motor drone

Here, φ_d (rad) is the desired roll angle, φ (rad) represents the measured roll angle, e_φ (rad) is the roll error and the required roll torque is represented as the U_4 (N.m). K_{P_t} (s^{-2}), K_{D_t} (s^{-1}) are control parameters and I_{XX} (N.m) is the moment of inertia of the body around the X-axis. This block diagram is made by considering the equation ($\ddot{\varphi} = \frac{U_4}{I_{XX}}$) which is resulted to the roll control U_4.

Yaw controller:
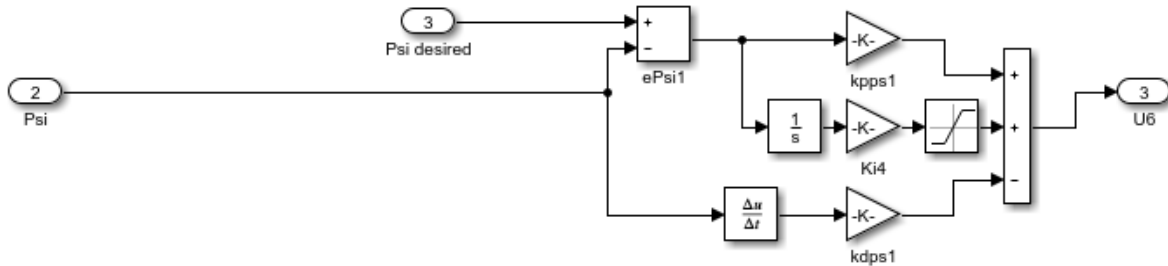
Figure 4-21: Yaw control block diagram for 6-motor drone

Where, ψ_d (rad) is the desired yaw angle, ψ (rad) represents the measured yaw angle, e_ψ (rad) is the yaw error and the required yaw torque is represented as the U_6 (N.m). $K_{P_{ps}}$ (s^{-2}), $K_{D_{ps}}$ (s^{-1}) are control parameters for the yaw control and I_{ZZ} (N.m) is the moment of inertia of the body around the Z-axis. This block diagram is built by considering the equation ($\ddot{\psi} = \frac{U_6}{I_{ZZ}}$) which is resulted to the yaw control U_6.

96

The second block of the control system is the inverted movements equations. By using the four basic motion signals from the first block, the propellers' squared speed are computed by the motion equation (4-8).

The motion equations can be inverted to identify the relationship between the U and Ω, in order to nonzero determinant of this equation. The inverted equations are written as the equation (4-12).

$$\begin{cases} \Omega_1^2 = \dfrac{1}{4\,b}U_2 - \dfrac{1}{4d}U_4 \\[4pt] \Omega_2^2 = \dfrac{1}{4\,b}U_2 + \dfrac{1}{4d}U_4 \\[4pt] \Omega_3^2 = \dfrac{1}{4\,b}U_2 - \dfrac{1}{4d}U_4 \\[4pt] \Omega_4^2 = \dfrac{1}{4\,b}U_2 + \dfrac{1}{4d}U_4 \\[4pt] \Omega_5^2 = \dfrac{1}{2\,b}U_1 - \dfrac{1}{2d}U_3 \\[4pt] \Omega_6^2 = \dfrac{1}{2\,b}U_1 + \dfrac{1}{2d}U_3 \end{cases} \qquad (4\text{-}12)$$

In the above equation b and d are the coefficients of the lift and drag forces respectively. In this study, these dimensionless values are attained by the wind tunnel experiments which are described in the first part of this chapter.

The last block of the control system is the dynamics block. A screenshot of this block content is shown in figures (4-22 and 4-23). In this block, it is shown that the linear acceleration vector (ddx, ddy, ddz) and the angular acceleration vector (dp, dq, dr) are resulted and by double integrating them, the position and the Euler angles of the vehicle are all achieved, respectively.
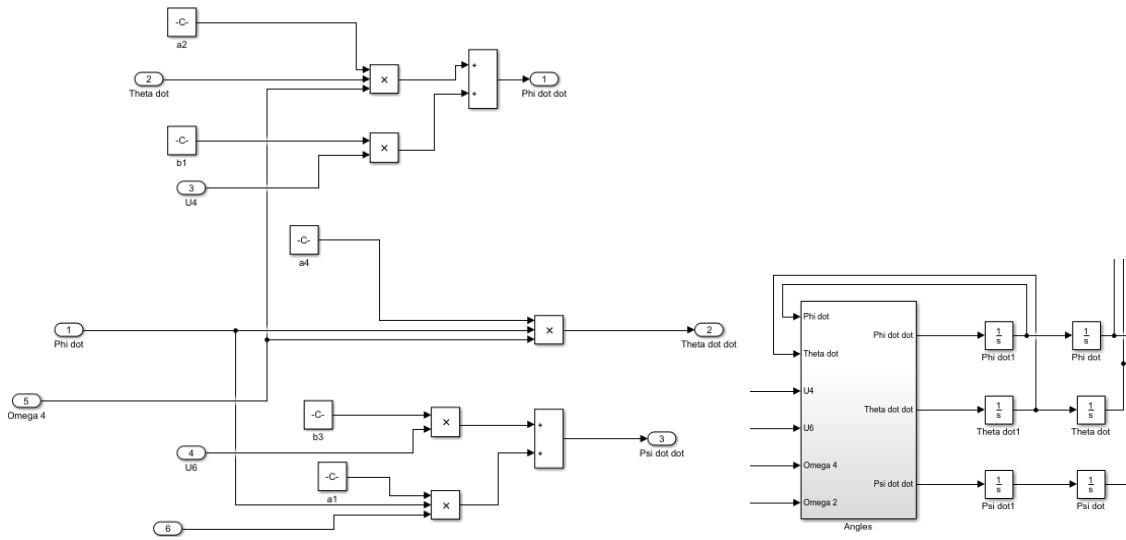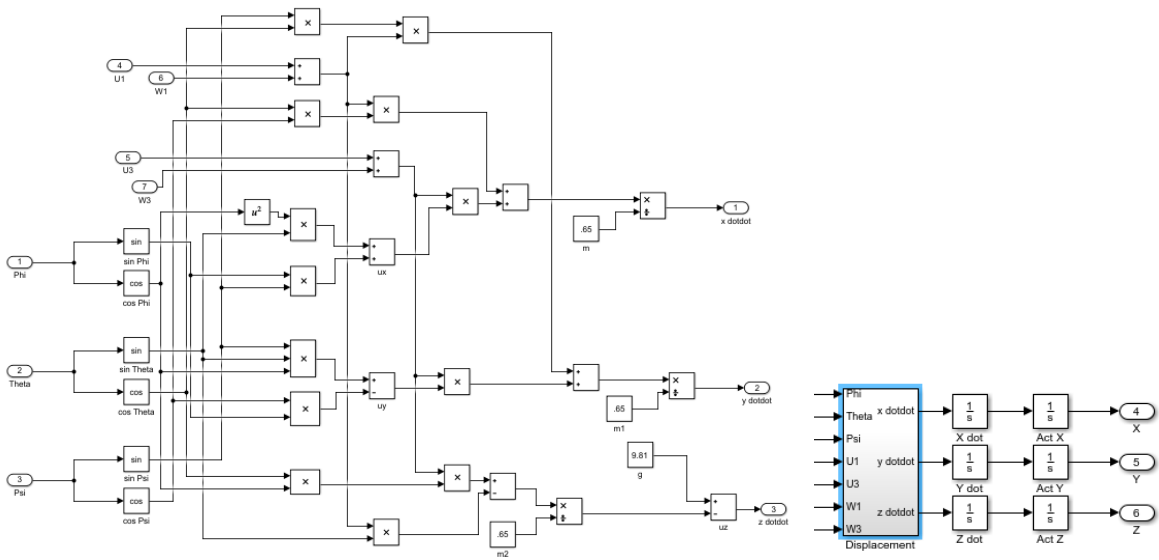
Figure 4-22: The Euler angles (dynamics)

Figure 4-23: The displacements (dynamics)

4-2-4 The Simulation Results of Both Vehicles

The last section of part two represents the simulation results for both quadcopter and 6-motor drone under normal flight conditions. The PID controller model is used in simulation by commanding vehicles to follow the desired inputs.

The desired input items of these two vehicles are different since their controllable items are different. In case of the standard quadcopter, Euler angles and altitude are assumed as the controllable items, while for the 6-motor drone, φ, ψ, x, z are considered to control the vehicle in accordance with the discussion in chapter two and three. The physical parameters of the standard quadcopter and the 6-motor drone are illustrated as the table 4-3 and 4-4, respectively.

Table 4-3: Quadcopter physical parameters

Name	Parameter	Value	Unit
Mass	m	0.1	Kg
Inertia on x axis	I_{xx}	4.6×10^{-4}	$Kg.m^2$
Inertia on y axis	I_{yy}	4.6×10^{-4}	$Kg.m^2$
Inertia on z axis	I_{zz}	3.9×10^{-4}	$Kg.m^2$
Thrust coefficient	b	41×10^{-4}	$N.s^2$
Arm length	l	.23	m
Propeller inertia	J_p	2.4×10^{-8}	$Kg.m^2$
Motor inertia	J_m	2.7×10^{-6}	$Kg.m^2$
Gearbox efficiency	η	12.73	%
Gearbox ratio	r	6.2	$Nill$

Table 4-4: 6-motor drone physical parameters

Name	Parameter	Value	Unit
Mass	m	0.12	Kg
Inertia on x axis	I_{xx}	4.7×10^{-4}	$Kg.m^2$
Inertia on y axis	I_{yy}	5.5×10^{-4}	$Kg.m^2$
Inertia on z axis	I_{zz}	4.3×10^{-4}	$Kg.m^2$
Thrust coefficient	b	41×10^{-4}	$N.s^2$
Arm length	l	.23	m
Propeller inertia	J_p	2.4×10^{-8}	$Kg.m^2$
Motor inertia	J_m	2.7×10^{-6}	$Kg.m^2$
Gearbox efficiency	η	12.73	%
Gearbox ratio	r	6.2	$Nill$

The purpose of this study is to prove the possibility to maintain the equilibrium by considering the desired input values. The comparison of the desired inputs and the overall attitude of the vehicle resulted in errors. By rectifying the errors, systems would be balanced.

The outcome data of simulation shows the control parameters with the quantitative results. All four motions of the vehicle (roll, pitch, yaw and height) are demonstrated by the PID controller. The simulation achievement is satisfactory and are illustrated as the following figures.

In the following figures, six parameters $(\varphi, \theta, \psi, x, y, z)$ are illustrated. For controllable parameters $(\varphi, \theta, \psi, z)$ of the standard quadcopter, two plots are shown in the same figure, the desired plot and the resulted plot. The desired plot is the proposed goal and the resulted plot is the achieved result. These two types of plots are compared to depict the error of the system.
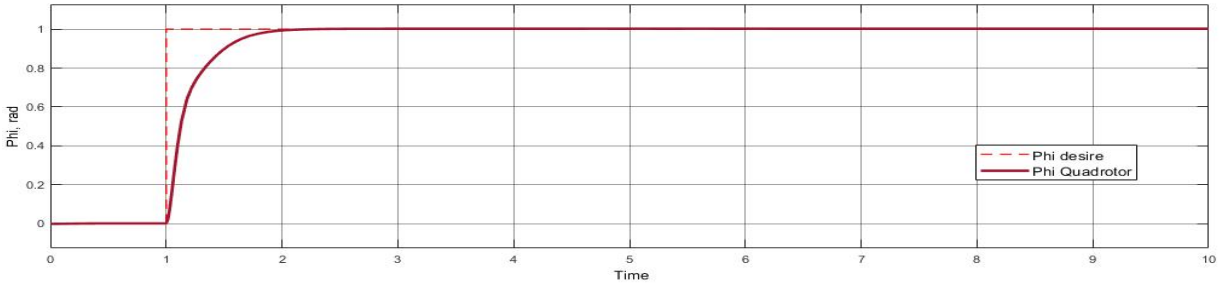
Figure 4-24: Roll [rad] plot of the quadrotor

As it is shown in figure (4-24), the resulted φ is 0 rad from 0 to 1 seconds (same as the desired φ). After 1 second, the desired φ is considered as 1 rad but the resulted φ graph shows that it takes 95% of the second to reach 1 rad. It means that the resulted φ reaches to 1 rad at 1.95 second. Therefore, there is 0.95 second error for the control system of the quadcopter to reach the desired φ.

Figure 4-25: Pitch [rad] plot of the quadrotor

Figure (4-25) shows that the resulted θ is 0 rad from 0 to 1 seconds (same as the desired θ). After 1 second, the desired θ is considered as 1 rad but the resulted θ graph shows that it takes 85% of the second to reach 1 rad. It means that the resulted θ reaches to 1 rad at 1.85 second. Therefore, there is 0.85 second error for the control system of the quadcopter to reach the desired θ.

Figure 4-26: Yaw [rad] plot of the quadrotor

As it is shown in figure (4-26), the resulted ψ is 0 rad from 0 to 1 seconds (same as the desired ψ). After 1 second, the desired ψ is considered as 1 radian but the resulted ψ graph shows that it takes one second to reach 1 radian. It means that the resulted ψ reaches to 1 radian at 2nd second. Therefore, there is 1 second error for the control system of the quadcopter to reach the desired ψ.
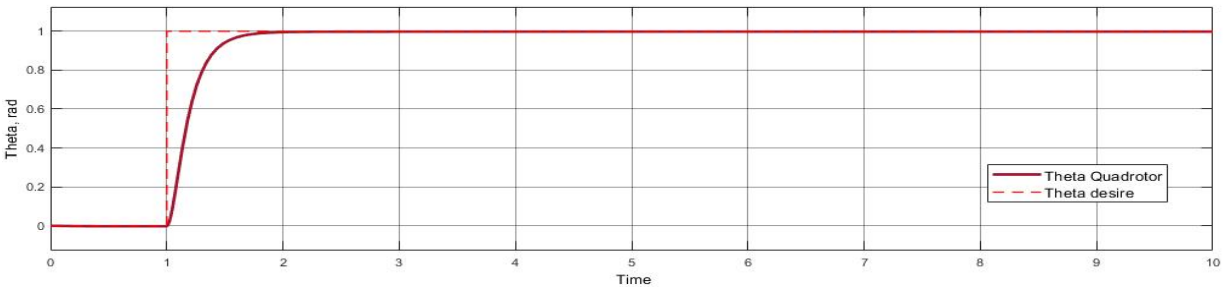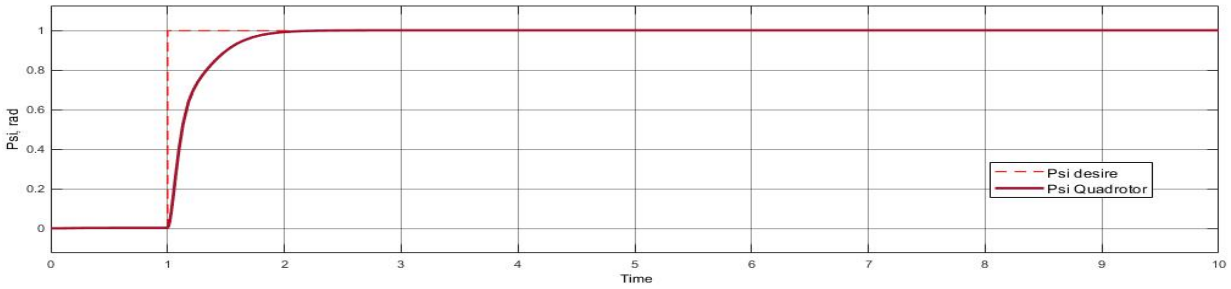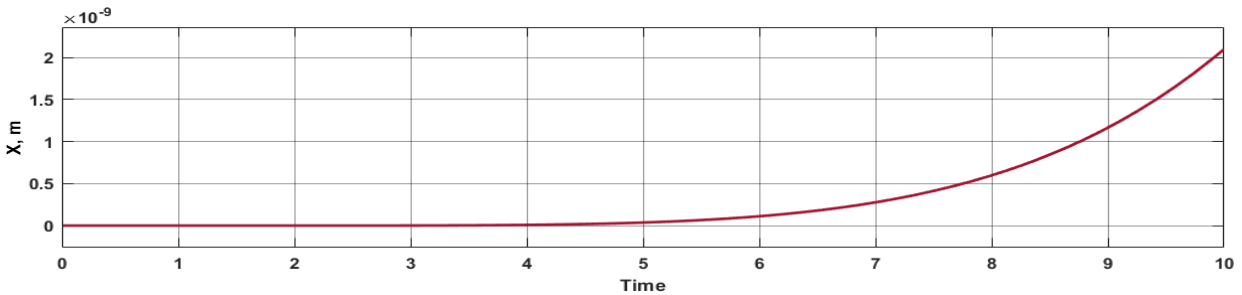

Figure 4-27: x [m] plot of the quadrotor

For the standard quadcopter, the desired graph is not included in the x and y plots. Since x and y are not controllable parameters in the quadcopter. Therefore, making zero changes in these displacements are not achieved but their changes are small amount as illustrated in figures 4-29 and 4-30. The x plot (figure 4-27) shows that from 0 to 4.5 seconds, there is no movement in the x direction and the graph shows 0 m. After 4.5 second, x starts to increase slightly.
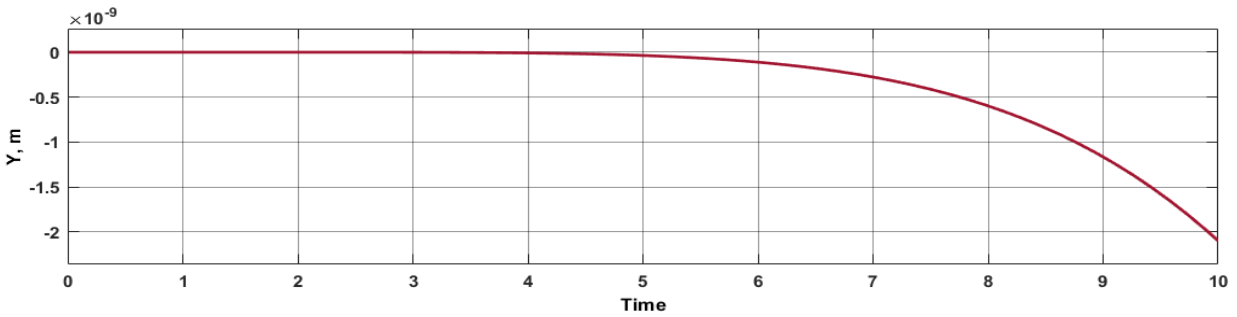
Figure 4-28: y [m] plot of the quadrotor

Figure (4-28) depicts that the quadcopter does not move in the y direction from 0 to 4.5 seconds. After 4.5 second, its value starts to decrease lightly and the vehicle moves in the negative direction of the y axes.
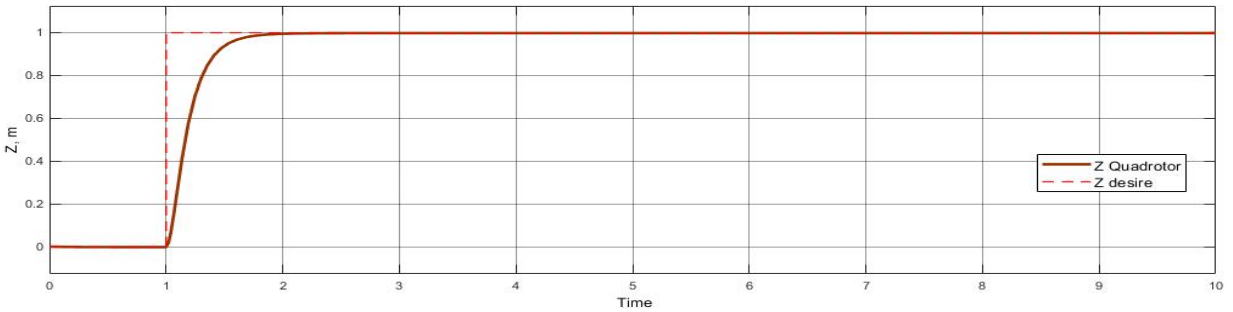
Figure 4-29: z [m] plot of the quadrotor

Figure (4-29) shows the altitude changes of the vehicle. Because of being controllable parameter, desired value is considered for this parameter. Between 0 to 1 seconds, the desired plot is considered 0 m and the resulted plot shows the same value. After 1 second the desired value is considered 1 m, while the resulted z plot shows that it takes 80% of the second to reach 1 m. It means that the resulted z reaches to 1 meter at 1.8 second. Therefore, there is 0.8 second error for the control system of the quadcopter to reach the desired z.
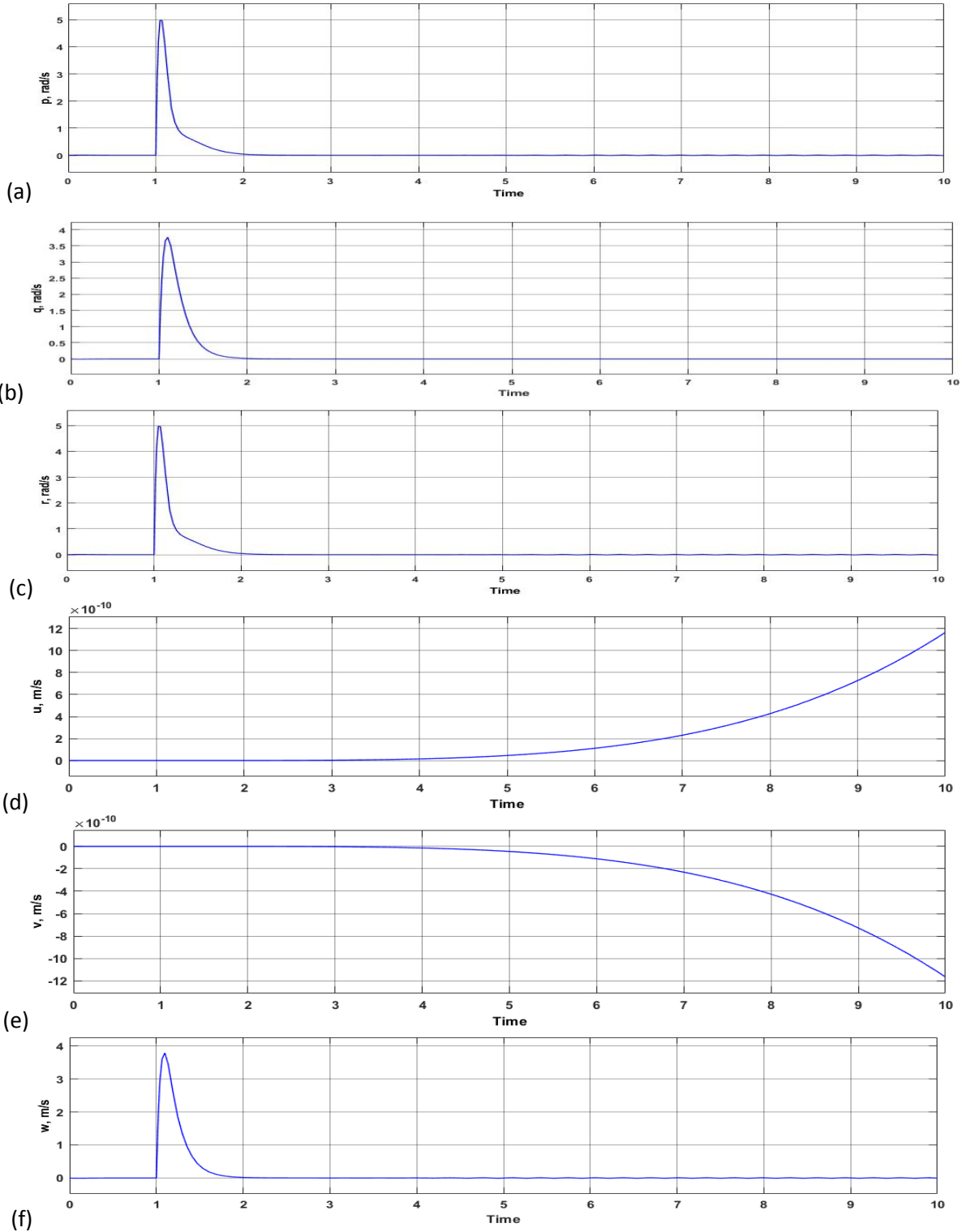
Figure 4-30: Linear and angular velocities of the standard quadcopter: (a) p [rad/s], (b) q [rad/s], (c) r [rad/s], (d) u [m/s], (e) v [m/s], (f) ω [m/s]

104

Figure (4-30) shows all the angular velocities and linear ones for the quadcopter. The first plot determines the angular velocity about φ angle and it is driven to zero. There is a sharp curve which shows the increasing and decreasing of the velocity to increase the angle 1 rad and then makes it stable and constant.

The next two plots are the angular velocities about θ and ψ angles, respectively. There are the same shapes for these two plots as the first one. Since their desired and resulted angle changes are the same.

The forth plot shows the linear velocity in the x direction. It illustrates the increment of the velocity which leads to the increment of the displacement in this direction. But the amount of increment is not remarkable as it shows in the first 10 seconds.

The fifth plot is the linear velocity in the y direction. It shows the decrement of the velocity which leads to the decrement of the displacement in the y direction. But the amount of decrement is not remarkable as it shows in the first 10 seconds.

The last plot is the linear velocity in the z direction. This plot is driven to zero after a sharp curve. This curve shows that the velocity in the z direction increases and decreases and then stables to zero. The increment and decrement of the velocity in the z direction leads to the 1-meter displacement changing in the z direction.

For the six-motor design, the following graphs are depicted as the results of the simulation. The following figures show the linear position and the Euler angles. The desired commands are considered as φ, ψ, x, z in order to the equations in chapter 3. By considering the specific purpose of this design which is fast forward flight, x is considered as one of the significant trajectory parameters. The x plot shows that the resulted x is almost the same as the desired x. Therefore, there is no loss of performance by comparing the 6-motor design with the quadrotor. Moreover, the mobility in the x direction is a controllable parameter.
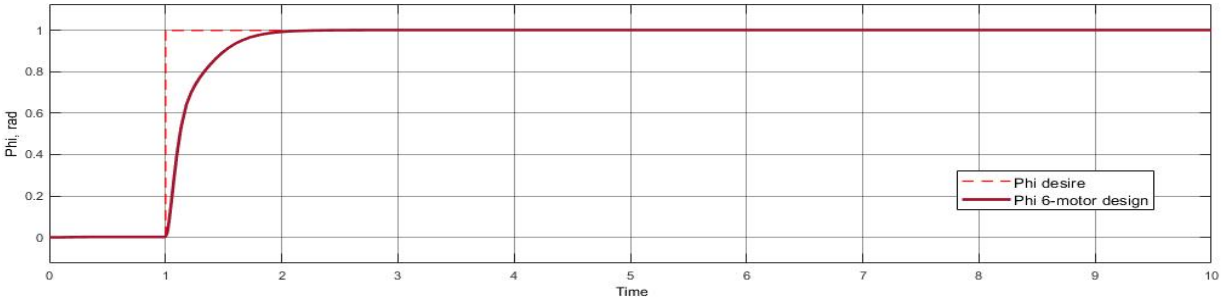
Figure 4-31: Roll [rad] of the 6-motor design

As it is shown in figure (4-31), the resulted φ is 0 rad from 0 to 1 seconds (same as the desired φ). After 1 second, the desired φ is considered as 1 rad but the resulted φ graph shows that it takes one second to reach 1 rad. It means that the resulted φ reaches to 1 rad at 2nd second. Therefore, there is 1 second error for the control system of the 6-motor design to reach the desired φ.

Figure 4-32: Pitch [rad] of the 6-motor design

For the six-rotor vehicle, the desired graph is not included in the θ graph. Since it is not controllable parameter in the six-rotor vehicle. Figure (4-32) shows that θ is 0 and there is no rotation and movement around this angle (θ) .

106
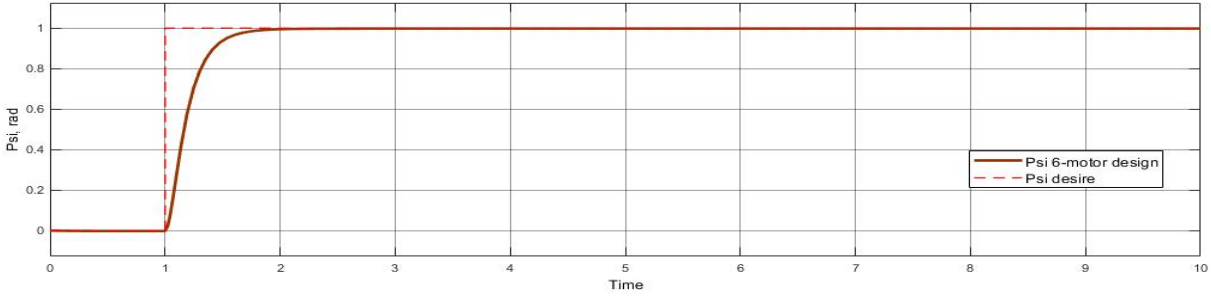
Figure 4-33: Yaw [rad] of the 6-motor design

Figure (4-33) shows that the resulted ψ is 0 rad from 0 to 1 seconds (same as the desired ψ). After 1 second, the desired ψ is considered as 1 rad but the resulted θ graph shows that it takes 95% of the second to reach 1 rad. It means that the resulted ψ reaches to 1 rad at 1.95 second. Therefore, there is 0.95 second error for the control system of the 6-motor design to reach the desired ψ.
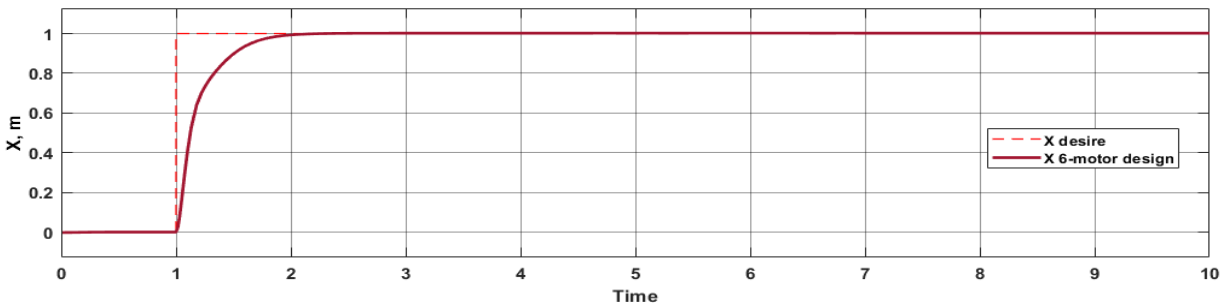
Figure 4-34: x [m], six-motor design

Figure (4-34) shows the movement of the vehicle in the x direction. Because of being controllable parameter, desired value is considered for this parameter. Between 0 to 1 seconds, the desired plot is considered 0 m and the resulted plot shows the same value. After 1 second the desired value is considered 1 m, while the resulted x plot shows that it takes one second to reach 1 m. It means that the resulted x reaches to 1 meter at 2nd second. Therefore, there is 1 second error for the control system of the 6-motor design to reach the desired x.
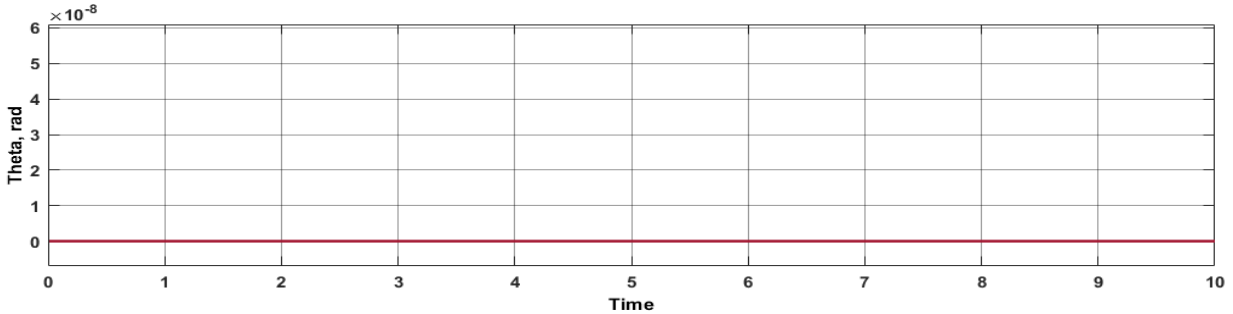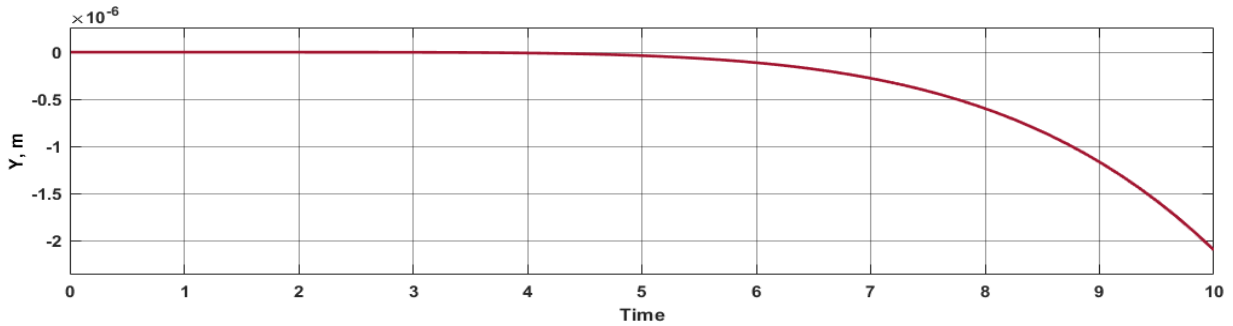
Figure 4-35: y [m], six-motor design

For the six-motor vehicle, the desired graph is not included in the y plot. Since it is not the controllable parameter of the vehicle. Therefore, making zero changes in y displacement is not achieved but its changes is small amount as illustrated in figure (4-35). It is depicted that the vehicle does not move in the y direction from 0 to 4.75 seconds. After 4.75 second, its value starts to decrease lightly and the vehicle moves in the negative direction of the y axes.
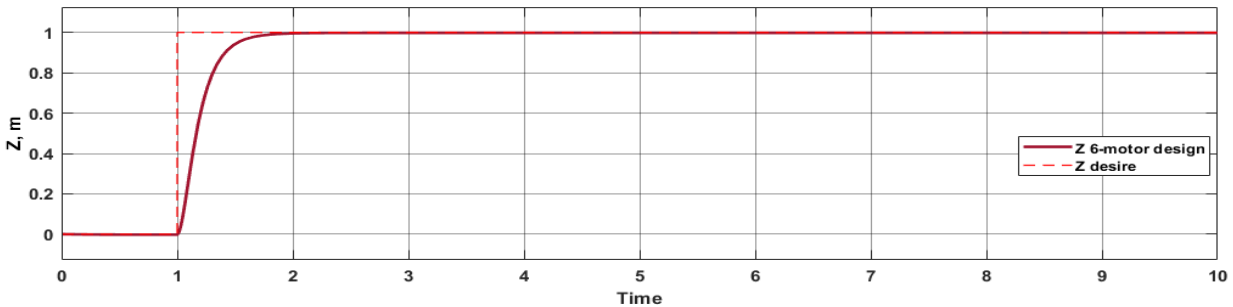
Figure 4-36: z [m], six-motor design

Figure (4-36) shows the altitude changes of the vehicle. Because of being controllable parameter, desired value is considered for this parameter. Between 0 to 1 seconds, the desired plot is considered 0 m and the resulted plot shows the same value. After 1 second the desired value is considered 1 m, while the resulted z plot shows that it takes 85% of the second to reach 1 m. It means that the resulted z reaches to 1 meter at 1.85 second. Therefore, there is 0.85 second error for the control system of the quadcopter to reach the desired z.

(a)

(b)

(c)

(d)

(e)

(f)
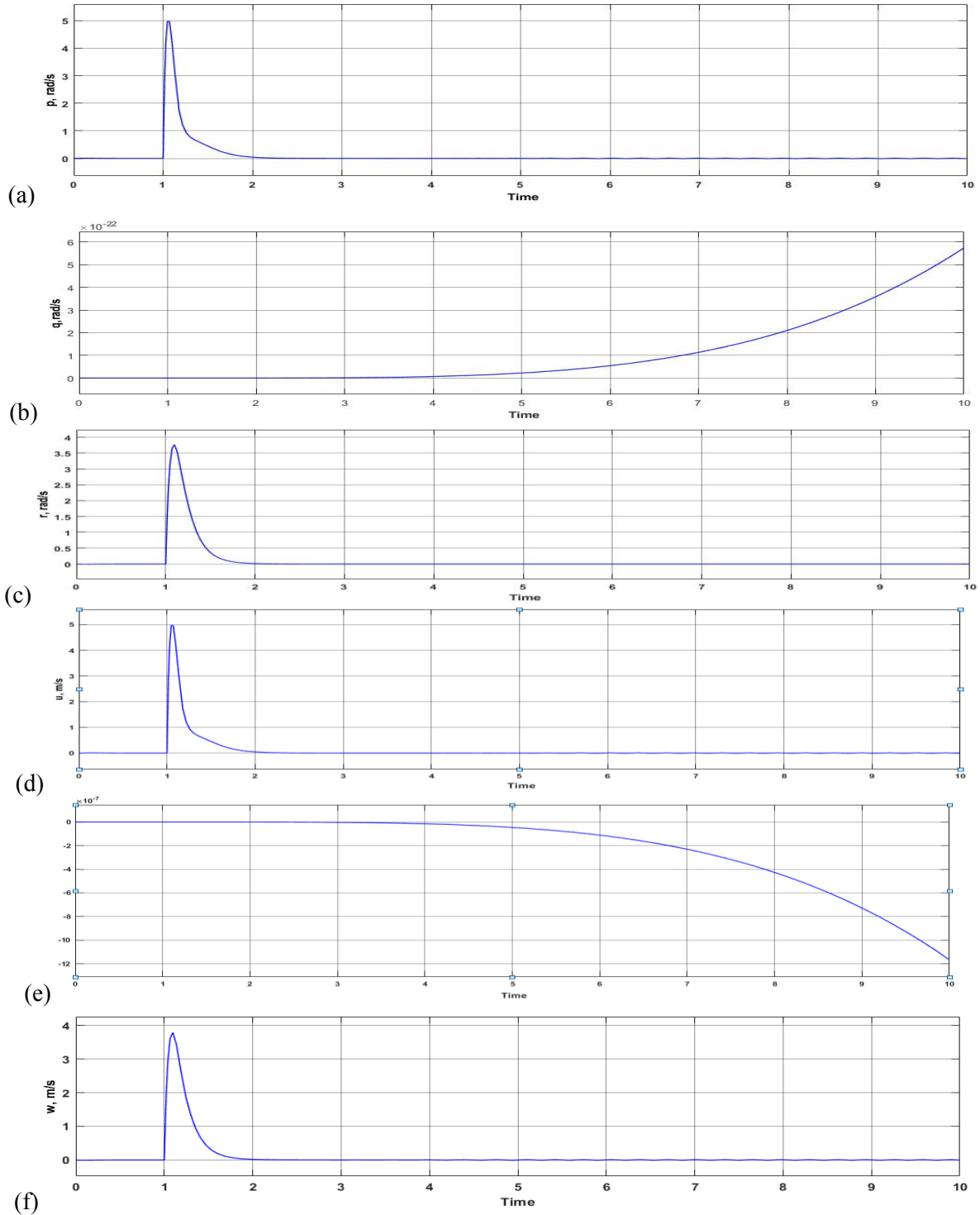
Figure 4-37: Linear and angular velocities of the six-motor design: (a) p [rad/s], (b) q [rad/s], (c) r [rad/s], (d) u [m/s], (e) v [m/s], (f) ω [m/s]

110

Figure (4-37) shows all the angular velocities and linear ones for the six-motor design. The first plot determines the angular velocity about φ angle and it is driven to zero. Only there is a sharp curve which shows the increasing and decreasing of the velocity to increase the angle 1 rad and then makes it stable and constant. The second plot shows the angular velocity about the θ angle. It illustrates an increment slightly which leads to some ignorable changes in the θ angle.

The third plot is the angular velocity about ψ angle. This plot is driven to zero after a sharp curve. This curve shows that the velocity about the ψ angle increases and decreases and then stables to zero. The increment and decrement of the velocity leads to the 1 rad changing about the ψ angle.

The forth plot shows the linear velocity in the x direction. This plot is driven to zero after a sharp curve. This curve shows that the velocity in the x direction increases and decreases and then stables to zero. The increment and decrement of the velocity in the x direction leads to the 1 (m) displacement changing in the x direction.

The fifth plot is the linear velocity in the y direction. It shows the decrement of the velocity which leads to the decrement of the displacement in the y direction. But the amount of decrement is not remarkable as it shows in the first 10 seconds.

The last plot is the linear velocity in the z direction. This plot is driven to zero after a sharp curve. This curve shows that the velocity in the z direction increases and decreases and then stables to zero. The increment and decrement of the velocity in the z direction leads to the 1 meter displacement changing in the z direction.

Comparing the simulation results of these two vehicles shows that both are figured in the equilibrium statuses and the desired positions and Euler angles are resulted. Moreover, the resulted plots of the six-motor UAV design show that the performance of the standard quadrotor and the six-motor UAV design are the same in both modeling which are considered in hover status. While, in the modeling of the six-motor UAV design, displacement in the x direction is the controllable component and the desired value is able to be achieved. Hence, the six-motor UAV design can be controlled in the x direction. While, x is not the controllable component in the quadrotor modeling. Because one of the goal of the six-motor UAV design is fast forward flight, by being able to control the displacement in the x direction, the forward direction motion

would be controlled. Moreover, by comparing both vehicles simulating, it is clear that the movement in the y direction is very small amount. Since, there is not any motor to produce force and torque in the y direction for both vehicles.

Chapter 5

Conclusions and Future Work

5-1 Conclusions

The purpose of this study is to investigate the feasibility to design a type of drone that could move fast forward. This design is an enhanced model of a quadrotor with two more propellers which produce thrust in the horizontal direction. The main goal of this six-rotor is to increase the forward flight speed, while maintaining controllability, maneuverability characteristics and the hovering stability of the standard quadcopter. This designed vehicle is able to perform a trajectory which include five main stages of the mission as it follows:

1) Vertical take-off and hover. 2) Orienting the appropriate direction. 3) Fast forward flight to reach the planned point of the mission. 4) Making and setting the required orientation for landing. 5) Hover and landing.

The feature which is not common to quadrotors is the fast forward motion which contributes to the decrease the flight time while the vehicle is able to stop and hover at any point of the flight to eventually collect more information on any specific point of the mission.

The first step of this project consists of considering all forces and torques on the vehicle. Hence, the mathematical approach further used for the design is investigated. All kinematics and dynamic equations of the standard quadcopter and its actuators are demonstrated by the Newton-Euler formulations.

The mathematical model of the proposed vehicle is presented by using the standard quadcopter mathematical model as the basic model. This model is further used to ensure that the design is feasible and functionally feasible and reliable. The actuators equations of the design follow the standard approach and they are implemented in both classical model and the proposed model. The dynamic performances of the two different systems are then compared. Although no prototype was built, a small quadrotor was used to carry out measurements in the wind tunnel. The measurements in the wind tunnel revealed the lift and drag coefficients for the model. Those

values were used in assessing the performances of the quadrotor. The performance of the six motors drone was obtained from the simulation and compared with the results obtained by the standard quadrotor. The performance of the two systems reveals as being similar.

This study used as solver for the simulation problem the standard Simulink of MATLAB. The control approaches in both vehicles are performed through their controllable actuators. Thus, the controllability of the vehicles is measured and examined by their mathematical models and the results of the simulations are analyzed.

A PID controller is used for both vehicles simulation models. The control system contains three components. The dynamics of both vehicles are divided into three subsystems; motors, angular and linear displacements.

The last step is analyzing the simulation results of both vehicles. The quantitative evaluation of the Simulink results is used to compare the performance of the six-rotor design system with the standard quadcopter. The main objective of this part of the study is to validate the feasibility of the controllers. The simulation results represent the effectiveness of both vehicle models. The built models reveal that both systems respond of same manner to commands. The targeted values are achieved by simulating the two models. In addition, the other parameters of the model which are not evaluated as the targeted parameters are estimates and show the suitable values by considering the vehicles features and mission. All the evaluated compared results illustrate the performance of the concept design. The results of the simulation of the two models indicate that this vehicle is able to perform the fast forward flight and be able to hover at any point of the flight.

Moreover, the aerodynamic forces were estimated by means of the wind tunnel tests. These forces are applied in the vehicles modeling and simulation.

There are multiple feasible applications for this design which the most impressive one is the human transportation. It is known that airplanes fly in corridors. Then the design should be able to deliver a flight height path to prohibit accidents. Therefore, high speed flight in horizontal direction represent an appropriate feature of this type of application to comply with the requirements in the crowded cities transportation. There is no requirement of inclination at of the platform for the proposed design as the standard quad would require some inclination and hence

a lower forward speed. The flight efficiency of the proposed model is improved as the drag of a drone structure is lower when in horizontal attitude vs an inclination of 15°. The proposed model offers less drag force and more lift force as well as thrust in the forward direction.

Although this study carried out using a toy, it is possible to build this design for practical implementations as like as the human transportation vehicle or the precise agricultural drone for monitoring the soil or crops condition.

5-2 The Future Work

Diverse other aspects could be considered as the future work of this study. This design could be analyzed by simulating the model performances while using different types of controls, namely PID controller, LQ controller, Back-stepping controller and etc. The results of various control systems could be compared to select the most appropriate control system.

Aerodynamic performance of the vehicle is another potential direction of research. CFD models could be built and the performance evaluated. The analysis of energy flow in the equipment and the possibility to harvest energy while flying is another potential direction of research.

After validation of the design concept, the next phase of a complex project would be to develop it as a prototype product. The functional prototype would demonstrate the features of the design of a practical manner. Hence, this theoretical idea could be investigated as an aerial vehicle in which one should consider all the real constraints. Wind could be one of the constraints which has impressive significant influence on the light aerial vehicles. The wind influences on the prototype of the vehicle would be evaluated to improve the conceptual design.

Investigating the sizing of the vehicle could represent another aspect of the further studies. Different sizes of this design for various applications can be considered. It could be discussed as a range of sizes namely, the toy size or the human transportation vehicle size.

The design could be further improved by using optimization as the following work of this study. The constraints could be considered as the wind, sensors, dynamic features and so on. Under the considered constraints, the desired factors would be maximized and the undesired factors would be reduced. Therefore, the highest performance would be achieved in order to utilize

optimization tools for modeling of the design. The controllability, maneuverability and stability of the vehicle might be enhanced after performing the optimization of the design.

APPENDIX A

The Rotation Matrix

In this model, the first step is to reach the rotational and translational matrix for more calculations, therefor, the process of getting these two matrixes are explained in detail in this appendix. The following figures are illustrated these three rotations schematics.

- Rotation about the Y-axis of the θ angle (Pitch) through R (y, θ) figure (2-1(a)).
- Rotation about the X-axis of the φ angle (Roll) through R (x, φ) figure (2-1(b)).
- Rotation about the Z-axis of the ψ angle (Yaw) through R (z, ψ) figure (2-1(c)).
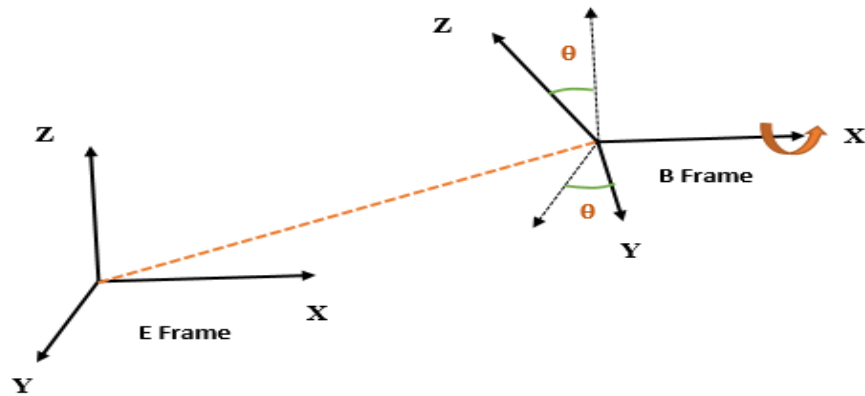
Fig 2-1(a): Rotation about X-axis by considering E-Frame as a fix frame
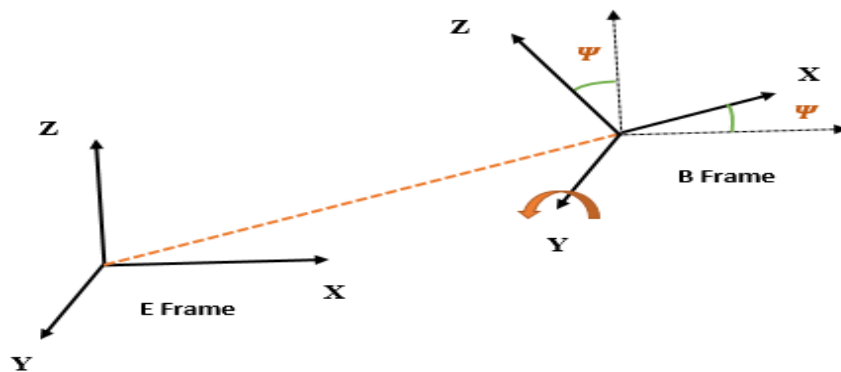
Fig 2-1(b): Rotation about Y-axis by considering E-Frame as a fix frame
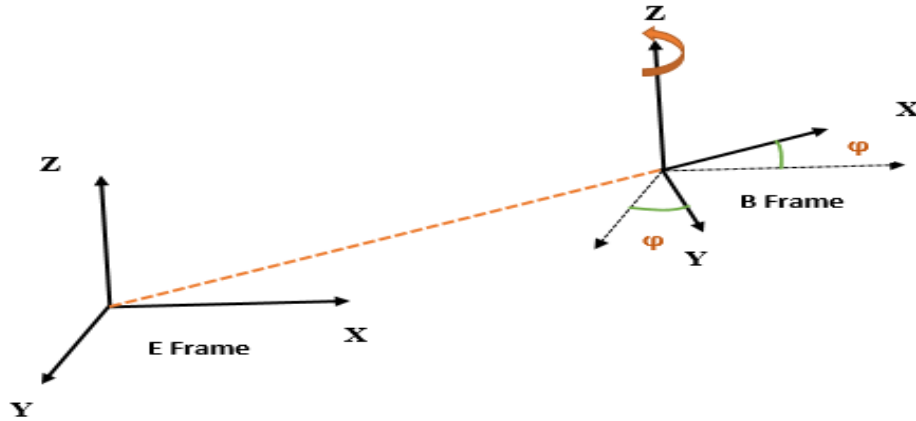
Fig 2-1(c): Rotation about Z-axis by considering E-Frame as a fix frame

Thanks to the book "Introduction to Robotics", the below matrixes are written for all three above rotations.

$$R_{x(\varphi)} = \begin{bmatrix} 1 & 0 & 0 \\ 0 & \cos\varphi & -\sin\varphi \\ 0 & \sin\varphi & \cos\varphi \end{bmatrix} \qquad (2\text{-}1)$$

$$R_y(\theta) = \begin{bmatrix} \cos\theta & 0 & \sin\theta \\ 0 & 1 & 0 \\ -\sin\theta & 0 & \cos\theta \end{bmatrix} \qquad (2\text{-}2)$$

$$R_z(\psi) = \begin{bmatrix} \cos\psi & -\sin\psi & 0 \\ \sin\psi & \cos\psi & 0 \\ 0 & 0 & 1 \end{bmatrix} \qquad (2\text{-}3)$$

By multiplying the above matrixes, a complete rotation matrix R_θ is concluded:

C and S are the symbols of cosine and sine respectively.

$$R_\theta = \begin{bmatrix} c\psi\, c\theta & -s\psi\, c\varphi + c\psi\, s\theta\, s\varphi & s\psi\, s\varphi + c\psi\, s\theta\, c\varphi \\ s\psi\, c\theta & c\psi\, c\varphi + s\psi\, s\theta\, s\varphi & -c\psi\, s\varphi + s\psi\, s\theta\, c\varphi \\ -s\theta & c\theta\, s\varphi & c\theta\, c\varphi \end{bmatrix} \qquad (2\text{-}4)$$

APPENDIX B

The Moments of Inertia Formulation and Calculation

When a body is rotating around a specific axis, its dynamic behavior is called the moment of inertia. This feature in rotational dynamics is same as the mass in the basic dynamics. It is defined as the scalar moment of inertia and moment of inertia tensor. The moment of inertia tensor is formulated as:

$$I = \iiint_V \rho r^2 dV \tag{B-1}$$

In the above equation, I $(kg\ m^2)$ is the moment of inertia, ρ $(kg\ m^{-3})$ is the spatial density, r (m) is the distance between the considered point and the axis of rotation and V (m^3) is the occupied volume by the object.

There are different moments of inertia about different axes of rotation for the same object. There is simple way to compress all moments of inertia of an object as one quantity, which is called the moment of inertia tensor. The following equation shows the moment of inertia tensor.

$$I = \begin{bmatrix} I_{XX} & I_{XY} & I_{XZ} \\ I_{YX} & I_{YY} & I_{YZ} \\ I_{ZX} & I_{ZY} & I_{ZZ} \end{bmatrix} \tag{B-2}$$

Where I_{XX} represents the moment of inertia about the x-axis when the object is rotating about the x-axis, I_{YX} represents the moment of inertia about the x-axis when the object is rotating about the y-axis and the other terms of the above matrix are the same.

Firstly, how to calculate the moment of inertia is described in detail for different object shapes that are used in this study (in this section, all the constants and variables are not defined in the abbreviation list. Since they are used only in this part of the appendix B and are not related to the other sections.).

Secondly, rotational and body moment of inertia which are two types of moment of inertia are calculated.

- Solid cylinder: radius = R, height = H, mass = M and constant density is defined as $\rho = \frac{M}{\pi R^2 H}$. The geometry of the solid cylinder is shown in figure B-1

Figure B-1: The geometry of the solid cylinder

$$I_X = \int_z \int_y \int_x \rho \; (y^2 + z^2) \, dx \, dy \, dz = \tag{B-3}$$

$$\rho \int_{-\frac{H}{2}}^{\frac{H}{2}} \int_{-\frac{R}{2}}^{\frac{R}{2}} \int_{-\sqrt{\left(\frac{R}{2}\right)^2 - y^2}}^{\sqrt{\left(\frac{R}{2}\right)^2 - y^2}} (y^2 + z^2) \, dx \, dy \, dz =$$

$$\rho \int_{-\frac{H}{2}}^{\frac{H}{2}} \int_0^{2\pi} \int_0^R (r^2 \sin^2 \theta + z^2) \, r \, dr \, d\theta \, dz =$$

$$\rho \left(H \int_0^R r^3 dr \int_0^{2\pi} \sin^2 \theta \, d\theta + 2\pi \int_0^R r dr \int_{-\frac{H}{2}}^{\frac{H}{2}} z^2 dz \right) =$$

$$\frac{M}{\pi R^2 H} \left(H \frac{R^4}{4} \pi + 2\pi \frac{R^2}{2} \frac{H^3}{12} \right) = M \left(\frac{R^2}{4} + \frac{H^2}{12} \right)$$

$$I_Y = \int_z \int_y \int_x \rho \, (x^2 + z^2) \, dx \, dy \, dz = \cdots = \tag{B-4}$$

$$\rho \int_{-\frac{H}{2}}^{\frac{H}{2}} \int_0^{2\pi} \int_0^R (r^2 \cos^2 \theta + z^2) \, r \, dr \, d\theta \, dz = \cdots = M \left(\frac{R^2}{4} + \frac{H^2}{12} \right)$$

$$I_Z = \int_z \int_y \int_x \rho \, (x^2 + y^2) \, dx \, dy \, dz = \cdots = \tag{B-5}$$

$$\rho \int_{-\frac{H}{2}}^{\frac{H}{2}} \int_0^{2\pi} \int_0^R (r^2 \cos^2 \theta + r^2 \sin^2 \theta) \, r \, dr \, d\theta \, dz = \cdots = M \left(\frac{R^2}{2} \right)$$

- Solid cylinder with variable density: radius = R, height = H, mass = M and constant density is defined as $\rho = \frac{M}{2\pi R H r}$. Its geometry is the same as the solid cylinder, figure B-1.
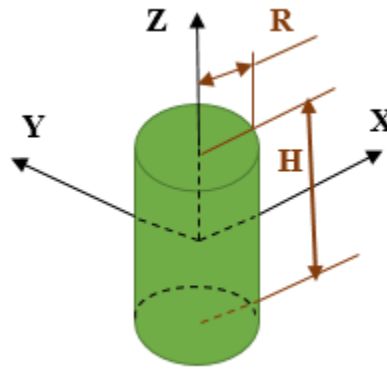
$$I_X = \int_z \int_y \int_x \rho \, (y^2 + z^2) \, dx \, dy \, dz = \tag{B-6}$$

$$\frac{M}{2\pi R H} \int_{-\frac{H}{2}}^{\frac{H}{2}} \int_{-\frac{R}{2}}^{\frac{R}{2}} \int_{-\sqrt{\left(\frac{R}{2}\right)^2 - y^2}}^{\sqrt{\left(\frac{R}{2}\right)^2 - y^2}} \frac{1}{r} \, (y^2 + z^2) \, dx \, dy \, dz =$$

$$\frac{M}{2\pi R H} \int_{-\frac{H}{2}}^{\frac{H}{2}} \int_0^{2\pi} \int_0^R \frac{1}{r} \, (r^2 \sin^2 \theta + z^2) \, r \, dr \, d\theta \, dz =$$

$$\frac{M}{2\pi R H} \left(H \int_0^R r^2 dr \int_0^{2\pi} \sin^2 \theta \, d\theta + 2\pi \, R \int_{-\frac{H}{2}}^{\frac{H}{2}} z^2 dz \right) =$$

$$\frac{M}{2\pi R H} \left(H \frac{R^3}{3} \pi + 2\pi \, R \frac{H^3}{12} \right) = M \left(\frac{R^2}{6} + \frac{H^2}{12} \right)$$

$$I_Y = \int_z \int_y \int_x \rho\,(x^2 + z^2)\,dx\,dy\,dz = \cdots = \tag{B-7}$$

$$\frac{M}{2\pi R H} \int_{-\frac{H}{2}}^{\frac{H}{2}} \int_0^{2\pi} \int_0^R \frac{1}{r}\,(r^2 \cos^2\theta + z^2)\,r\,dr\,d\theta\,dz = \cdots = M\left(\frac{R^2}{6} + \frac{H^2}{12}\right)$$

$$I_Z = \int_z \int_y \int_x \rho\,(x^2 + y^2)\,dx\,dy\,dz = \cdots = \tag{B-8}$$

$$\frac{M}{2\pi R H} \int_{-\frac{H}{2}}^{\frac{H}{2}} \int_0^{2\pi} \int_0^R \frac{1}{r}(r^2 \cos^2\theta + r^2 \sin^2\theta)\,r\,dr\,d\theta\,dz = \cdots = M\left(\frac{R^2}{3}\right)$$

- Solid rectangular prism: length = L, width = W, height = H, mass = M and constant density is defined as $\rho = \frac{M}{L\,W\,H}$. The geometry of the solid rectangular prism is shown in figure (B-2).
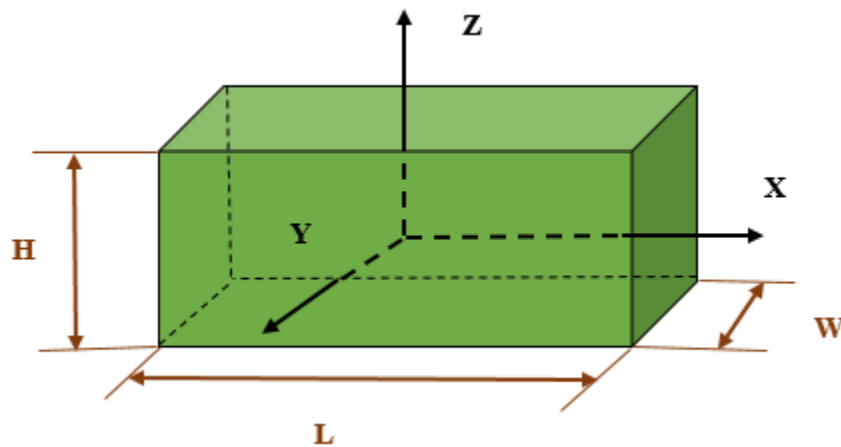
Figure B-2: The geometry of the solid rectangular prism

$$I_X = \int_z \int_y \int_x \rho \ (y^2 + z^2) \ dx \ dy \ dz = \tag{B-9}$$

$$\rho \int_{-\frac{H}{2}}^{\frac{H}{2}} \int_{-\frac{W}{2}}^{\frac{W}{2}} \int_{-\frac{L}{2}}^{\frac{L}{2}} (y^2 + z^2) \ dx \ dy \ dz =$$

$$\rho \left(LH \int_{-\frac{W}{2}}^{\frac{W}{2}} y^2 dy + L W \int_{-\frac{H}{2}}^{\frac{H}{2}} z^2 dz \right) =$$

$$\frac{M}{L\,W\,H} \left(LH \ \frac{W^3}{12} + LW \frac{H^3}{12} \right) = M \left(\frac{W^2}{12} + \frac{H^2}{12} \right)$$

$$I_Y = \int_z \int_y \int_x \rho \ (x^2 + z^2) \ dx \ dy \ dz = \tag{B-10}$$

$$\rho \int_{-\frac{H}{2}}^{\frac{H}{2}} \int_{-\frac{W}{2}}^{\frac{W}{2}} \int_{-\frac{L}{2}}^{\frac{L}{2}} (x^2 + z^2) \ dx \ dy \ dz = \cdots = M \left(\frac{L^2}{12} + \frac{H^2}{12} \right)$$

$$I_Z = \int_z \int_y \int_x \rho \ (x^2 + y^2) \ dx \ dy \ dz = \cdots = \tag{B-11}$$

$$\rho \int_{-\frac{H}{2}}^{\frac{H}{2}} \int_{-\frac{W}{2}}^{\frac{W}{2}} \int_{-\frac{L}{2}}^{\frac{L}{2}} (x^2 + y^2) \ dx \ dy \ dz = \cdots = M \left(\frac{L^2}{12} + \frac{W^2}{12} \right)$$

If the axes origin is not corresponded with the object center of mass, the moment of inertia is calculated by the parallel axes theorem. In this theorem, if the axis of rotation displacement of the center of mass (COM) of the object is shown by a distance D from the axis of rotation, the following equation (B-12) and figure (B-3) illustrated the displaced and the center moments of inertia.

$$I_{displaced} = I_{center} + MD^2 \tag{B-12}$$
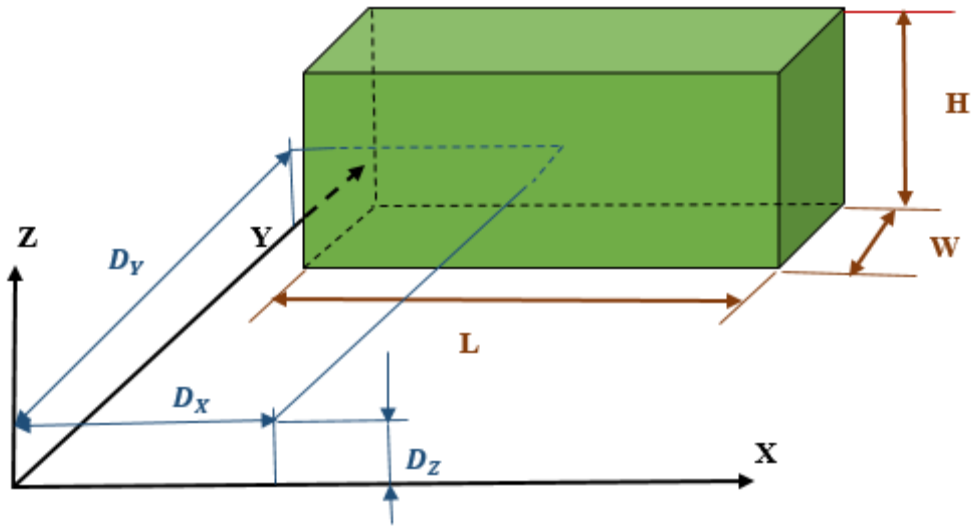
Figure B-3: The solid rectangular prism displaced

B.2: Measurement of the vehicles geometry

In this part by using the former equations of this appendix and the basic measurements of the vehicles, the body and rotational moments of inertia are calculated.

At first, the total rotational moment of inertia around the motor axis is calculated. These calculations for the standard quadcopter and 6-motor drone are the same. Since for both vehicles, the same motor and gear and dimensions are used. This moment of inertia contains the rotational moment of inertia around the motor axis $J_M [N \, m \, s^2]$ and the rotational moment of inertia around the propeller axis $J_P [N \, m \, s^2]$. Figure B-3 depicts the rotational moment of inertia of the motor – gearbox – propeller system in details.
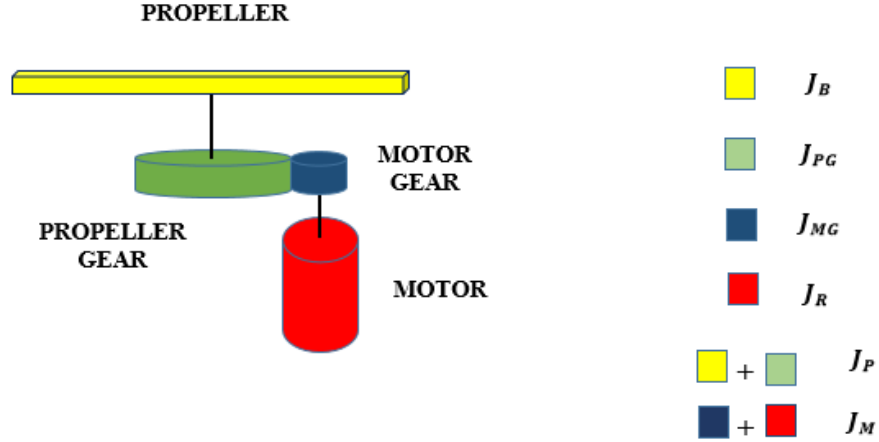
Figure B-4: Rotor inertia

J_{M_T} contains two quantities: the motor gear and the motor rotational moment of inertia (J_M [$N\ m\ s^2$] and J_{MG} [$N\ m\ s^2$]). They are considered as a solid cylinder, thus their moments of inertia are calculated as follows:

$$J_M = \frac{1}{2}\ M_M\ R_M^2 = 2.45 \times 10^{-8} \tag{B-13}$$

$$J_{MG} = \frac{1}{2}\ M_{MG}R_{MG}^2 = 2 \times 10^{-10} \tag{B-14}$$

$$J_{M_T} = J_R + J_{MG} = 2.47 \times 10^{-8} \tag{B-15}$$

In addition, J_{P_T} contains two quantities: the propeller gear and propeller rotational moments of inertia (J_B [$N\ m\ s^2$] and J_{PG} [$N\ m\ s^2$]). The propeller gear is considered as a solid cylinder and the propeller is assumed as a flat plate. Therefore, their moments of inertia are calculated as follows:

$$J_P = \frac{1}{12}\ M_P\ (W_P^2 + L_P^2) = 2.67 \times 10^{-6} \tag{B-16}$$

$$J_{PG} = \frac{1}{2}\ M_{PG}R_{PG}^2 = 3.5 \times 10^{-8} \tag{B-17}$$

$$J_{P_T} = J_P + J_{PG} = 2.79 \times 10^{-6} \tag{B-18}$$

By considering the equations (2-60) and (2-65), the total motor inertia around the motor axis J_{TM} $[N\ m\ s^2]$ and the total motor inertia around the propeller axis J_{TP} $[N\ m\ s^2]$ are as equations (B-19) and (B-20) respectively. The

$$J_{TM} = J_{M_T} + \frac{J_{P_T}}{\eta\ N^2} = 3.04 \times 10^{-8} \tag{B-19}$$

$$J_{TP} = J_{P_T} + \eta\ N^2\ J_{M_T} = 14.87 \times 10^{-6} \tag{B-20}$$

Secondly, the body moment of inertia is calculated which there are some differences between the standard quadcopter and 6-motor drone by considering the geometry displacement of the components. At first, the body moment of inertia of the standard quadcopter is calculated and then the body moment of inertia of the 6-motor drone is calculated. In this contribution, the dynamic behavior of the whole body when rotating around a defined axis is calculated. In order to the symmetric structure, the inertia tensor of the body is simplified as a diagonal matrix. Therefore, the three body moments of inertia I_{XX}, I_{YY}, and I_{ZZ} are derived to find the moment of inertia matrix. Then, the whole body of the vehicle can be divided to some parts with simpler geometry. The following parts are the components which must be considered to model the vehicle.

1. The main structure, as a two solid narrow cylinders which are crossed and fastened in the middle.
2. The electrical box that include the MCU (main computer unit) and the battery. It is considered as a rectangular parallelepiped.
3. Four motors with their gears which are considered as solid cylinders.
4. Four propellers which are considered as solid cylinders.
5. Four propeller gears which are considered as solid cylinders.
6. The camera which is considered as solid cylinder.

For the all above components, three moments of inertia around the x-axis, y-axis and z-axis must be calculated.

Figure (B-4) shows two narrow cylinders which are crossed with the radius R_B of $1.7 \times 10^{-2}(m)$, the length L_B of $.26(m)$ and the mass M_B of $35 \times 10^{-3}(kg)$. The symmetric cross

structure leads to the equality for the moment of inertia around the x-axis I_{BX} $[N\ m\ s^2]$ and around the y-axis I_{BY} $[N\ m\ s^2]$.
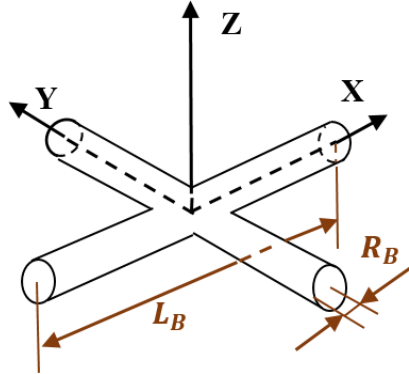
Figure B-5: The body

$$I_{BX} = I_{BY} = M_B\left(\frac{R_B^2}{4} + \frac{L_B^2}{12}\right) + \frac{1}{2}M_B R_B^2 = 2 \times 10^{-4} \tag{B-21}$$

$$I_{CZ} = M_B\left(\frac{R_C^2}{4} + \frac{L_C^2}{12}\right) + M_B\left(\frac{R_C^2}{4} + \frac{L_C^2}{12}\right) = 4 \times 10^{-4} \tag{B-22}$$

Figure (B-6) shows the rectangular parallelepiped of the electronics box with the length L_E of $.04\ (m)$, the width W_E of $2.5 \times 10^{-2}(m)$, the height H_E of $8.2 \times 10^{-3}(m)$ and the mass M_E $25 \times 10^{-3}(kg)$.
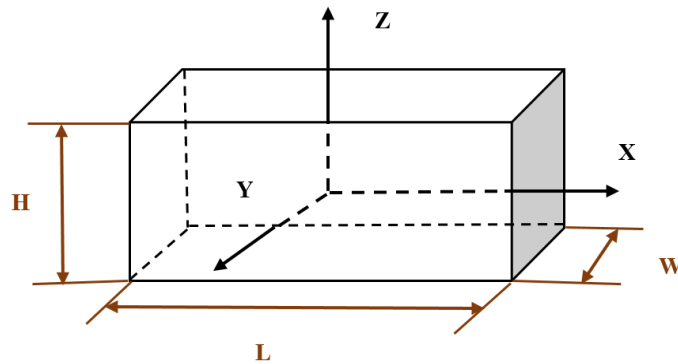
Figure B-6: The electronics box

The moments of inertia around the x-axis I_{EX} $[N\ m\ s^2]$, y-axis I_{EY} $[N\ m\ s^2]$ and z-axis I_{EZ} are derived as follows:

$$I_{EX} = M_E \left(\frac{W_E^2}{12} + \frac{H_E^2}{12} \right) = 1.4 \times 10^{-6} \tag{B-23}$$

$$I_{EY} = M_E \left(\frac{L_E^2}{12} + \frac{H_E^2}{12} \right) = 1.4 \times 10^{-6} \tag{B-24}$$

$$I_{EZ} = M_E \left(\frac{L_E^2}{12} + \frac{W_E^2}{12} \right) = 4.6 \times 10^{-6} \tag{B-25}$$

Figure (B-7) shows one of the motors with its gear as a symmetric cylinder. It has the radius R_M of $3.5 \times 10^{-3}(m)$, the height H_M of $2.2 \times 10^{-2}(m)$, the mass M_M of $6 \times 10^{-3}(m)$. There are distances from the COM around the x-axis D_{XM}, y-axis D_{YM} and z-axis D_{ZM} that are measured as 7.4×10^{-2} (m), 7.4×10^{-2} (m) and $1 \times 10^{-2}(m)$ respectively.
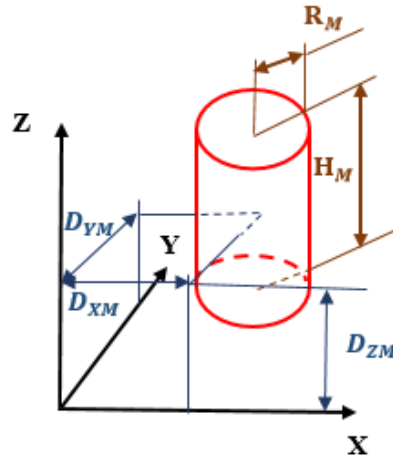
Figure B-7: The motor

The moments of inertia around the x-axis I_{M1X} $[N\ m\ s^2]$, y-axis I_{M1Y} $[N\ m\ s^2]$ and z-axis I_{M1Z} are derived as follows:

$$I_{M1X} = M_M \left(\frac{R_M^2}{4} + \frac{H_M^2}{12} + D_{YM}{}^2 + D_{ZM}{}^2 \right) = 35 \times 10^{-6} \tag{B-26}$$

$$I_{M1Y} = M_M \left(\frac{R_M^2}{4} + \frac{H_M^2}{12} + D_{XM}{}^2 + D_{ZM}{}^2 \right) = 35 \times 10^{-6} \tag{B-27}$$

$$I_{M1Z} = M_M \left(\frac{R_M^2}{4} + D_{XM}{}^2 + D_{YM}{}^2 \right) = 65 \times 10^{-6} \tag{B-28}$$

All above moments of inertia (B-26), (B-27) and (B-28) for the first motor are the same as other motors in order to the symmetric geometry. So, it is written as:

$$I_{M1X} = I_{M2X} = I_{M3X} = I_{M4X} \tag{B-29}$$

$$I_{M1Y} = I_{M2Y} = I_{M3Y} = I_{M4Y} \tag{B-30}$$

$$I_{M1Z} = I_{M2Z} = I_{M3Z} = I_{M4Z} \tag{B-31}$$

Figure (B-8) shows one of the propellers as a symmetric cylinder. It has the radius R_P of $2.5 \times 10^{-3} (m)$, the height H_P of $1.4 \times 10^{-2} (m)$, the mass M_P of $1.8 \times 10^{-3} (m)$. There are distances from the COM around the x-axis D_{XP}, y-axis D_{YP} and z-axis D_{ZP} that are measured as $8 \times 10^{-2} (m)$, $8 \times 10^{-2} (m)$ and $8 \times 10^{-2} (m)$ respectively.


Figure B-8: The propeller

The moments of inertia around the x-axis I_{P1X} [$N\,m\,s^2$] , y-axis I_{P1Y} [$N\,m\,s^2$] and z-axis I_{P1Z} are derived as follows:

$$I_{P1X} = M_P\left(\frac{R_P^2}{4} + \frac{H_P^2}{12} + D_{YP}{}^2 + D_{ZP}{}^2\right) = 12 \times 10^{-6} \qquad \text{(B-32)}$$

$$I_{P1Y} = M_P\left(\frac{R_P^2}{4} + \frac{H_P^2}{12} + D_{XP}{}^2 + D_{ZP}{}^2\right) = 12 \times 10^{-6} \qquad \text{(B-33)}$$

$$I_{P1Z} = M_P\left(\frac{R_P^2}{4} + D_{XP}{}^2 + D_{YP}{}^2\right) = 23 \times 10^{-6} \qquad \text{(B-34)}$$

All above moments of inertia (B-32), (B-33) and (B-34) for the first motor are the same as other motors in order to the symmetric geometry. So, it is written as:

$$I_{P1X} = I_{P2X} = I_{P3X} = I_{P4X} \qquad \text{(B-35)}$$

$$I_{P1Y} = I_{P2Y} = I_{P3Y} = I_{P4Y} \qquad \text{(B-36)}$$

$$I_{P1Z} = I_{P2Z} = I_{P3Z} = I_{P4Z} \qquad \text{(B-37)}$$

Figure (B-9) shows one of the propellers gears as a symmetric cylinder. It has the radius R_{PG} of $2.5 \times 10^{-3}(m)$, the height H_{PG} of $1.4 \times 10^{-2}(m)$, the mass M_{PG} of 1.8×10^{-3} (m). There are distances from the COM around the x-axis D_{XPG}, y-axis D_{YPG} and z-axis D_{ZPG} that are measured as 8×10^{-2} (m), 8×10^{-2} (m) and $8 \times 10^{-2}(m)$ respectively.
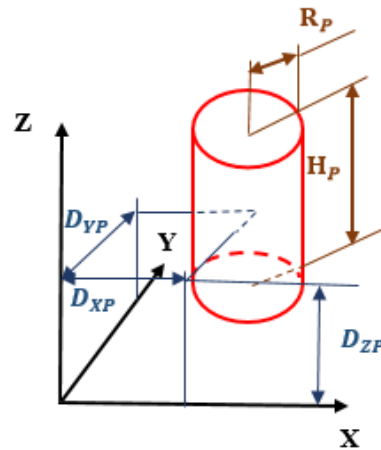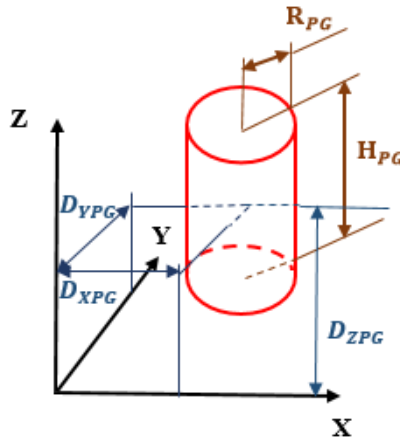
Figure B-9: The propeller gear

The moments of inertia around the x-axis I_{PG1X} $[N\ m\ s^2]$,y-axis I_{PG1Y} $[N\ m\ s^2]$ and z-axis I_{PG1Z} are derived as follows:

$$I_{PG1X} = M_{PG} \left(\frac{R_{PG}^2}{4} + \frac{H_{PG}^2}{12} + D_{YPG}^2 + D_{ZPG}^2 \right) = 16 \times 10^{-6} \tag{B-38}$$

$$I_{PG1Y} = M_{PG} \left(\frac{R_{PG}^2}{4} + \frac{H_{PG}^2}{12} + D_{XPG}^2 + D_{ZPG}^2 \right) = 16 \times 10^{-6} \tag{B-39}$$

$$I_{PG1Z} = M_{PG} \left(\frac{R_{PG}^2}{4} + D_{XPG}^2 + D_{YPG}^2 \right) = 32 \times 10^{-6} \tag{B-40}$$

All above moments of inertia (B-38), (B-39) and (B-40) for the first motor are the same as other motors in order to the symmetric geometry. So, it is written as:

$$I_{PG1X} = I_{PG2X} = I_{PG3X} = I_{PG4X} \tag{B-41}$$

$$I_{PG1Y} = I_{PG2Y} = I_{PG3Y} = I_{PG4Y} \tag{B-42}$$

$$I_{PG1Z} = I_{PG2Z} = I_{PG3Z} = I_{PG4Z} \tag{B-43}$$

Figure (B-10) shows one of the camera as a symmetric cylinder. It has the radius R_C of $1.2 \times 10^{-2}(m)$, the height H_C of $5 \times 10^{-2}(m)$, the mass M_C of $9.4 \times 10^{-3}\ (m)$. There is distances from the COM around the z-axis D_{ZC}, $2.3 \times 10^{-2}(m)$.
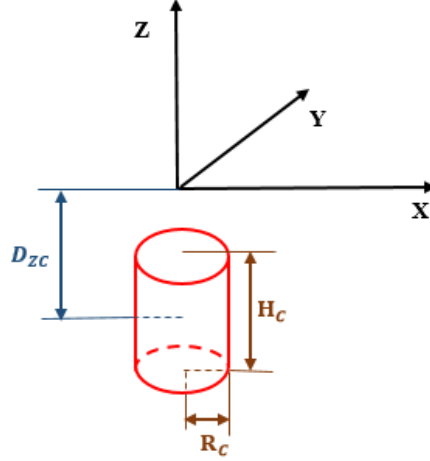
Figure B-10: The camera

The moments of inertia around the x-axis I_{CX} $[N\ m\ s^2]$, y-axis I_{CY} $[N\ m\ s^2]$ and z-axis I_{CZ} are derived as follows:

$$I_{CX} = M_C\left(\frac{R_C^2}{4} + \frac{H_C^2}{12} + D_{YC}^2 + D_{ZC}^2\right) = 7.2 \times 10^{-6} \tag{B-44}$$

$$I_{CY} = M_C\left(\frac{R_C^2}{4} + \frac{H_C^2}{12} + D_{XC}^2 + D_{ZC}^2\right) = 7.2 \times 10^{-6} \tag{B-45}$$

$$I_{CZ} = M_C\left(\frac{R_C^2}{4} + D_{XC}^2 + D_{YC}^2\right) = 6.7 \times 10^{-7} \tag{B-46}$$

Finally, the total moments of inertia around the x-axis I_{XX}, y-axis I_{YY} and z-axis I_{ZZ} are calculated as follows:

$$I_{XX} = I_{BX} + I_{EX} + I_{M1X} + I_{M2X} + I_{M3X} + I_{M4X} + I_{P1X} + I_{P2X} + I_{P3X} + I_{P4X} \tag{B-47}$$
$$+ I_{PG1X} + I_{PG2X} + I_{PG3X} + I_{PG4X} + I_{CX} = 4.6 \times 10^{-4}$$

$$I_{YY} = I_{BY} + I_{EY} + I_{M1Y} + I_{M2Y} + I_{M3Y} + I_{M4Y} + I_{P1Y} + I_{P2Y} + I_{P3Y} + I_{P4Y} \qquad \text{(B-48)}$$
$$+ I_{PG1Y} + I_{PG2Y} + I_{PG3Y} + I_{PG4Y} + I_{CY} = 4.6 \times 10^{-4}$$

$$I_{ZZ} = I_{BZ} + I_{EZ} + I_{M1Z} + I_{M2Z} + I_{M3Z} + I_{M4Z} + I_{P1Z} + I_{P2Z} + I_{P3Z} + I_{P4Z} \qquad \text{(B-49)}$$
$$+ I_{PG1Z} + I_{PG2Z} + I_{PG3Z} + I_{PG4Z} + I_{CZ} = 3.94 \times 10^{-4}$$

The equations (B-47), (B-48) and (B-49) show that the moment of inertia around the x and y axes are the same. Moreover, the moment of inertia around the z axis has a close value to the x and y axes. Therefore, this vehicle has a high degree of symmetry by considering these axes and the simplicity of the changing of the angular speed on all axes are the same.

Body moments of inertia calculations for 6-motor drone

In case of the 6-motor design, the calculations of the moments of inertia for the cross structure as a body, the electronics part and camera are the same as the standard quadcopter moments of inertia. Therefore, the moments of inertia of the 6-motor design for the motor, propeller and propeller gear are calculated as follows:

All four vertical motors in this design have the same moment of inertia as the standard quadcopter. Figure (B-11) shows one of the horizontal motors of the 6-motor design with its gear as a symmetric cylinder. It has the radius R_M of $3.5 \times 10^{-3} (m)$, the height H_M of $2.2 \times 10^{-2} (m)$, the mass M_M of $6 \times 10^{-3} (m)$. There are distances from the COM around the x-axis D_{XM} and z-axis D_{ZM} that are measured as 6×10^{-2} (m) and $2 \times 10^{-2} (m)$ respectively.

Figure B-11: The horizontal motor of the 6-motor design

The moments of inertia around the x-axis I_{M_H1X} $[N\ m\ s^2\ ]$,y-axis I_{M_H1Y} $[N\ m\ s^2]$ and z-axis I_{M_H1Z} are derived as follows:

$$I_{M_H1X} = M_M \left(\frac{R_M^2}{4} + \frac{H_M^2}{12} + D_{ZM}{}^2 \right) = 2.66 \times 10^{-6} \tag{B-50}$$

$$I_{M_H1Y} = M_M \left(\frac{R_M^2}{4} + \frac{H_M^2}{12} + D_{XM}{}^2 + D_{ZM}{}^2 \right) = 23 \times 10^{-6} \tag{B-51}$$

$$I_{M_H1Z} = M_M \left(\frac{R_M^2}{4} + D_{XM}{}^2 \right) = 21 \times 10^{-6} \tag{B-52}$$

All above moments of inertia (B-50), (B-51) and (B-52) of the first horizontal motor are the same for the second motor in order to the symmetric geometry. So, it is written as:

$$I_{M_H1X} = I_{M_H2X} \tag{B-53}$$

$$I_{M_H1Y} = I_{M_H2Y} \tag{B-54}$$

$$I_{M_H1Z} = I_{M_H2Z} \tag{B-54}$$

All four vertical propellers in this design have the same moment of inertia as the standard quadcopter. Figure (B-12) shows one of the horizontal propellers as a symmetric cylinder. It has

the radius R_P of $2.5 \times 10^{-3} (m)$, the height H_P of $1.4 \times 10^{-2} (m)$, the mass M_P of $1.8 \times 10^{-3} (m)$. There are distances from the COM around the x-axis D_{XP} and z-axis D_{ZP} that are measured as $7 \times 10^{-2} (m)$ and $2 \times 10^{-2} (m)$ respectively.

Figure B-12: The horizontal propeller of the 6-motor design

The moments of inertia around the x-axis I_{PH1X} $[N\ m\ s^2]$, y-axis I_{PH1Y} $[N\ m\ s^2]$ and z-axis I_{PH1Z} are derived as follows:

$$I_{PH1X} = M_P \left(\frac{R_P^2}{4} + \frac{H_P^2}{12} + D_{YP}^2 + D_{ZP}^2 \right) = 75 \times 10^{-8} \tag{B-55}$$

$$I_{PH1Y} = M_P \left(\frac{R_P^2}{4} + \frac{H_P^2}{12} + D_{XP}^2 + D_{ZP}^2 \right) = 95 \times 10^{-7} \tag{B-56}$$

$$I_{PH1Z} = M_P \left(\frac{R_P^2}{4} + D_{XP}^2 + D_{YP}^2 \right) = 88 \times 10^{-7} \tag{B-57}$$

All above moments of inertia (B-55), (B-56) and (B-57) of the first horizontal propeller are the same for the second propeller in order to the symmetric geometry. So, it is written as:

$$I_{PH1X} = I_{PH2X} \tag{B-58}$$

$$I_{PH1Y} = I_{PH2Y} \tag{B-59}$$

$$I_{PH1Z} = I_{PH2Z} \tag{B-60}$$

All four vertical propellers' gears in this design have the same moment of inertia as the standard quadcopter Figure (B-13) shows one of the horizontal propellers' gears as a symmetric cylinder.

It has the radius R_{PG} of $2.5 \times 10^{-3} (m)$, the height H_{PG} of $1.4 \times 10^{-2} (m)$, the mass M_{PG} of $1.8 \times 10^{-3} (m)$. There are distances from the COM around the x-axis D_{XPG} and z-axis D_{ZPG} that are measured as $7 \times 10^{-2} (m)$ and $2 \times 10^{-2} (m)$ respectively.
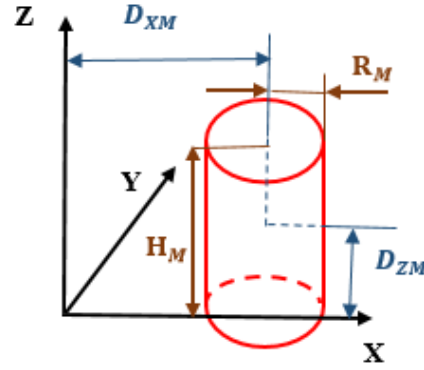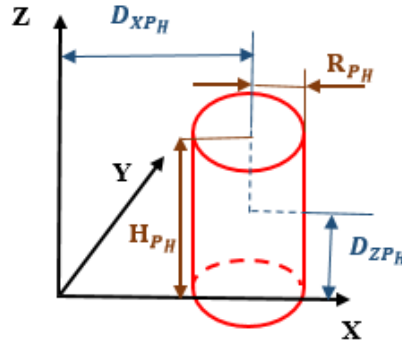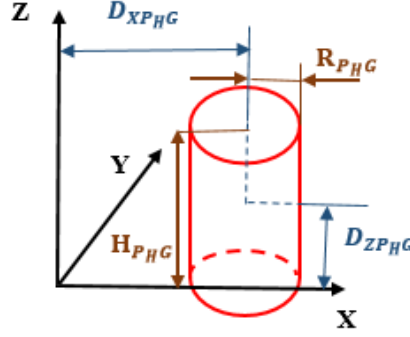

Figure B-13: The horizontal propeller gear of the 6-motor design

The moments of inertia around the x-axis I_{P_HG1X} $[N \ m \ s^2]$,y-axis I_{P_HG1Y} $[N \ m \ s^2]$ and z-axis I_{P_HG1Z} are derived as follows:

$$I_{P_HG1X} = M_{PG} \left(\frac{R_{PG}^2}{4} + \frac{H_{PG}^2}{12} + D_{YPG}{}^2 + D_{ZPG}{}^2 \right) = 16 \times 10^{-6} \tag{B-61}$$

$$I_{P_HG1Y} = M_{PG} \left(\frac{R_{PG}^2}{4} + \frac{H_{PG}^2}{12} + D_{XPG}{}^2 + D_{ZPG}{}^2 \right) = 16 \times 10^{-6} \tag{B-62}$$

$$I_{P_HG1Z} = M_{PG} \left(\frac{R_{PG}^2}{4} + D_{XPG}{}^2 + D_{YPG}{}^2 \right) = 32 \times 10^{-6} \tag{B-63}$$

All above moments of inertia (B-61), (B-62) and (B-63) of the first horizontal propeller gear are the same for the second propeller gear in order to the symmetric geometry. So, it is written as:

$$I_{P_HG1X} = I_{P_HG2X} \tag{B-64}$$

$$I_{P_HG1Y} = I_{P_HG2Y} \tag{B-65}$$

$$I_{P_HG1Z} = I_{P_HG2Z} \tag{B-66}$$

Finally, the total moments of inertia around the x-axis I_{XX}, y-axis I_{YY} and z-axis I_{ZZ} are calculated as follows:

$$I_{XX} = I_{BX} + I_{EX} + I_{M1X} + I_{M2X} + I_{M3X} + I_{M4X} + I_{M_H1X} + I_{M_H2X} + I_{P1X} + I_{P2X} \qquad \text{(B-67)}$$
$$+ I_{P3X} + I_{P4X} + I_{P_H1X} + I_{P_H2X} + I_{PG1X} + I_{PG2X} + I_{PG3X} + I_{PG4X}$$
$$+ I_{P_HG1X} + I_{P_HG2X} + I_{CX} = 4.7 \times 10^{-4}$$

$$I_{YY} = I_{BY} + I_{EY} + I_{M1Y} + I_{M2Y} + I_{M3Y} + I_{M4Y} + I_{M_H1Y} + I_{M_H2Y} + I_{P1Y} + I_{P2Y} \qquad \text{(B-68)}$$
$$+ I_{P3Y} + I_{P4Y} + I_{P_H1Y} + I_{P_H2Y} + I_{PG1Y} + I_{PG2Y} + I_{PG3Y} + I_{PG4Y}$$
$$+ I_{P_HG1Y} + I_{P_HG2Y} + I_{CY} = 5.5 \times 10^{-4}$$

$$I_{ZZ} = I_{BZ} + I_{EZ} + I_{M1Z} + I_{M2Z} + I_{M3Z} + I_{M4Z} + I_{M_H1Z} + I_{M_H2Z} + I_{P1Z} + I_{P2Z} \qquad \text{(B-69)}$$
$$+ I_{P3Z} + I_{P4Z} + I_{P_H1Z} + I_{P_H2Z} + I_{PG1Z} + I_{PG2Z} + I_{PG3Z} + I_{PG4Z}$$
$$+ I_{P_HG1Z} + I_{P_HG2Z} + I_{CZ} = 4.3 \times 10^{-4}$$

The equations (B-67), (B-68) and (B-69) show that the moment of inertia around the x and z axes are almost the same. Moreover, the moment of inertia around the z axis has a close value to the x axes. Therefore, this vehicle has a high degree of symmetry by considering these axes.

APPENDIX C

The Dynamics Model's Basic Steps

The second law of Newton has stated the equation (C-1) where, m (kg) is the mass of the vehicle, a (ms^{-2}) is the acceleration and F (N) is the force, while $\ddot{\tau}^E$ (ms^{-2}) is the linear acceleration (by considering $\tau^E[m]$ as the linear position) with respecting the E-frame the second law can be rewritten as equation (C-2).

$$ma = F \tag{C-1}$$

$$m\,\ddot{\tau}^E = F^E \tag{C-2}$$

The linear acceleration $\ddot{\tau}^E$ (ms^{-2}) is written in the B-frame as follows (C-3) where, R_θ is rotational matrix and V^B is linear velocity

$$\ddot{\tau}^B = \widehat{R_\theta \dot{V}^B} \tag{C-3}$$

Then the equation (C-2) is derived as the equation (C-4) and expanded as the equation (C-5) when the B-frame is considered.

$$m\,\widehat{R_\theta \dot{V}^B} = R_\theta\, F^B \tag{C-4}$$

$$m\,(\dot{R}_\theta V^B + R_\theta\, \dot{V}^B) = R_\theta\, F^B \tag{C-5}$$

The derivative of the rotation matrix is equal to the multiplication of the rotation matrix and the skew symmetric matrix of ω^B $(\frac{m}{s})$ (rotational velocity in the B-frame), equation (C-6). Then, it can be written as follows where the skew symmetric matrix for any given vector in general form of $k = [k_1 \quad k_2 \quad k_3]^T$ is defined as matrix (C-7). [7]

$$\dot{R}_\theta = R_\theta\, S(\omega) \tag{C-6}$$

$$S(k) = \begin{bmatrix} 0 & -k_3 & k_2 \\ k_3 & 0 & -k_1 \\ -k_2 & k_1 & 0 \end{bmatrix} \tag{C-7}$$

The skew symmetric matrix of ω^B $(\frac{m}{s})$ is derived by the above matrix template and external multiplication. Finally, the equation (C-5) is rewritten as the equation (C-8).

$$mR_\theta\left(\omega^B \times V^B + \dot{V}^B\right) = R_\theta\,F^{\,B}$$

$$m\left(\omega^B \times V^B + \dot{V}^B\right) = F^{\,B} \tag{C-8}$$

The above derivations resultant shows the expanded equation of $F^{\,B}$ (N). Therefore, for the momentum $T^{\,B}$ (N) the same derivations must be written, where $I(Nms^2)$ is the body inertia matrix, $\ddot{\theta}^E$ $(rad\;s^{-2})$ is the angular acceleration vector by considering the E-frame, Γ_θ is the translational matrix.

$$I\ddot{\theta}^E = T^{\,E} \tag{C-9}$$

$$I\widehat{\dot{\Gamma_\theta\,\omega}}^{\,B} = \Gamma_\theta\,T^{\,B} \tag{C-10}$$

$$I\left(\dot{\Gamma}_\theta\,\omega^B + \dot{\omega}^B\Gamma_\theta\right) = \Gamma_\theta\,T^{\,B} \tag{C-11}$$

Where, $\dot{T}_\theta = \Gamma_\theta\omega^B$, so after the substitution it will be as follows:

$$I(\Gamma_\theta\,\omega^B \times \omega^B + \dot{\omega}^B\,\Gamma_\theta) = \Gamma_\theta\,T^{\,B} \tag{C-12}$$

$$I(\omega^B \times \omega^B + \dot{\omega}^B) = T^{\,B} \tag{C-13}$$

The combination of two equations (C-8) and (C-13) can show the translational and rotational equations of motions of a 6 DOF rigid body which are formulated as equation (C-14):

$$\begin{bmatrix} mI_{3\times3} & 0_{3\times3} \\ 0_{3\times3} & I_{3\times3} \end{bmatrix} \begin{bmatrix} \dot{V}^B \\ \dot{\omega}^B \end{bmatrix} + \begin{bmatrix} \omega^B \times (mV^B) \\ \omega^B \times (I\omega^B) \end{bmatrix} = \begin{bmatrix} F^B \\ T^B \end{bmatrix} \qquad \text{(C-14)}$$

In the above equation, $I_{3\times3}$ is an identity matrix with the dimension of three by three and the first matrix is a diagonal constant matrix. $\dot{V}^B (m\ s^{-2})$ is the linear acceleration vector of the quadrotor in the B-frame where, $\dot{\omega}^B\ (rad\ s^{-2})$ is the angular acceleration of the quadrotor in the B-frame. Moreover, $F^B(N)$ and $T^B(N\ m)$ are the quadrotor forces vector and torques vector in the B-frame respectively. The equation (C-14) is valid for all rigid body that follow the mentioned simplification.

APPENDIX D

The Aerodynamics Contribution

The thrust and the drag coefficients are two significant quantities which are considered in the aerodynamics contribution. The aerodynamics characteristics of the rotating propellers are calculated by considering the combined momentum and blade element theories. They are explained as two different concepts respectively.

Momentum Theory

This theory is not sufficient for designing the rotor system and is not considered with the details of the rotor blades. It provides an estimation for the induced power requirement of the rotor and the ideal performance limit. In the momentum theory, there is a disk to produce energy as the rotor. There are some assumptions which are considered in the momentum theory as follows:

- A cylinder which is surrounded by a control volume with the radius of R_1 which lead to the rotor (disk) radius of R.
- The rotor is composed of an infinite number of blades and may be considered as an actuator disk.
- The actuator disk is infinitely thin, therefore there is no discontinuity in velocity of the air when it flows through the disk.
- The rotor is uniformly accelerating the air through the disk with no loss at the tips.
- The axial kinetic energy which is imported to the air in the slip stream is the power required to produce the thrust.
- The air is considered frictionless and incompressible. Therefore, there is no profile drag loss in the rotor disk.

As it is shown in figure (D-1), the rotor is pushing the air continuously down. Then, the air inside the slip stream acquires a velocity increment or momentum change. Therefore, an opposite and equal reaction force which is called rotor thrust acts on the rotor. The velocity increment of the air is in the opposite direction of the thrust. In this figure, rotor disk is a thin disk of area A, far upstream field is considered station 1, far downstream field is considered station 4, the pressure of the station 1 and 4 are atmospheric pressure P_0, stations 2 and 3 are

above and below the disk. It is noted that about the induced velocity, (v) is its symbol at the rotor disk and ω is its symbol at far field.
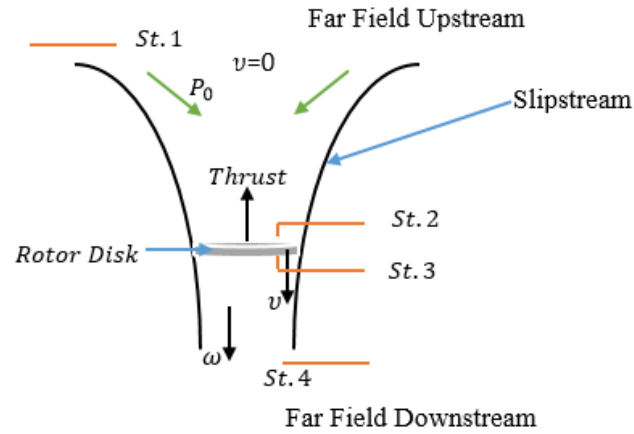
Figure D-1: Momentum theory

Based on the conservation laws, the mass flow rate is given as the equation (D-1). The momentum conservation is explained by the relation of the force to the rate of the momentum change, the equation (D-2).

$$\overset{\circ}{m} = \rho A v \tag{D-1}$$

$$T = \overset{\circ}{m}(\omega - 0) = \rho A v \omega \tag{D-2}$$

The energy conservation rate is described as the relation of the rate of the work done on the air to and its changes in the kinetic energy per second, as the equation (D-3).

$$Tv = \frac{1}{2}\overset{\circ}{m}(\omega^2 - 0) = \frac{1}{2}\overset{\circ}{m}\omega^2 \tag{D-3}$$

By substitution of T from the equation (D-1) in the equation (D-3) is resulted in the equation (D-4).

$$T = \rho A v 2v \tag{D-4}$$

By substituting ω in the equation (D-2), the induced velocity on the rotor disk is given by the equation (D-5).

$$v = \sqrt{\frac{T}{2\rho A}} \qquad \text{(D-5)}$$

The power is required to develop the thrust T is given as (D-6).

$$P = Tv = T\sqrt{\frac{T}{2\rho A}} \qquad \text{(D-6)}$$

The thrust coefficient is defined as (D-7).

$$C_T = \frac{T}{\rho A (\Omega R)^2} \qquad \text{(D-6)}$$

APPENDIX E

The Motion Vector Calculation Steps for 6-Motor Design

Motion vector $U_B(\Omega)$ expresses the thrust and drag forces of propellers F_{th} and torques around three coordinate axes T_{th}. It contains the multiplication of the motion matrix and the square of the propeller's rotational speed as the equation (E-1). [46, 47]

$$U_B(\Omega) = E_B\Omega^2 \tag{E-1}$$

The following formula (E-2) shows the F_{th} for both status of rotors, whenever the rotor axis is vertical either it is horizontal. For the first four rotors which are installed on the vehicle by the vertical axis, θ_i will be considered 90° and for the 5th and 6th rotors which are installed on the vehicle with the horizontal axis, θ_i will be equal to 0°. Therefore, by these substitutions the resulted matrix is written as formula (E-3) for the forces that are created by the rotors (F_{th}).

$$F_{th} = \begin{bmatrix} C\theta_1 & C\theta_2 & C\theta_3 & C\theta_4 & C\theta_5 & C\theta_6 \\ 0 & 0 & 0 & 0 & 0 & 0 \\ -S\theta_1 & -S\theta_2 & -S\theta_3 & -S\theta_4 & -S\theta_5 & -S\theta_6 \end{bmatrix} \begin{bmatrix} K\Omega_1^2 \\ K\Omega_2^2 \\ K\Omega_3^2 \\ K\Omega_4^2 \\ K\Omega_5^2 \\ K\Omega_6^2 \end{bmatrix} \tag{E-2}$$

$$F_{th} = \begin{bmatrix} 0 & 0 & 0 & 0 & K\Omega_5^2 & K\Omega_6^2 \\ 0 & 0 & 0 & 0 & 0 & 0 \\ -K\Omega_1^2 & -K\Omega_2^2 & -K\Omega_3^2 & -K\Omega_4^2 & 0 & 0 \end{bmatrix} = \begin{bmatrix} F_x \\ F_y \\ F_z \end{bmatrix} \tag{E-3}$$

By using the formula (E-4), the matrix (E-5) is defined for the T_{th} as the rotors momentum. There is a similarity in this step with the former step where θ_i must be considered for different propellers axis. Therefore, where $i = 1,..,4$ (rotor with vertical axis), θ_i are considered 90° and where $i = 5, 6$ (rotor with horizontal axis), θ_i are considered 0°.

$$M_{th} =$$

$$
\begin{bmatrix}
l_s S\theta_1 - C\theta_1\lambda_1 & l_s S\theta_2 - C\theta_2\lambda_2 & l_s S\theta_3 - C\theta_3\lambda_3 & l_s S\theta_4 - C\theta_4\lambda_4 & l_s S\theta_5 - C\theta_5\lambda_5 & l_s S\theta_6 - C\theta_6\lambda_6 \\
L_l S\theta_1 & L_l S\theta_2 & L_l S\theta_3 & L_l S\theta_4 & L_l S\theta_5 & L_l S\theta_6 \\
l_s C\theta_1 + S\theta_1\lambda_1 & -l_s C\theta_2 + S\theta_2\lambda_2 & l_s C\theta_3 + S\theta_3\lambda_3 & -l_s C\theta_4 + S\theta_4\lambda_4 & l_s C\theta_5 + S\theta_5\lambda_5 & -l_s C\theta_6 + S\theta_6\lambda_6
\end{bmatrix}
\quad \text{(E-4)}
$$

$$
* \begin{bmatrix} K\Omega_1^2 \\ K\Omega_2^2 \\ K\Omega_3^2 \\ K\Omega_4^2 \\ K\Omega_5^2 \\ K\Omega_6^2 \end{bmatrix}
$$

$$\text{(E-5)}$$

$$
M_{th} = \begin{bmatrix}
l_s & -l_s & -l_s & l_s & \lambda_5 & -\lambda_6 \\
-L_l & L_l & L_l & -L_l & 0 & 0 \\
-\lambda_1 & \lambda_2 & -\lambda_3 & \lambda_4 & l_s & -l_s
\end{bmatrix}
\begin{bmatrix} K\Omega_1^2 \\ K\Omega_2^2 \\ K\Omega_3^2 \\ K\Omega_4^2 \\ K\Omega_5^2 \\ K\Omega_6^2 \end{bmatrix}
= \begin{bmatrix} M_x \\ M_y \\ M_z \end{bmatrix}
$$

In the above equations (E-4) and (E-5), $\lambda_{1,2,3,4,5,6}$ are torque/force ratios which for counter clockwise rotating propellers λ_2, λ_4 and λ_6 are positive whereas λ_1, λ_3 and λ_5 are negative and for clockwise rotating ones. The distance of rotors to the center of gravity of the vehicle in the X and Y directions are defined as l_s and L_l.

Therefore, forces and torques which are produced by rotors can provide a unique matrix as movement matrix $E_B[+]$ and movement vector $U_B(\Omega)[+]$ that is written in the equation (E-6).

In this issue by considering the aerodynamics, it is clear that both forces and torques are related to the square of the propellers speed. Then by multiplication of the square of the rotation speed $\Omega^2 [rad\ s^{-1}]$ by the movement matrix $E_B[+]$, the movement vector $U_B(\Omega)[+]$ is resulted. Moreover the aerodynamic contributions (thrust $b[N\ s^2]$ and drag $d[N\ m\ s^2]$ factors) are derived in the appendix D.

$$U_B(\Omega) = E_B\Omega^2 = \begin{bmatrix} U_1 \\ U_2 \\ U_3 \\ U_4 \\ U_5 \\ U_6 \end{bmatrix} = \begin{bmatrix} b\Omega_5^2 + b\Omega_6^2 \\ 0 \\ b(\Omega_1^2 + \Omega_2^2 + \Omega_3^2 + \Omega_4^2) \\ bl(\Omega_4^2 - \Omega_2^2) + d(\Omega_5^2 - \Omega_6^2) \\ bl(\Omega_3^2 - \Omega_1^2) \\ d(\Omega_2^2 + \Omega_4^2 - \Omega_1^2 - \Omega_3^2) + bl(\Omega_5^2 - \Omega_6^2) \end{bmatrix} \tag{E-6}$$

In the above equation, $U_1, U_2, U_3, U_4, U_5, U_6$ are the movement vector components which are related to each propeller. In order to the vehicle trajectory which is the fast forward flight, there is no rotation and momentum. Therefore, only the drag and thrust forces are considered as the motion vector for the 6-motor design as the equation (E-7).

$$U_B(\Omega) = E_B\Omega^2 = \begin{bmatrix} U_1 \\ U_2 \\ U_3 \\ U_4 \\ U_5 \\ U_6 \end{bmatrix} = \begin{bmatrix} b\Omega_5^2 + b\Omega_6^2 \\ 0 \\ b(\Omega_1^2 + \Omega_2^2 + \Omega_3^2 + \Omega_4^2) \\ d(\Omega_5^2 - \Omega_6^2) \\ 0 \\ d(\Omega_2^2 + \Omega_4^2 - \Omega_1^2 - \Omega_3^2) \end{bmatrix} \tag{E-7}$$

Therefore, the motion matrix is defined as the equation (E-8):

$$E_B = \begin{bmatrix} 0 & 0 & 0 & 0 & b & b \\ 0 & 0 & 0 & 0 & 0 & 0 \\ b & b & b & b & 0 & 0 \\ 0 & 0 & 0 & 0 & d & -d \\ 0 & 0 & 0 & 0 & 0 & 0 \\ -d & d & -d & d & 0 & 0 \end{bmatrix} \tag{E-8}$$

APPENDIX F

List of Symbols and Abbreviations

Ω (rad/s)	Angular velocity
Ω_h (rad/s)	Angular velocity in hover
f_E	Earth frame
f_B	Body frame
m_1, m_2, m_3, m_4	Quadrotor motors
D (N)	Drag force
ρ (kg/m^3)	Density
V (m/s)	Speed of vehicle relative to the air
A (m^2)	Airfoil cross sectional area
c_d	Drag coefficient
c_l	Lift coefficient
b (N)	Thrust coefficient
T $[N]$	Thrust force
L (N)	Lift force
x, y, z (m)	Linear positions
φ, θ, ψ (rad)	Euler angles
$\boldsymbol{\tau}^E$ (m)	Linear position in the earth frame
$\boldsymbol{\theta}^E$ (rad)	Angular position in the earth frame
$\boldsymbol{\xi}$	Position in the earth-frame
R_θ	Rotational matrix
Γ_θ	Translational matrix
$\boldsymbol{V}^E = \dot{\boldsymbol{\tau}}^E$	Linear velocity matrix in the earth frame
$\boldsymbol{V}^B$	Linear velocity matrix in the body frame
u, v, w (m/s)	Linear velocities
$\boldsymbol{\omega}^E = \dot{\boldsymbol{\theta}}^E$	Angular velocity matrix in the earth frame
$\boldsymbol{\omega}^B$	Angular velocity matrix in the body frame

O_E	Earth frame base
O_B	Body frame base
$p, q, r \ (rad/s)$	Angular velocities
I	Inertia matrix
$\boldsymbol{F^E} \ (N)$	Force in the earth frame
$\boldsymbol{T^E} (Nm)$	Torque in the earth frame
$\dot{\boldsymbol{\xi}}$	Velocity vector
$m(kg)$	Quadrotor mass
$\ddot{\boldsymbol{\tau}}^E (ms^{-2})$	Linear acceleration
$\ddot{\boldsymbol{\theta}}^E \ (rad \ s^{-2})$	Angular acceleration
$S(\omega)$	Skew symmetric matrix of (ω)
$\boldsymbol{F^B} \ (N)$	Force vector in the body frame
$\boldsymbol{T^B} (Nm)$	Torque vector in the body frame
M_B	Inertia matrix
C_B	Coriolis-centripetal matrix
$\boldsymbol{Q}$	Generalized force vector
$\dot{\boldsymbol{\nu}}$	Generalized acceleration vector
$I_{XX} \ (kg \ m^2)$	Inertia on X axis
$I_{YY} \ (kg \ m^2)$	Inertia on Y axis
$I_{ZZ} \ (kg \ m^2)$	Inertia on Z axis
$G_\theta \ (\xi)$	Gravity force
$O_B(v)$	Gyroscopic propeller matrix
$E_B \Omega^2$	Motion force
$\boldsymbol{F_G^B}$	Gravity force vector in the body frame
$g(ms^{-2})$	Gravity acceleration
$J_{TP}(Nms^2)$	Total rotational moment of inertia about the propeller axis

$\boldsymbol{U_B}(\boldsymbol{\Omega})(m/s)$	Motion vector
$E_B(m\ s^{-1})$	Motion matrix
$l(m)$	Distance from the center of the propeller to CG
U_1, U_2, U_3, U_4	Motion vector components
$R\ (\Omega)$	Resistor
$L\ (H)$	Inductance
$v\ (V)$	Voltage source
$e(V)$	Potential generator
$i\ (A)$	Current
$K_E\ (V\ s\ rad^{-1})$	Motor force constant
$\omega_M(rad\ s^{-1})$	Motor angular speed
$J_{TM}(N\ m\ s^2)$	Total motor mass moment of inertia
$T_M(N\ m)$	Motor torque
$T_L(N\ m)$	Load torque
$K_M(N\ m\ A^{-1})$	Motor torque constant
$\omega_P(rad\ s^{-1})$	Propeller angular speed
η	Gear conversion efficiency
P_M	Mechanical power of the motor axis
$P_P\ (N\ m\ s^{-1})$	Mechanical power of the propeller axis
$T_{P_M}(N\ m)$	Propeller torque in the motor axis
$T_{M_P}(N\ m)$	Motor torque in the propeller axis
$J_M(N\ m\ s^2)$	Rotor moment of inertia about the motor axis
$J_P(N\ m\ s^2)$	The rotor moment of inertia about the propeller axis
$T_P(N\ m)$	Propeller torque
$D_P(N)$	Propeller drag force

❖ All the bolded symbols in the above list and in the context of this study is considered as the vector.

References

[1] N. Aldawoodi, "An approach to designing an unmanned helicopter autopilot using genetic algorithms and simulated annealing," Scholar Commons, Florida, 2008.

[2] T. P. Ehrhard, "Air Force UAVs The Secret History," *Mitchell Institute Press,Arlington,VA* , pp. 1-84, 2010.

[3] John F. Keane and Stephen S. Carr, "A Brief History of Early Unmanned Aircraft," *JOHNS HOPKINS APL TECHNICAL DIGEST, VOLUME 32, NUMBER 3* , pp. 558-571, 2013.

[4] Róbert SZABOLCSI, "A New Approach of Certification of the Airworthiness of the UAV Automatic Flight Control Systems," *Technical Sciences* , pp. 423-431, 2014.

[5] Richard K. Barnhart, Stephen B. Hottman Douglas, M. Marshall and Eric Shappee, Introduction to Unmanned Aircraft Systems, New York: CRC Press, Taylor & Francis Group , 2011.

[6] A. Cavoukian, "Privacy and Drones: Unmanned Aerial Vehicles," Ontario, 2012.

[7] KimonP.Valavanis and GeorgeJ.Vachtsevanos, Handbook on UAVs, Atlanta: Springer Science+Business Media Dordrecht , 2015.

[8] A. V. Koldaev, "Non-Military UAV Applications," *Research Gate,* 2007.

[9] I. Colomina, P. Molina, "Unmanned Aerial Systems for Photogrammetry and Remote Sensing: A review," *ISPRS Journal of Photogrammetry and Remote Sensing,* pp. 79-97, 2014.

[10] R.J. Bachmann, F.J. Boria, R. Vaidyanathan,P.G. Ifju, R.D. Quinn, "Biologically Inspired Micro-Vehicle Capable of Aerial and terrestrial Locomotion," *Mechanism and Machine Theory,* vol. 44, pp. 513-546, 2009.

[11] M. Hassanalian, A. Abdelkefi, "Classifications, applications, and design challenges of drones: A review," *Progress in Aerospace Sciences,* vol. 91, pp. 99-131, 2017.

[12] Dario Floreano, Robert J. Wood, "Science, technology and the future of small autonomous drones," *Nature,* vol. 521, pp. 460-466, 2015.

[13] Babak Ameri, David Meger, Keith Power, Dr. Yang Gao, "UAS Applications: Disaster & Emergency Management," GEOSYS Technology Solutions Ltd. , Vancouver, 2009.

[14] Rachel L. Finn, David Wright, "Unmanned Aircraft Systems: Surveillance, Ethics and Privacy in Civil Applications," *Computer Law & Security Review,* vol. 28, pp. 184-194, 2012.

[15] Lina Tang, Guofan Shao, "Drone remote sensing for forestry research and practices," *Springer,* vol. 26, no. 4, pp. 791-797, 2015.

[16] Haitao Xiang, Lei Tian, "Development of a Law-cost Agricultural Remote Sensing System Based on an Autonomous Unmanned Aerial Vehicle (UAV)," *Biosystem Engineering,* vol. 108, pp. 174-190, 2011.

[17] J. Torres-Sanchez, J.M. Pena, A.I. DE Castro, F. Lopez-Granados, "Multi-Terporal Mapping of the Vegetation Fraction in Early-Season Wheat Fields Using Images from UAV," *Computer and Electronics in Agriculture,* vol. 103, pp. 104-113, 2014.

[18] José Manuel Peña, Jorge Torres-Sánchez, Ana Isabel de Castro, Maggi Kelly, Francisca López-Granados, "Weed Mapping in Early-Season Maize Fields Using Object-Based Analysis of Unmanned Aerial Vehicle (UAV) Images," *PLOS ONE,* vol. 8, no. 10, pp. 1-11, 2013.

[19] P.J. Zarco-Tejada, R.Diaz-Varela, V.Angileri, P. Loudjani, "Tree Hight Quantification Using Very High Resolution Imagery Acquired from an Unmanned Aerial Vehicle (UAV) and Automatic 3D Photo-Reconstruction Methods," *European Journal of Agronomy,* vol. 55, pp. 89-99, 2014.

[20] Cornelius A. Thiels, DO, Johnathon M. Aho, MD, Scott P. Zietlow, MD, and Donald H. Jenkins, MD, "Use of Unmanned Aerial Vehicles for Medical Product Transport," *Air Medical Journal ,* vol. 34, no. 2, pp. 104-108, 2015.

[21] Leila A. Haidari, Shawn T. Brown, Marie Ferguson, Emily Bancroft, Marrie Spiker, Allen Wilcox, Ramya Ambikapathi, Vidya Sampath, Diana L. Connor, Bruce Y. Lee, "The economic and Operational Value of Using Drones to Transport Vaccines," *Vaccine,* vol. 34, pp. 4062-4067, 2016.

[22] SANDEEP S., GURURAJ B TENNALI, DEEPAK A. YARAGUPPI, SANDEEP S.,NITISH K., "Nanobotz in Cancer Detection & Trearment," *Journal of Medicine and Pharmaceutical ,* vol. 1, pp. 7-14, 2015.

[23] M. Balasingam, "Drones in Medicine—The Rise of the Machines," *Clinical Practice ,* pp. 1-4, 2017.

[24] Judy E. Scott, Carlton H. Scott, "Drone Delivery Models for Healthcare," *Hawaii International Conference on System Sciences,* pp. 3297-3304, 2017.

[25] Francesco Nex & Fabio Remondino, "UAV for 3D mapping applications: a review," *Appl Geomat,* vol. 6, pp. 1-15, 2014.

[26] F. Remondino, L. Barazzetti , F. Nex , M. Scaioni , D. Sarazzi , "UAV Photogrammetry for Mapping and 3D modeling-Current Status and Future Perspectives," *International Archives of the Photogrammetry, Remote Sensing and Spatial Information Sciences,* Vols. XXXVIII-1/C22 , pp. 1-7, 2011.

[27] R. E. Weibel, "Safety Considerations for Operation of Different Classes of Unmanned Aerial Vehicle in the National Airspace System," MIT, Massachusetts, 2005.

[28] Richard Voyles, Guangying Jiang, "Hexrotor UAV Platform Enabling Dextrous Interaction with Structures - Preliminary Work," *IEEE,* pp. 1-7, 2012.

[29] H. Eisenbeiss, "UAV Photogrammetry," Zurich, 2009.

[30] M. A. Boon, A. P. Drijfhout S. Tesfamichael, "Comparison of a Fixed-Wing and Multi-Rotor UAV for Environmental Mapping Applications: A Case Study," *The International Archives of the Photogrammetry, Remote Sensing and Spatial Information Sciences,* Vols. XLII-2/W6, pp. 47-54, 2017.

[31] D. Norris, Build Your Own Quadcopter, McGraw-Hill Education, 2014.

[32] M.Bangura, "Aerodynamics and Control of quadrotor," Uppsala, 2017.

[33] Čedomir Lj. Kostića, Boško P. Rašuo, ""AERODYNAMIC AIRFOIL AT CRITICAL ANGLES OF ATTACK,"," *MILITARY TECHNICAL COURIER,* vol. 64, no. 3, pp. 784-811, 2016.

[34] H. Babinsky, "How do wings work," *PHYSICS EDUCATION,* pp. 497-503, 2003.

[35] S. Bouabdallah, "Design and Control of Quadrotors with Application to Autonomous Flying," Lausanne, 2007.

[36] T. Bresciani, "Modelling, Identification and Control of a quadrotor helicopter," Milano, 2008.

[37] M.Ranjbaranhesarmaskan, "Fault Recovery of an Under-Actuated Quadrotor Aerial Vehicle," Montreal, 2010.

[38] S.A.Raza, "Design and Control of a Quadrotor Unmanned Aerial Vehicle," Ottawa, 2010.

[39] F. Hamano, "Derivative of Rotation Matrix – Direct Matrix Derivation of Well-Known Formula in Green Energy and Systems," Long Beach, CA, 2013.

[40] A. Bostrom, "Rigid Body Dynamics," Gothenburg, 2012.

[41] S. Zhao, "Time Derivative of Rotation Matrices," Sheffield, 2016.

[42] A. Persson, "How Nweton might have derived the Coriolis acceleration," Uppsala, 2017.

[43] I. Osgar John Ohanian, "Mass Properties Calculation and Fuel Analysis in the Conceptual Design of Uninhabited Air Vehicles," Virginia Tech Electronic Theses and Dissertations, Blacksburg, Virginia, 2003.

[44] D.B. Marghitu, M. Dupac, "Advanced Dynamics: Analytical and Numerical Calculations with MATLAB," no. Chapter 2, 2012.

[45] W. Jordan, "Transmission for Driving Counter-rotating Propellers, Lubrication System, and Associated Methods," United State Patent No.6478641 B2, 2002.

[46] Kaan T. Oner, Ertugrul Cetinsoy, Mustafa Unel, Mahmut F. Aksit, Ilyas Kandemir, Kayhan Gulez, "Dynamic Model and Control of a New Quadrotor Unmanned Aerial Vehicle with Tilt-Wing Mechanism," in *International Conference on Control, Automation, Robotics and Vision*, Paris, 2008.

[47] Kaan Taha ¨ONER1, Ertu˘grul C¸ET˙INSOY1, Efe SIRIMO˘GLU1, Cevdet HANC¸ER1, "Mathematical modeling and vertical flight control of a tilt-wing UAV," *Turk J Elec Eng & Comp Sci, Tubitak,* vol. 20, no. 1, pp. 149-157, 2012.

[48] J. C. Lerner, "Wind Tunnels in Engineering Education," in *Wind Tunnels and Experimental Fluid Dynamics Research* , InTech, 2011, p. 709.

[49] A. Durai, "Experimental Investigation of Lift and Drag Characteristics of a Typical MAV under Propeller Induced Flow," *International Journal of Micro Air Vehicles,* vol. 6, no. 1, pp. 63-72, 2014.

[50] John B. Brandt∗ and Michael S. Selig†, "Propeller Performance Data at Low Reynolds Numbers," AIAA Aerospace Sciences Meeting , Urbana, 2011.

[51] A. Knight, Basics of MATLAB and Beyond, Washington, D.C.: CHAPMAN & HALL/CRC, 2000.

[52] M. D. Schmidt, "SIMULATION AND CONTROL OF A QUADROTOR UNMANNED AERIAL VEHICLE," UKnowledge, Kentucky, 2011.

[53] A. Noth, S. Bouabdallah and R. Siegwart, "Dynamic Modeling of Fixed-Wing UAVs," ETH, Zurich, 2006.

[54] Andre Noth, Walter Engel and Roland Siegwart, "Design of an Ultra-Lightweight Autonomous Solar Airplane for Continuous Flight," ResearchGate, Zurich, 2016.

[55] M. Khaghania, J. Skalouda, "AUTONOMOUSNAVIGATIONOFSMALLUAVSBASEDONVEHICLEDYNAMIC MODEL," *The International Archives of the Photogrammetry, Remote Sensing and Spatial Information Sciences,* Vols. XL-3/W4, pp. 117-122, 2016.

[56] A. Sanchez, J. Escareño, O. Garcia and R. Lozano, "Autonomous Hovering of a Noncyclic Tiltrotor UAV: Modeling, Control and Implementation," The International Federation of Automatic Control , Seoul, 2008.

[57] A. Elsayed Ahmed, A. Hafez, A. N. Ouda, H. Eldin Hussein Ahmed, H. Mohamed Abd-Elkader, "Modeling of a Small Unmanned Aerial Vehicle," *World Academy of Science, Engineering and Technology ,* vol. 9, no. 3, pp. 413-421, 2015.

[58] M.D.Schmidt, "Simulation and Control of a Quadrotor Unmanned Aerial Vehicle," Lexington, 2011.

[59] L. S. A. F. J. M.-T. R. K. Anshuman Bhardwaj, "UAVs as Remote Sensing Plateform in Glaciology: Present Applications and Future Prospects," *Remote Sensing of Environment,* vol. 175, pp. 196-204, 21016.